Ben Gurion University of the Negev

Faculty of Natural Sciences

Investigating the Use of Rock Bolts to Mitigate Rock Bursts Using the Discrete Element DDA Method

Thesis submitted in partial fulfillment of the requirements for the M.Sc. Degree in the faculty of Natural Sciences

By:

Nachum Kazaz

Under supervision of Prof. Yossef. H. Hatzor

July 2018

Ben Gurion University of the Negev

Faculty of Natural Sciences

Investigating the Use of Rock Bolts to Mitigate Rock Bursts Using the Discrete Element DDA Method

Thesis submitted in partial fulfillment of the requirements for the M.Sc. Degree in the faculty of natural sciences

By:

Nachum Kazaz

UNDER THE SUPERVISION OF Prof. Yossef Hatzor

Signature of student: _____ Date: _____

Signature of supervisor: __ Y. Hatzor. _____ Date: _____

Signature of chairperson

Of the committee for graduate studies: _____ Date: _____

July 2018

Acknowledgment

I would like to thank my thesis advisor Professor Yossef H. Hatzor, for his support and professional supervision throughout this research.

I would like also to thank my friends Aviran Feldhiem, Yair Gordin, Omri Shitrit, Dr. Ben-Gou He, Yuval Kiser, Doron Morad, Itzik Yadid and Alexandra Zaslav for the assistance they provided me. I would like also the thank Rivka Eini and Zahla Sharabi for their huge help in maneuvering through University bureaucracy, and to Avishay Krif for the technical support.

Finally, I want to thank my family for their enormous support along the way.

Abstract

This thesis explores the rock-burst phenomenon and the ways to mitigate it with the use of active support elements, such as rock-bolts and rock-anchors.

Rock-bursts are defined as rapid releases of strain energy, which initiate displacement of rock mass volume from the tunnel free surface toward the tunnel space. The phenomenon is related to strain release due to the new opening of the tunnel space. Rock-bursts are very complex and are related to several mechanisms including buckling, high velocity sliding on discontinuities and block ejections due to seismic energy of remote source. Rock-bursts pose a high threat to workers and equipment in tunneling sites, and can cause considerable difficulties for project managers and planners; each year several deaths and equipment loss are reported around the world due to rock-bursts.

Energy absorbing rock bolts are effective and moderately inexpensive instruments to manage rock bursts when there is a pre-existing problem. The role of the bolts is to retain key blocks in their position during the event and to increase the frictional resistance in the system, thus conserving the structural stability via arching mechanisms. The main differences between regular traditional bolts to energy absorbing bolts is the ability to undergo substantial deformation with high load in a short period of time.

In this study, we analyzed the performance of energy absorbing rock bolts during and after a rock burst event using the numerical DDA method. DDA is a discrete-element numerical modeling method that uses pre-specified

polygons (blocks) that do not undergo any plastic deformation during the analysis. The displacement of the blocks is governed by kinematical equations and by Coulomb's shear strength criterion between block edges. The main assumption of the DDA method is that failures in the rock mass occur primarily through slip across pre-existing rock discontinuities rather than fracture of intact rock. This study focuses on three main subjects:

In the first part we study the role of rock bolts in the DDA model during non-damped dynamic simulations. Dynamic simulation is different in essence from static simulation: in dynamic simulation the kinetic energy is translated from one time step to the next, whereas in static simulation it does not. We conduct a numeric 'drop test', in which a fixed rock bolt is subjected to different types of loads, while recording the load and strain it undergoes. The results show that the original DDA bolt model behaves like a pure spring, which undergoes simple harmonic motion when subjected to any kind of load, either external or due to self-weight of the block. The velocity which governs the kinetic energy associated with rock bursts only has a minor role on the rock bolt operation. Finally, we determine the optimal bolt stiffness that should be used in a rock burst prone area.

The second part of this research focuses on the performance of the rock-bolt under stress induced rock-bursts as a function of bolt stiffness, bolt installation geometry and the rock mass condition. During the geometrical installation of the bolts, their length and spacing were found to be of decisive importance in absorbing rock bursting energy. We find that it is important that the installed

bolting pattern be as dense as possible in order to anchor as many free key blocks and to preserve the overall structure of the tunnel, by increasing the frictional resistance in the system. We also find that the bolt must be long enough, up to one diameter from the tunnel free surface, to ensure effective restraining of the released energy. Rock mass quality, which in our study was scaled by the RMR rating method, has a significant impact on the energy absorbing performance of the supporting elements. We find that while the poorly rated rock mass will absorb up to 32 kJ/m^2, well-rated rock-masses will absorb less than 1 kJ/m^2 on average. The results proved that DDA displays a strong prediction ability of the energy load excreted on the rock bolting pattern, with resulting values close to estimated and measured values by researchers worldwide.

In the third part of the study, we explore rock bursts triggered by dynamic loads caused by nearby explosions. We want to examine the effect of blast energy on the loads that developed on rock bolt pattern, and test for variations depending on the distance between the blast and the tunnel, and the friction angle of the rock discontinuities. To test this, we use a blast element: a geometric installation which transfers radial stress of 30 MPa to the tunnel, without initial stress applied in the simulation. The results show that the dominant factor influencing the bolt load is the distance of the blast element from the tunnel free surface. Excess load values reach up to 2.08 kJ. The friction angle also has an important role in determining the bolt load: load reduction of up to 1.7 kJ were recorded when the friction angle was raised from 20^o to 60^o. Further study

should be conducted which also incorporates initial stresses in the blast study, to determine if this impacts our results.

Thesis Contents

List of figures

List of tables

Chapter 1 : Introduction

1.1: The rock burst phenomenon

Rock-burst is a physical phenomenon observed in depths greater than 1000 meters, an environment that is characterized by high *in-situ* stresses (Cai, 2013). When rock-burst event occurs, a volume of rock abruptly ejects at high velocity from the free surface of a tunnel toward the tunnel space (Stacey, 2011). There are two common types of rock-bursts: 1) strain-bursts, 2) dynamically induced rock-bursts. The main focus of this thesis is the high velocity sliding on pre-existing discontinuities that can derive from both mechanisms. **Strain-bursts** relate to strain relaxation occurring as a result of the new opening. This new opening enables the accumulated elastic strain to release. The rock starts to undergo buckling / sliding on joints / splitting processes, to a point that discrete elements (rock blocks) might eject into the tunnel space at high velocity. Strain-burst is typically related to hard/brittle rock masses. The second mechanism, **dynamically induced rock-bursts,** occurs when seismic energy travels from afar and thus produces rock-block ejections toward the tunnel. Dynamically induced rock-burst can occur in almost any sort of rock mass. The two mechanisms are illustrated in Figure 1-1. The nature of the rock burst phenomena is yet to be fully understood. Durrheim et al. (1998), reported that during a rock-burst event one panel of the tunnel was severely damaged while the other was perfectly unscathed.

The mitigation of to the rock-burst hazard is based on two components:

1) Smart planning of excavation outlines, such as geometry, mining in sequence, minimal explosion usage and avoidance from geological hazards (faults, dykes etc.).

2) A good support system that can absorb the majority of the energy released in the event without damaging the excavation.

In this thesis, we focus on the planning of a support system that aims to reduce the risk coming from rock-bursts. We studied the likelihood of mitigating rock-bursts using rock-bolts. This effective and economic support measure can possibly reduce the risk level

associated with rock-burst hazard. The study is conducted using the Discontinuous Deformation Analysis (DDA) method, a discrete element numerical method that enables us to insert discontinuities to the mesh, simulating blocky rock masses. DDA also has the option to add purely elastic springs to the mesh, simulating rock-bolts, with no limit on elongation and load bearing.

1.2: The influence of rock-bursts on tunneling projects

Due to their unpredictable and violent nature, rock-bursts can cause injuries and fatalities to workers as well as damage to the mining equipment (Cai, 2013). For this reason, it is imperative to determine how to counter this problem. Nevertheless, the relatively infrequent but often serious instances of rock-burst damage in tunnels have consequently not received the attention that is warranted (Ortlepp, 1994).

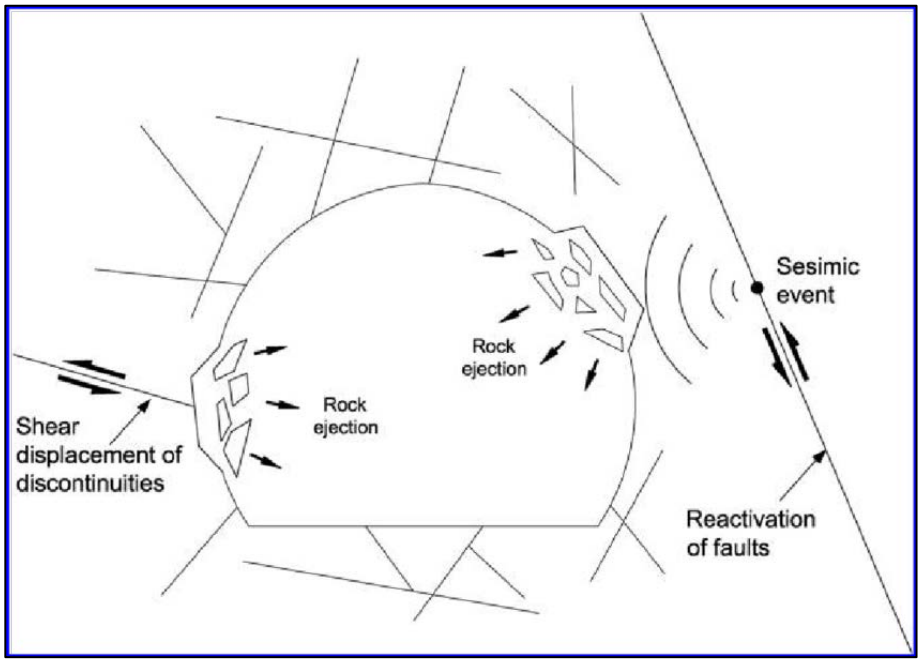

Figure 1-1: Rockburst mechanism illustration. Rock ejection due to the arrival of far distance seismic energy caused by fault slip (right). Rock ejection due to shearing on pre-existing discontinuities at tunnel free surface (left). (Modified after Ortlepp and Stacey 1994)

Rock-burst prediction and prevention can also come in the form of smart mining planning before tunneling. For example, Durrheim et al. (1998) found that the rock-burst source mechanism is often controlled by the mine layout and regional structures such as faults and

dykes. When the problem already exists, it can be alleviated with special support elements. One of the useful support elements is the **energy absorbing rock-bolt**, with theoretically, no limit on elongation and load bearing capacity.

1.3: Support systems in tunneling

We summarize the role of support system elements in deep tunneling projects. Then, we focus on the implementation of rock-bolts in tunneling projects with special attention to energy absorbing rock-bolts.

The support system and its role in deep tunneling

The support in rock-burst prone area consists of two functions, passive support and active support:

1) The passive support system aims to sustain the rock-burst event and transfer the energy to the active support; it includes shotcrete lining, steel mesh and steel sets (steel arch) connected with special plates to the active support.

2) Active support mainly consists of rock-bolts anchored to stabilize the rock beyond the plastic zone circling the tunnel space - usually several meters away from the tunnel free surface where there are no rock deformations. The bolts are attached to the passive support via steel plates. The role of the active support is to retain the key-blocks in their position, to increase frictional resistance across joints, and to increase compressive strength. A schematic illustration of rock bolts is shown in Figure 1-2.

This support method is very common in the industry. Starting in the early 1970s, fully grouted steel rebars, usually with mesh and lacing, became the common method to support deep underground tunnels throughout the gold-mining industry (Ortlepp, 1994).

Active support system in Rock-burst prone area

An active support system includes three different types of rock-bolts that can be installed during the tunneling process. Each element has its own role in terms of load capacity, deformation ability, and energy absorption (Figure 1-3). The active element should be chosen carefully based on the site's condition:

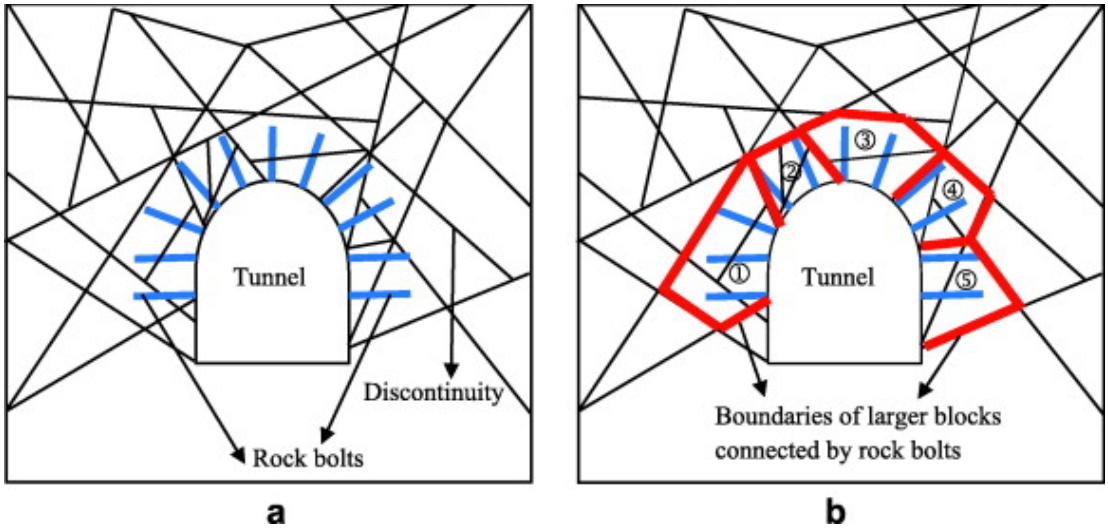

Figure 1-2: (a) Concept of rock bolts in jointed rock mass. (b) The bolts retain the potential key block (marked in red) and also stabilize the structure and prevent it from collapse ((Fu and Ma, 2014)*)*

1) Stiff bolts: Tunnel sites at shallow depth, under low stress field, can be supported by simple stiff rock-bolts because they can carry only the dead load of the free block at the tunnel surface. Those bolts are usually a simple rebar with diameter of $2-5\ cm$, and are capable of carrying a high load range of $150-800\ kN$. However, the bolt strength may be exceeded even after a relatively small amount of deformation.

2) Deformable bolts: Suitable for tunnel sites with large movements in the rock mass, i.e. weak or flowing ground. These bolts have low bearing capacity, up to $50\ kN$, and are usually based on friction between the bolt and the rock. The split set is the most common deformable rock-bolt.

3) Energy absorbing rock-bolt: In the case of tunnel sites with both large movements and high load due to an extremely high stress field, bolts designed to be installed in such environments need to have the ability to undergo high deformation and high impact load without failing. The bolt needs to exhibit elongation ability at the range of up to 15 % and sustain impact load up to $400\ kN$.

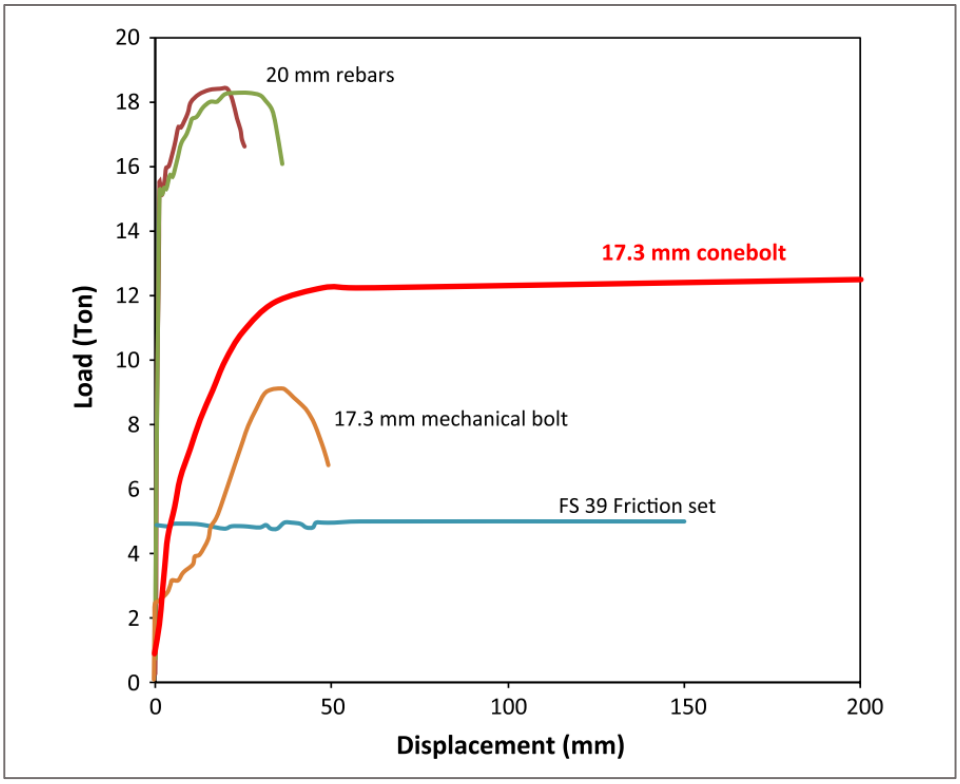

Figure 1-3: The different types of rock-bolts available in the market today. The rock-bolts are sorted into three groups: load bearing bolts (noted as 20 mm rebars). Strain bearing bolts (noted as FS 39 Friction set). Energy absorbing bolts (noted as 17.3 mm Conbolt). (Li 2010).

A special rock-bolt for rock-burst conditions named D-Bolt (Li, 2010) is presented in Figure 1-4. This bolt consists of long deformable steel rods linking each other with wiggle shaped anchors (Figure 1-4, a). This rock-bolt uses the plastic behavior of steel when deformation occurs. Even if parts of the rock-bolt fail, the other anchored wiggle is still functioning and absorbing more energy. D-Bolts are tested by a laboratory test called 'drop test', in which a 1 ton mass is dropped on a special plate that transfers a dynamic load to a tube containing the rock-bolt (Figure 1-4, b). The results of the 'drop test' (Figure 1-4, c) demonstrate that the D-Bolt has high impact load capacity, up to 315 kN, deformation ability of 17.7 % and energy absorption ability of 39 kJ, all achieved in less than 50 $msec$. These numbers are widely accepted by the scientific community (Cai, 2013;Kaiser and Cai, 2013; Ortlepp, 1994).

Although the importance of energy absorbing rock-bolts is accepted by many, in reality, the majority of rock-bolts are still stiff, do not behave like an energy absorbing tool, and

will probably fail under dynamic conditions. Observations and in-situ reports from the past years indicate that the use of regular stiff rebars is still dominant in deep tunnels, mostly because of cost reduction. Ortlepp (1994) concluded that the continuing failure of such elements to counter the problem should have led to an urgent revision of tunnel design procedures based on stiff rebars.

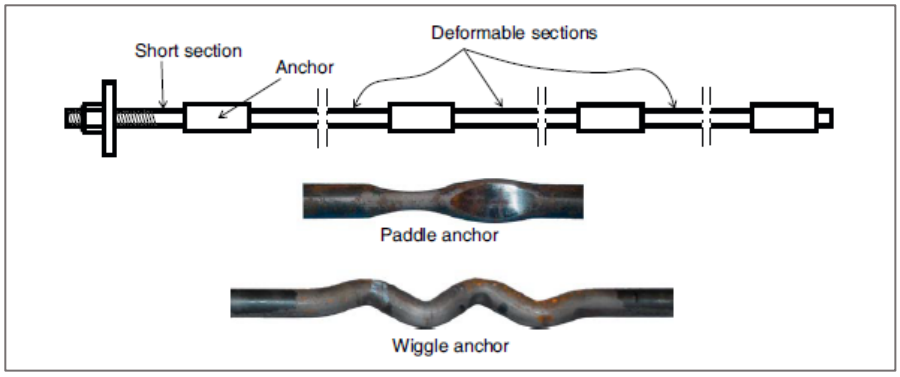

Figure 1.4 (a)

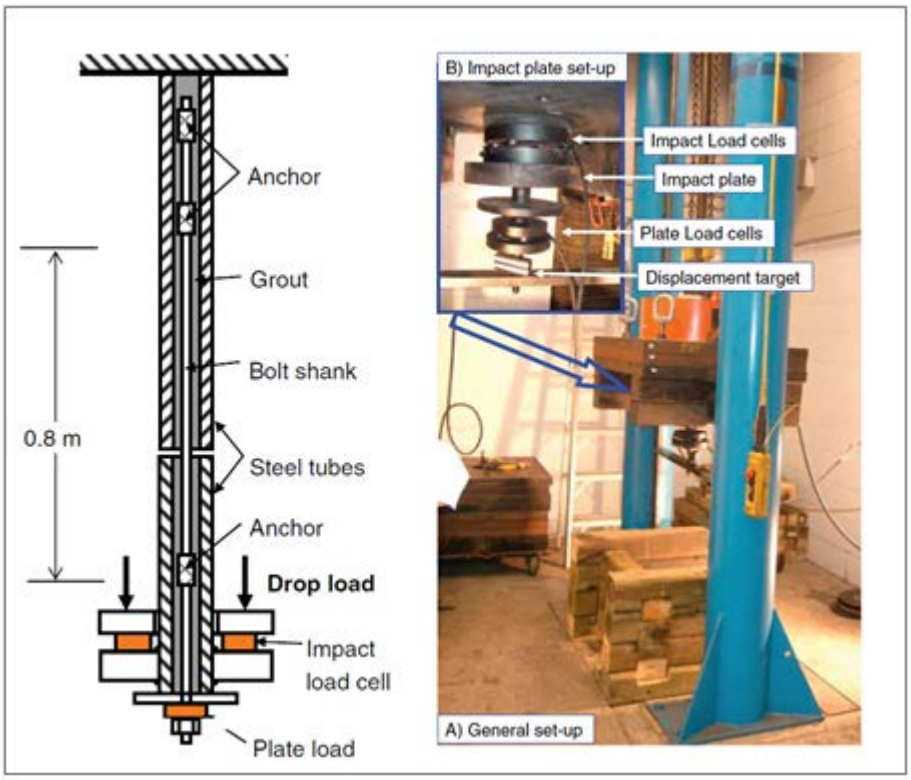

Figure 1.4 (b)

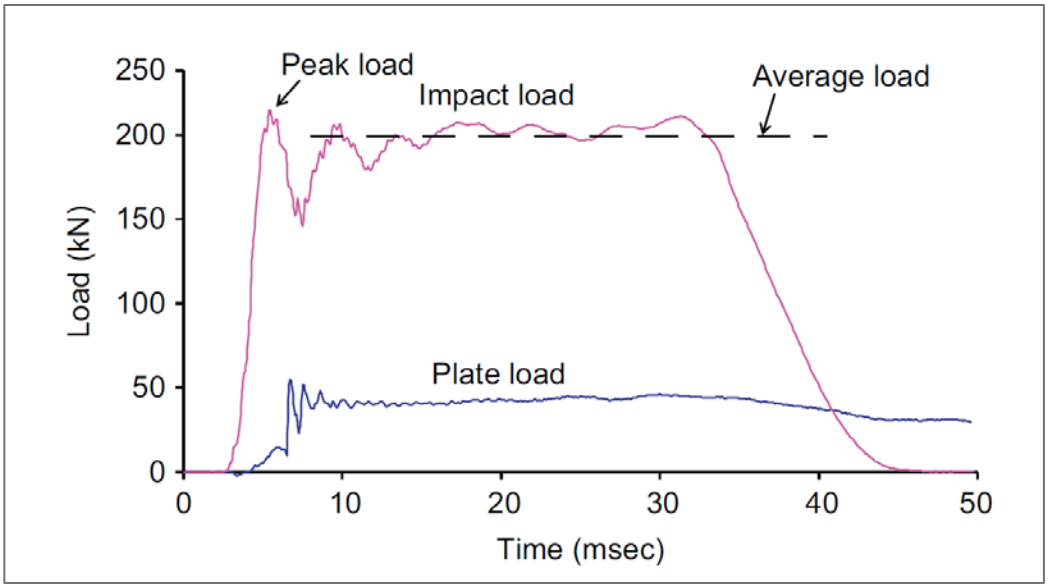

Figure 1.4 (c)

Figure 1-4: The D-Bolt and the special anchors (a). Rock-bolt dynamic experiment tested behavior under Rockburst conditions (b) the experiment aparatus used to test the bolt, by dropping mass of 1 ton on plate connecting to the bolt (b). D-Bolt force history graph (c).

Rock burst mitigation using energy absorbing rock bolts

The history of energy absorbing rock-bolts begins in 1968 when Ortlepp, a prominent South African scientist, suggested a new concept: a rock-bolt with the ability to undergo large deformations, thus absorbing most of the energy of a rock-burst event.

Over the next twenty years, numerous attempts have been made to develop this tool, but without much success. The suggested rock-bolts, which developed over that period, have the ability to undergo large deformations, but failed in the end because of the large impact load. For example, the Friction bolt cannot carry more than $50\ kN$ of load while the rock burst impact reaches more than $2000\ kN$ (Cai, 2013).

In the early 1990's, a new device was introduced, the Cone-bolt. This bolt consists of two parts: 1) a cone shaped anchor, 2) a smaller diameter metal rod attached to the cone (see Figure 1-5). The bolt is inserted into a drill hole and filled with cement. In normal static conditions the Cone-bolt functions like a regular stiff bolt and carries the static load. When

the Cone-bolt is subjected to a high impact load, such as a rock burst event, the cone anchor is dragged through the cement along the drill-hole. Due to the friction force between the cone and the cement, the bolt can undergo high deformations and absorb a high impact load. The Cone bolt proved its abilities in reality when it managed to keep a tunnel safe during a 3.2 magnitude rock burst in a Canadian mine: the bolt elongated $18\,cm$ thus absorbing much of the energy (Cai, 2013). It is worth mentioning that in contrast to other shafts in the mine, where regular rebars were installed, large damages occurred. Today there are dozens of other energy absorbing rock bolts present in the market as well.

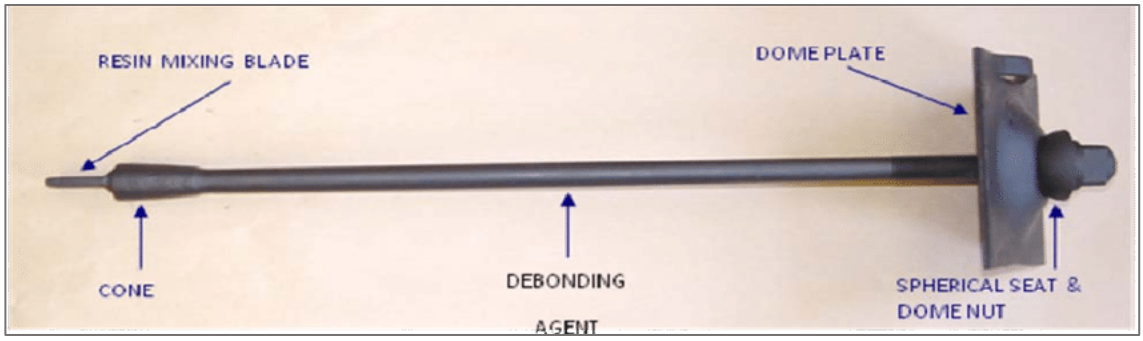

Figure 1-5: The Conebolt rock bolt used in high load high deformable rock-mass envioments

1.4: thesis objectives

Rock-bolt is an efficient and economical instrument to ease the severity of rock-bursts. Here we focus on **blocky** rock-masses that are abundant in tunneling projects around the world. In blocky rock masses, sliding mechanism is the primary source of rock-bursts. In this case, when high strain energy is stored in the surrounding rock mass, and the finite block ("keyblock" in Goodman and Shi's (1985) Block Theory terminology) has the kinematic ability to move, the accumulated strain can release abruptly. The abrupt release produces a rock-burst event followed by block ejection towards the tunnel space (Figure 1-1). Since rock-bolts are the last barrier to absorb the energy of a rock-burst event, good rock-bolting design can significantly reduce the damage while retaining the key blocks in their position.

In this study, we assume elastic deformation of intact block material and a plastic deformation along discontinuities. Specifically, we want to answer two main questions:

1. Can rock bolts mitigate the rock burst phenomenon, and if so, how can they accomplish this, in terms of bolt parameters?
2. And, what will be the energy load, on the bolt system, during the time of the event?

We will study several aspects, including grade of rock mass, type of load, and the rock bolt's support system parameters. First, we aim to understand the loading mechanism during rock-burst event, both dynamic and static. Later, we will examine several parameters that influence rock bolt behavior during rock-burst event:

1. Bolt spacing
2. Bolt length
3. Bolt stiffness
4. Rock mass properties as scaled by RMR classification
5. Type of load: static and dynamic
6. The performance and limitation of the bolt element in the original DDA code

Simulation of tunneling in DDA consists of installation of radial rock-bolts and the removal of the tunnel material. Although it might not be perceived as realistically feasible, the process is similar to the construction method for the Olmos Irrigation Tunnel Project under the Andes Mountains in Peru. In this instance, due to severe rock-burst problems the tunnel was excavated using a TBM without pre-cast concert slab. After excavating one segment, they used steel mesh and rock-bolts to support the tunnel and only after the strain energy was released were the concrete segments put in place (Clark and Chorley, 2014).

Chapter 2 : Research Methods

2.1: The numerical DDA method

The development of engineering geology in the recent decades has been coupled with an effort to predict rock behavior in complicated rock masses. One way to make those predictions feasible is through numerical modeling. Numerical modeling in rock mechanics consists mainly of two main approaches. The Finite Element Method (FEM), is based on load/displacement transfer through pre-specified mesh. In such an approach, we assume connection between all particles in the observed media. FEM is very useful for continuous rocks with known material properties. The Discrete Element Method (DEM) was developed to better address rock masses containing discontinuities. DDA belongs to the DEM family and solves the displacements between discrete block elements, each having six degrees of freedom (Shi, 1993). The DDA method focuses on surface interaction between well-defined blocks that are assumed stiff and simply deformable, namely the block deformation is calculated for the center of mass and the block is assumed to deform homogenously. The developers of DDA based the method on the assumption that most of the deformation in geological rock masses is concentrated on the boundaries between stiff elements (rock blocks), namely across pre-existing rock discontinuities such as joints, faults, shears, bedding and foliation planes, and that the blocks remain intact during the deformation (Goodman and Shi, 1985). The computed displacement between blocks is controlled by the mechanical properties of the discontinuities, namely cohesion and friction angle, as Coulomb friction is assumed to act across discontinuities. The paramount idea of DDA is system energy minimization, as per the second law of thermodynamics, any system will tend to go in a direction that leads to minimum energy.

The program uses a set of equations for the first order (linear) displacement of variables in pre-specified time, called time-step. The equations are formulated such that all energy components can be minimized. In each time-step, the simultaneous equilibrium equations of all the blocks in the system are formulated and solved repeatedly until none of the blocks penetrate one another and there is no tension between blocks. In the end of the process,

when kinematic equilibrium is achieved, the final system displacement is the accumulation of all displacements in each time step, and the energy left in the system can be converted to stress that in time can be examined for each block.

For point (x, y) inside a block, six first order deformation variables can be the source of displacement:

$$\begin{pmatrix} u \\ v \end{pmatrix} = \begin{pmatrix} 1 & 0 & -(y-y_0) & (x-x_0) & 0 & (y-y_0)/2 \\ 0 & 1 & (x-x_0) & 0 & (y-y_0) & (x-x_0)/2 \end{pmatrix} \begin{pmatrix} u_0 \\ v_0 \\ r_0 \\ \varepsilon_x \\ \varepsilon_y \\ \gamma_{xy} \end{pmatrix} \quad (1)$$

where, u and v are the point displacement along the X and Y axis respectively, x_0 and y_0 are the block centroid coordinate, u_0 and v_0 are the translation components, r_0 is the rotation component around the centroid, ε_x and ε_y are the block strains, and γ_{xy} is the shear strain. This formula can be presented in the following form:

$$\begin{pmatrix} u \\ v \end{pmatrix} = [T_i][D_i] = \begin{pmatrix} t_{11} & t_{12} & t_{13} & t_{14} & t_{15} & t_{16} \\ t_{21} & t_{22} & t_{23} & t_{24} & t_{25} & t_{26} \end{pmatrix} \begin{pmatrix} d_{1i} \\ d_{2i} \\ d_{3i} \\ d_{4i} \\ d_{5i} \\ d_{6i} \end{pmatrix} \quad (2)$$

Equation 2 is used to construct the simultaneous equilibrium equations. A block system is defined by contacts between individual blocks and constrains on specific blocks. The simultaneous equilibrium equations can be written in compact form as:

$$[K][D] = [F]$$

Or:

$$\begin{pmatrix} K_{11} & K_{12} & K_{13} & & K_{1n} \\ K_{21} & K_{22} & K_{23} & \cdots & K_{2n} \\ K_{31} & K_{32} & K_{33} & & K_{3n} \\ & \vdots & & \ddots & \vdots \\ K_{n1} & K_{n2} & K_{n3} & \cdots & K_{nn} \end{pmatrix} \begin{pmatrix} D_1 \\ D_2 \\ D_3 \\ \vdots \\ D_n \end{pmatrix} = \begin{pmatrix} F_1 \\ F_2 \\ F_3 \\ \vdots \\ F_n \end{pmatrix} \quad (3)$$

Each element K is a 6×6 matrix that contains the derivatives of all components in the

system that could produce energy (i.e. elastic energy) with respect to the six deformation variables. Submatrices K_{ii} represent energy derivatives for the single block and depend on block material properties. Submatrices K_{ij} represent energy derivatives for interactions between two blocks and depend on the interaction properties between blocks i and j. D_i is a 6×1 submatrix representing the deformation variables of block i. F_i is a 6×1 submatrix representing derivatives of external loading acting on block i (for example initial stress) with respect to each deformation variable. The energy derivatives with respect to single block deformation variables are of the form:

$$\frac{\partial \Pi}{\partial dr_i} = 0\,, \quad r = 1, \dots, 6 \tag{4}$$

where Π is the potential energy for block i, and dr_i are the six deformation variables. The total potential energy is minimized by setting the equation equal to zero. For interactions between two blocks, the equations are of the form:

$$\frac{\partial^2 \Pi}{\partial r_i \partial s_j} = 0, \qquad r, s = 1, \dots, 6 \tag{5}$$

representing the equilibrium of energy derivative of interaction between blocks i and j. Another partial derivative is the derivative we take with respect to external forces that form vector $[F]$ in the simultaneous equilibrium equation, namely:

$$\frac{\partial \Pi(0)}{\partial r_i} = f_r, \qquad r = 1, \dots, 6 \tag{6}$$

representing the derivatives of minimum energy of block i when $[D] = 0$.

There are several forces and stresses in a rock system that could produce energy. These include elastic stresses, point loads, line loads, volume loads, initial stresses, viscosity and inertia forces. These forces can be modeled in DDA. The process to define the components of the simultaneous equations repeat itself in all cases, first defining the energy expression and then taking its derivative with respect to all deformation variables. The development and differentiation of the energy expressions are computed separately for all deformation variables and then added together. This enables us to make changes in the parameters of the energy produced in each time step, thus modeling non-linear rock behavior. The complete mathematical treatment can be found in Shi's book (1993).

DDA No-tension and No-penetration principle

In the previous section we briefly discussed principles for a single block analysis. Now we wish to extend our discussion to a multi-block system that simulates the rock mass. Two main principles govern the analysis: 1) tension is not allowed between blocks, 2) penetration is not allowed between blocks. Those principles are enforced by sets of equations and inequalities imposed on the simultaneous equations (see Figure 2-1). Stiff springs are attached at identified contacts that constrain movement in one or two directions. In the case that tensile force is created between two blocks, the blocks simply separate. The simultaneous equilibrium equations are solved repeatedly until no penetration and no tension is obtained at all contacts. When friction and cohesion along the block boundaries are taken into account, the interaction between blocks is governed by Coulomb's criterion. The simultaneous equation changes accordingly, and a new component is added to the equations.

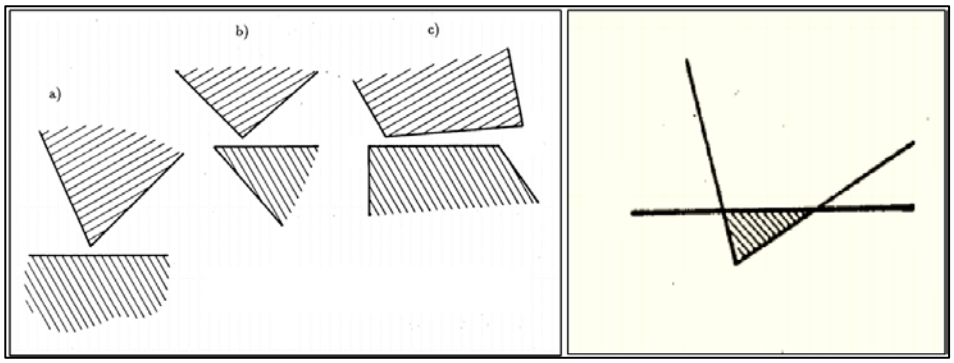

Figure 2-1: Allowed contact between block (right) and disallowed contact (left) (Shi, 1993)

Dynamic simultaneous equations

DDA simultaneous equations can be extended to dynamic analysis by adding a term for acceleration force and velocity, given by the equation:

$$M\ddot{D} + \mu\dot{D} + kD = F \tag{7}$$

where M, μ and K are the mass, viscous damping and stiffness matrices, respectively. In the current research, no viscous damping is applied, hence $\mu = 1$. The term for the acceleration with initial condition $D_0 = 0$, is:

$$\ddot{D} = \frac{2}{\Delta_i^2}\left(D - \dot{D}_0\right) \tag{8}$$

where Δi is the time step, $\dot{D}_0$ is the velocity at the beginning of the current time step. In the next time step Δ_{i+1}, $\dot{D}$ should be:

$$\dot{D} = \frac{2}{\Delta_i} D - \dot{D}_0 \tag{9}$$

By inserting those two equation (8) and (9) to the simultaneous equation (7) and rearranging, we have a new form:

$$KD = F \tag{10}$$

which is the form of the simultaneous equation for dynamic analysis.

DDA time integration scheme

The time integration in DDA is based on a Newmark integration scheme (Tsesarsky et al., 2002). The integration is in the form:

$$u_{i+1} = u_i + \Delta t \dot{u}_i + 0.5\Delta t^2 \ddot{u}_{i+1} \tag{11}$$

$$\dot{u}_{i+1} = \dot{u}_i + \Delta t \ddot{u}_{i+1} \tag{12}$$

Where Δt is the time step, u_i is the displacement in the current time step, $\dot{u}_i$ is the velocity in the current time step, $\ddot{u}_{i+1}$ is the acceleration in the next time step. The displacement of a block in the next time step is therefore dependent on the current displacement, the current velocity, and the acceleration of the next time step. This mechanism insures an implicit solution that is unconditionally stable (Tsesarsky et al., 2002). For further elaboration see (Wang et al., 1996).

Rock bolt in DDA

Rock-bolts in DDA can be seen as purely elastic springs, with specific spring stiffness K, and linear geometry that remains constant throughout the numeric simulation. The springs

connect two fixed points in two different blocks. In the simulation, when extension of the bolt takes place between point (r_i) and (r_j) of blocks i and j respectively, the meaning is that the bolt now has new strain energy, and that the displacement of the block depends on the bolt stiffness (Figure 2-2). We can use that property to measure the force exerted by the blocks during displacement. The DDA purely elastic springs represent a realistic approximation for energy absorbing rock bolts, implying that the high elongation ability and high bearing capacity are beneficial for the study of rock-burst phenomenon. Simulating the behavior of a rock-bolt in the rock-mass however is more complicated than the simplistic spring representation in the original DDA method. Several researches around the world are studying the possibility to improve the reliability of using rock bolt in DDA. Nie et al. (2014) conducted several studies on the coupled model to explore the grouted cement interface between the bolt and the rock mass using DDA, and proposed a new model for the shear stress developed between the grout and the bolt. Moosavi et al. (2006) studied the option to focus the load building along the bolt length, and especially focused on the stress build up next to a discontinuity (Figure 2-3). Their model was a double analysis whereby in each time step a special code calculated the stress along the bolt and inserted the new data to the DDA program of the next time step.

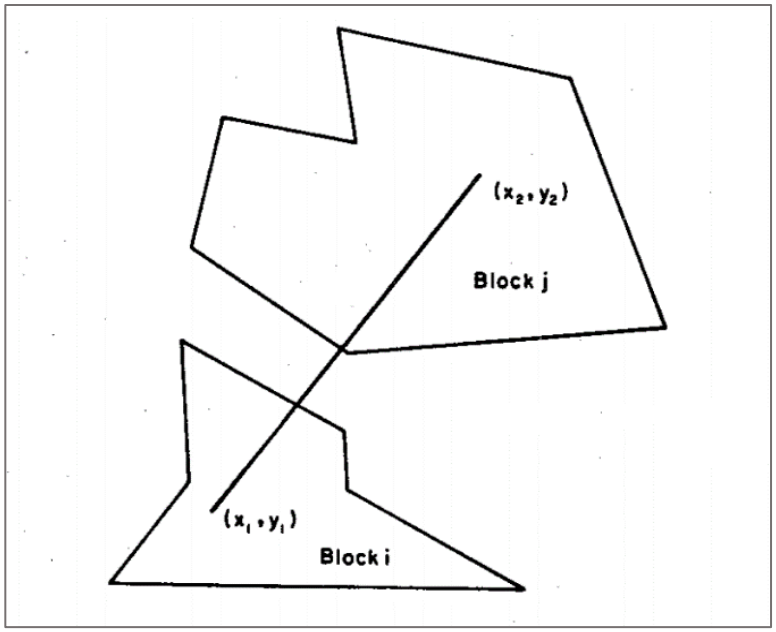

Figure 2-2: DDA schematic model of spring like, one-dimensional rock-bolt connecting two blocks (Shi, 1993)

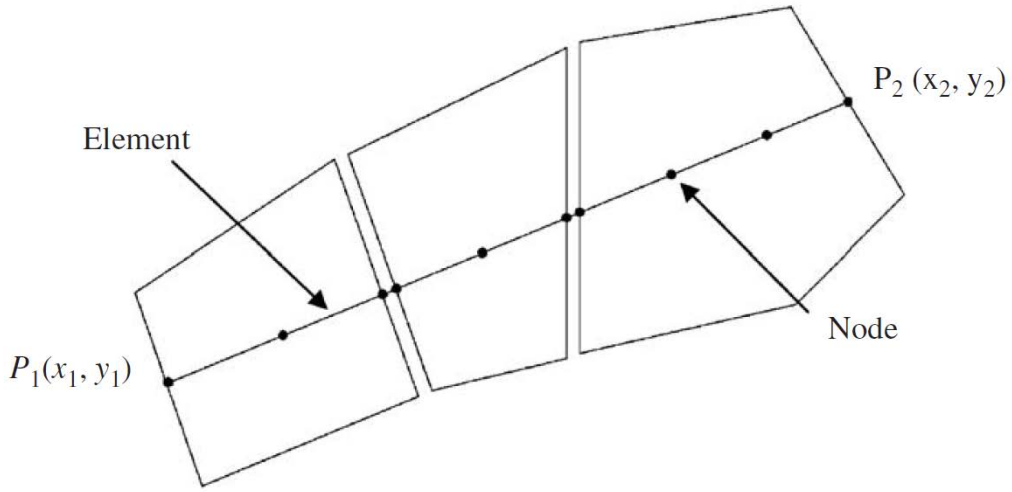

Figure 2-3: Advanced multi-nodes rock-bolt model for DDA, the use of multiple nodes along the bolt length to examine the load concentration near joints in the rock mass (M. Moosavi, 2006).

The DDA bolt model versus physical reality

A rock-bolt in reality is generally comprised of two parts: 1) the bolt itself, typically a steel rebar of several inch diameter, 2) cement through which the bolt is attached to the rock mass (Moosavi and Grayeli, 2006). In this study, for physical and numerical purposes, rock-bolts are assumed to be a linear spring connecting two fixed points in the numerical mesh (see chapter 2), and the cement bonding strength is ignored. A spring can endure purely elastic strain along its full length to some extent before it becomes permanently plastic. The ability of the spring to undergo elastic deformation depends on its stiffness (eq 12).

It is reasonable to conduct our study using DDA spring-like rock-bolt for three major reasons:

1) Rock-bolts are generally made from metal, and thus have the elastic characteristic of a metal rod (similar to a spring). The elastic elongation of a metal depends on its Young's modulus, its cross section and length, and can be expressed by the elongation equation:

$$\Delta l = \frac{F * l_0}{E * A} \tag{13}$$

where E is the Yong's modulus, A is the metal cross section, F is the applied force and l_0 is the initial length. The constant (EA/l_o) is in fact the stiffness of the bolt.

2) Rock-bolts in rock-burst prone areas need to sustain high deformation including the ability to resist high loads. The DDA rock-bolt feature, which is a pure spring, has limitless load/strain capacity.

3) The DDA rock-bolts are easy to handle and analyze.

In this study we use load and energy approach for our analysis. To derive the spring energy, we use Hooke's law. The one-dimensional spring stiffness is given by:

$$k = \frac{F}{\Delta l} \tag{14}$$

where F is the force acting on the spring and Δl is the spring extension (elongation). The spring energy due to elongation is given by:

$$U_{spring} = \frac{1}{2} k \Delta l^2 \tag{15}$$

Substituting equation 12 into 13 we get:

$$U_{spring} = \frac{F^2}{2k} \tag{16}$$

Note that the spring energy is inversely proportional to the spring stiffness. For an elastic rod with a cross sectional area *A*, the stiffness is:

$$k = \frac{EA}{l} \tag{17}$$

where E is Young's modulus and l is the rod length. By considering the cross sectional area, we can now revert to stress and strain instead of force and elongation. The energy per unit volume in terms of stresses and strains is given by integration on the stress-strain curve:

$$U_{rod} = \int_{\epsilon_0}^{\varepsilon} \sigma(\varepsilon)\, d\varepsilon = \int_{\epsilon_0}^{\varepsilon} E\epsilon\, d\varepsilon = E\, \frac{\varepsilon^2}{2} = \frac{\sigma^2}{2E} \tag{18}$$

substituting equation 15 to 16 we get:

$$U_{rod} = \frac{\sigma^2 A}{2kl} \tag{19}$$

by multiplying the rod volume, we get the total rod energy over its volume:

$$U_{rod} = \frac{\sigma^2 A^2}{2k} \tag{20}$$

As would be expected, the rod energy is inversely proportional to the rod stiffness as in the one-dimension case. This basic principle is graphically illustrated in Figure 2-4.

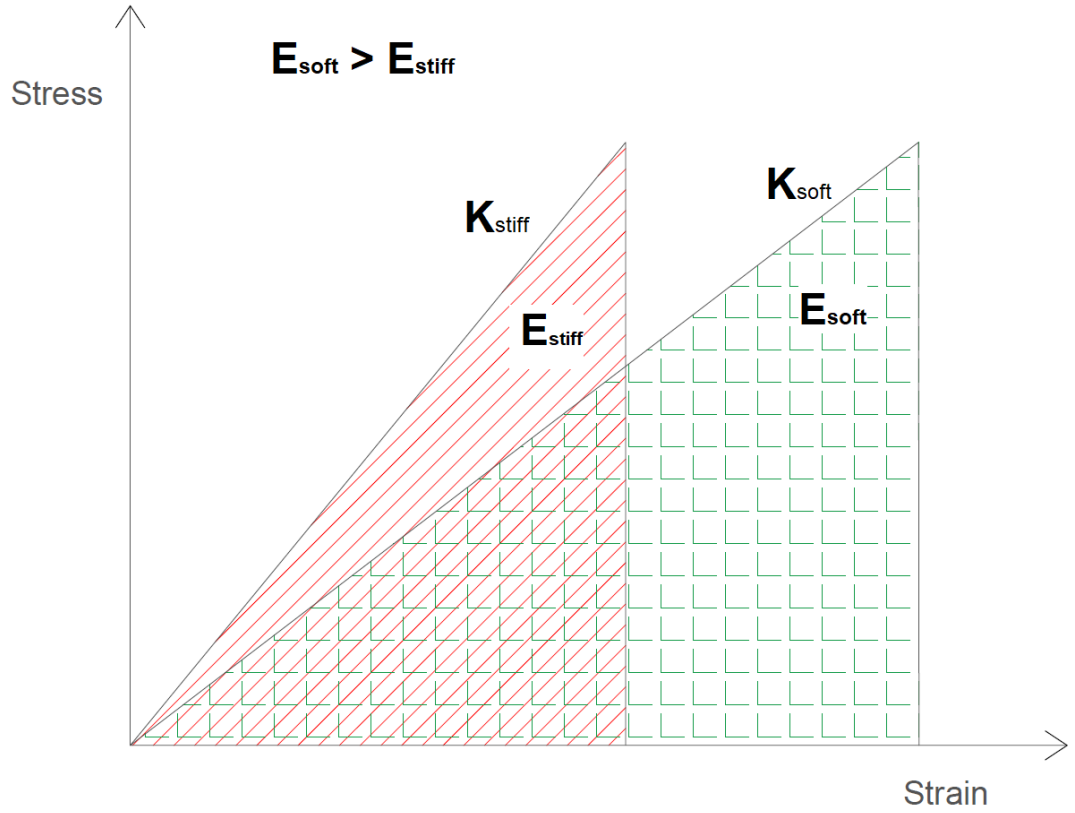

Figure 2-4: Schematic image of energy absorption in different bolt stiffness for a given constant stress. It is noticeable that low stiffness bolt absorb more energy when loaded.

User-defined numerical control parameters in DDA

The numerical control parameters required to define an input in DDA are:

1) k_{01} - is the dynamic control parameter. There are few mechanisms that consume energy in DDA. Because we are dealing with a first order approximation, all blocks are assumed homogeneous, so energy can dissipate only by linear elastic deformation of the blocks or through shear along the pre-existing discontinuities. In the original DDA 'artificial' energy loss does not exist, although it is reasonably needed, because energy can be lost due to heat generation, and inelastic deformation (breaking blocks corners, plastic deformation, etc.) that are part of rock systems deformation. Analysis that ignores such considerations will exaggerate prediction of deformation. Laboratory research done by comparison of DDA dynamic results to shaking table experiments (Tsesarsky et al., 2002) suggests 2 % damping to be realistic for dynamic simulations.

2) g_0 – the contact spring stiffness, also expressed as "k", in order to minimize penetration and tension. The g_0 is a parameter that has a large effect on the results of the analysis, therefore, it must be selected carefully. If possible, it should be selected by comparing the DDA results to an existing analytical solution, and preforming iterations until a satisfying agreement is obtained. According to the DDA user manual (Shi, 1996), a suitable value for g_0 is $E * L$, where E is Young's modulus and L is the average diameter of a block in the analyzed domain.

3) g_1 - the time step interval. This factor is the duration of the time step. It maintains a large influence on the accuracy and the efficiency of the analysis. There is no precise method to determine this number, therefore previous experiences in numeric analysis and geological engineering experiences in real world problem behavior are required. One way to asses this parameter in DDA is to examine the number of iterations per each time step required for convergence until the simultaneous equations satisfy the condition of no tension and no penetration in all contacts. Each trial to fit such a solution is one iteration. A high number of iterations indicates inappropriate time step length (a reasonable number should be less than four). This number should be small enough to guarantee infinitesimal displacements at each time step. Attentive and educated selection of $g1$ value will ensure both high efficiency and high accuracy of the numerical solution.

4) g_2 – the assumed maximum displacement per time step ratio, a dimensionless quantity related to the size of the model. It is used to find possible contacts between blocks, and it should be small enough to ensure infinitesimal displacement in each time step, and the convergence of the solution. Maximum displacement factor ($g2$) given by:

$$\delta_{max} = 2 * g_2 * y \tag{21}$$

where δ_{max} is the maximum displacement in each time step and y is the domain length in the Y axis.

2.2: DDA modification and improvements

The DDA code used in this research is an enhanced version of the original code developed by Shi (1993). The DDA method has developed extensively along the years. Since its first publication in 1988, many modifications and developments have been introduced including high order approximation (Doolin and Sitar, 2004), sequential excavation (Tal et al., 2014), coupled rock-mass and rock-bolt interaction during tunnel excavation (Moosavi and Grayeli, 2006). Typical applications that use such enhancements include dynamic simulations like earthquake effects on masonry structures and blasting effects on tunnels (Kamai and Hatzor, 2008; Yagoda-Biran and Hatzor, 2010; Zelig et al., 2015), and even the solution of water flow problems (Kim et al., 1999). The code was designed to handle different applications focusing mainly on tunneling, slope failure, failure behavior of joints, fracturing and fragmentation processes of geological and structural materials, and earthquake effects. In this research, we will focus on dynamic behavior of the mass and its influence on the support system using two recent DDA enhancements.

New viscous boundary condition in DDA

One of the problems that arises when running a dynamic analysis is the finite distance of the model domain. Since DDA uses fixed frame boundaries, the energy does not dissipate as it does in real life, but reflects from the boundaries, thus producing errors to the simulation results. One way to deal with this problem is to introduce non-reflective boundary conditions. Non-reflective boundaries are sets of viscous energy equations that have the ability to absorb the energy that reaches the edge of the model domain. This process if effective because DDA is based on a minimum energy principle. The derivatives of the energy component are added easily to the stiffness matrices $[k]$.

Bao et al. (2012) used an analytical solution proposed by Lysmer and Kuhlemeyer (1969) to implement a new viscous boundary submatrix with high absorbing efficiency for the DDA method, thus constructing a viscous boundary condition in the model. The method to set a viscous boundary condition is based on independent dashpots in the normal and tangential direction of the model domain boundaries. Each block in the boundaries has two pairs of dashpots. The dashpots can absorb and dampen the velocity energy arriving to the

boundary domain. In their work, Bao el al. (2012) showed the high performance of the model in handling both P-wave and S-wave propagation problems. The viscous boundary sub-matrices consist of derivatives of potential energy components that are stored in the boundary dashpot. The potential energy in a dashpot must equal the work of the reacting force in the dashpot. For each single time step the viscous force in the dashpot is assumed to be proportional to the velocity of the dashpot at the attaching point.

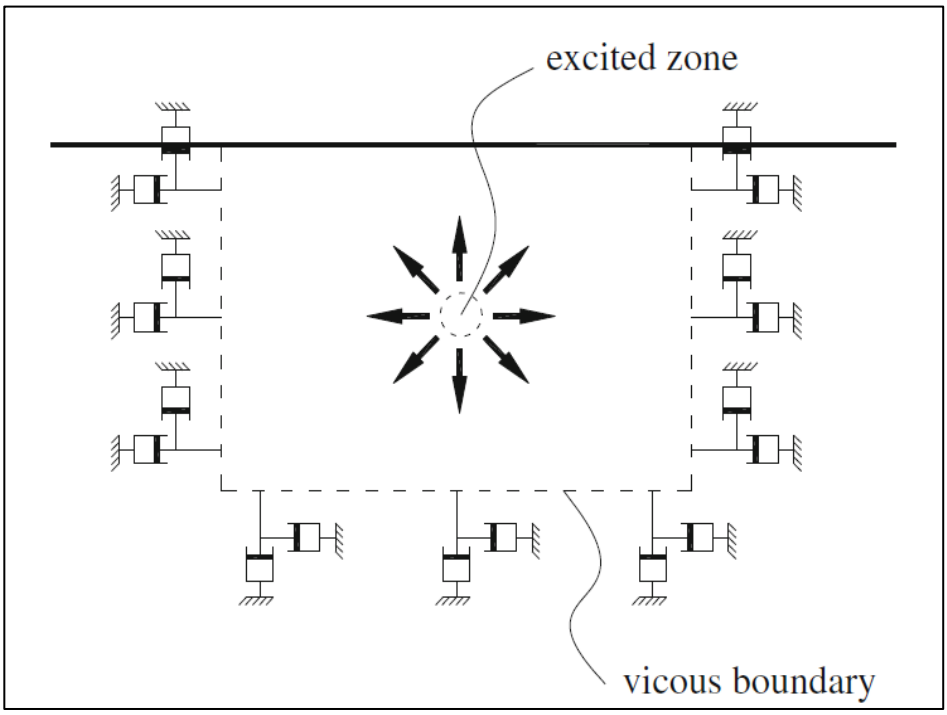

Figure 2-5: Concept of viscous non-reflective boundaries in DDA (Bao et al, 2012)

The non-reflective boundary condition of Bao el al. (2012) involves infinitesimal dashpots oriented normal and tangential to the boundary. The resistance forces of the dashpots are:

$$F_n = -a\rho V_p v_n l_0 \tag{22}$$

$$F_t = -a\rho V_s v_t l_0 \tag{23}$$

where l_0 is the length of the boundary to which the dashpot are attached, ρ is the unit mass, V_p and V_s are the velocities of P-wave and S-wave in the material of the boundary, v_n and

v_t are the velocities of the boundary block, and α is a dimensionless parameter related to the incident angle. The characteristic *P* and *S* wave velocities for a material are:

$$V_p = \sqrt{\frac{E(1-\upsilon)}{\rho(1+\upsilon)(1-2\upsilon)}} \tag{24}$$

$$V_s = \sqrt{\frac{E}{2\rho(1+\upsilon)}} \tag{25}$$

where E, υ are the material's Young's modulus and Poisson's ratio respectively. Finally, to use the formula in a DDA Cartesian coordinate system, the following transformation is used:

$$v_n = v_x \sin\alpha - v_y \cos\alpha \tag{26}$$

$$v_t = v_x \cos\alpha + v_y \sin\alpha \tag{27}$$

Where α is the direction angle of the boundary edge corresponding to x-axis; v_x and v_y are the block velocities in the x and y directions, respectively.

New sequential excavation capability in DDA

DDA-R is a development of the original DDA code made by Yuval Tal in his M. Sc. studies at Ben-Gurion University (Tal et al., 2014). DDA-R significantly improves simulation modeling, including rock-bursts. When DDA was first released, the cavity, or the excavation, was included in the mesh from the beginning of the analysis. However, when running a simulation without letting the interactions between all the blocks achieve stress equilibrium, errors were produced in terms of wrong stress-strain build-up and friction mobilization. Excavation sequence, or Gravity Turn On, can be compared to the process of geological burial during which elastic strain is stored in the block system before the tunnel is created. During that stage all block contacts are allowed to "set" until the correct stress state is developed everywhere in the modeled domain, only then is the opening space removed from the mesh. This enhancement makes DDA-R analysis more accurate where the role of initial stresses in the modeled domain is an important issue. Moreover, frictional

resistance between blocks is governed by the friction coefficient and the magnitude of the normal stress acting on the joints. If the stresses are not allowed to fully develop in the analyzed domain before the excavation is removed, access displacements will be computed because of lower than actual frictional resistance in the modeled domain. The modified DDA code contains two stages:

(1) At the beginning of the simulation, one or several temporary blocks are placed in the future tunnel excavation space. A static simulation ($K_{01} = 0$) is executed until equilibrium is attained everywhere in the modeled domain.

(2) The temporary block(s) are removed either at once or gradually, to simulate the sequence of tunnel excavation. A dynamic simulation is executed ($K_{01} = 1$).

Blast modeling in DDA

The use of explosives in hard rock tunneling is very common due to their efficiency and low price, in comparison with other excavation methods. In the drill and blast method, small diameter holes are drilled in the tunnel face in a specific pattern (ISEE Blaster's Handbook, 2011), after which explosive charges are inserted into the holes. When the blast occurs, the high pressure of the expanding gases breaks the rock to small fragments. Later, when the support system installation is complete, new holes are drilled to continue the tunneling process. Blasting is an operation that produces a large amount of energy during a short time period. The energy is released in two forms: via stress waves, and pressurized gases. Previous research has shown that in hard rock, like granite gneiss, only $10 - 18$ % of the energy released is in the form of stress waves. In soft rock, like salt, that number is much lower and can diminish to ~ 2 % (Kutter and Fairhurst, 1971). The remaining energy in both hard and soft rocks expands in the form of highly pressurized gas. The blast penetration through the rock mass depends on blast chamber volume and time; other parameters that affect the penetration are the blast angle, location, rock type, number and orientation of discontinuities, and the surrounding pressure.

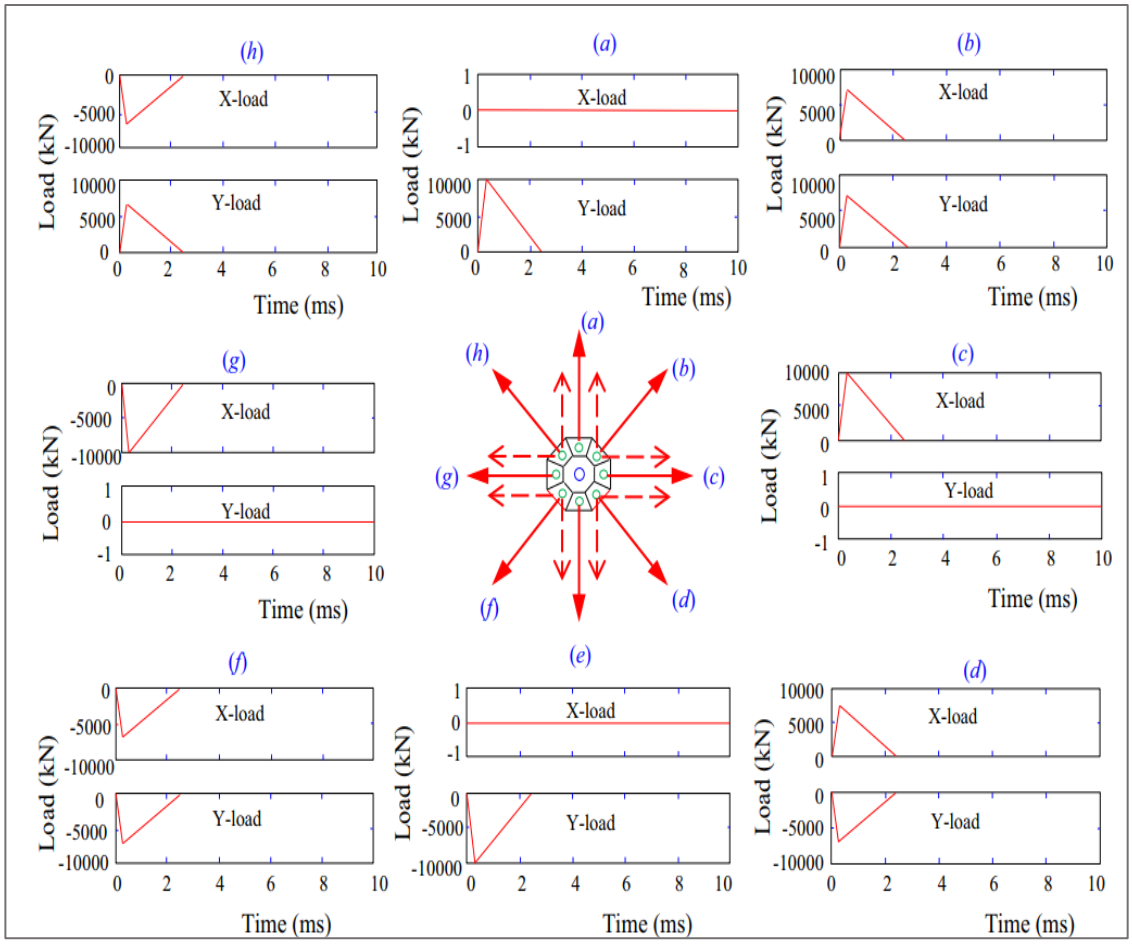

Figure 2-6: The blast model and time history of the blast function by direction invented by Zelig et al., in order to create radial load each load point recive specified loads in the X and Y axes when the net results pointed radialy (Zelig, 2015)

In the original DDA code, a blast option does not exist. To simulate such blast Zelig et al. (2015) developed a new blast option based on special geometry and the usage of DDA loading points arranged in a specific manner. Several assumptions were made: 1) the blast is an adiabatic process with no energy converted to heat, 2) the gas produces equal radial pressure in all directions. The geometry of the proposed blast option is shown in Figure 2-6. In the figure, an octagon shape comprised of eight blocks is arranged around a hole point. In DDA, a hole point set inside a block, implies that this block will be removed at the beginning of the simulation. The outer edge of each block is $1\,m$ in length and at the centroid of each polygon there is a load point. Each load point produces a time dependent force vector, with respect to the radial direction. The force function produces a load based

on a linearization of typical blast stress function comprised from two phases. The final outcome is a stress of 10 MPa radiating in a normal direction from each edge.

Mesh construction using AutoCAD software

The original DDA software package consists of four programs (Shi 1996):

1) The line-generating program DDA Lines (dl) generates lines representing joints, the boundary of the joint domain, and perimeter tunnels. The line representing joints can be generated statistically.

2) The block generating program DDA cut (dc), generates the block system by forming all possible blocks from individual line segments.

3) The analysis program DDA forward (df), performs the DDA forward static or dynamic analysis of a block system. The system of simultaneous equilibrium equations formulated in DDA are solved by either a direct method with non-zero storage or a successive over-relaxation (SOR) iteration method.

4) The graphic output program DDA Graph (dg) is a graphic post-processor, which produces graphic output on the screen and postscript files for printing.

The AutoCAD software package is beneficial in the process of block cutting in complex mesh. In order to produce a precise medium, we used AutoCAD to create all of the geometry elements that compose our problem: tunnel, rock bolt, absorbing boundary etc. The modeling of multi-block structure in 2D-DDA is based on augmentation made by (Yagoda-Biran, 2008) . The steps for constructing a mesh in the 2D-DDA using AutoCAD are described briefly in Figure 2-7.

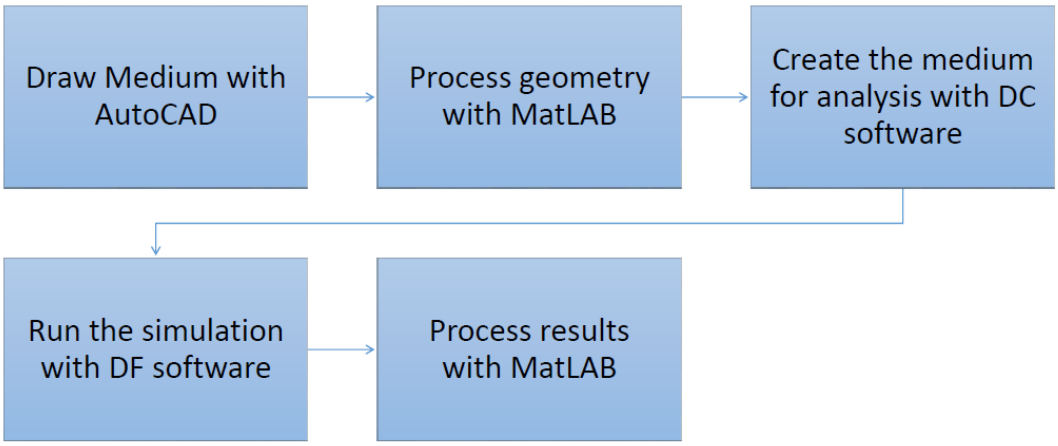

Figure 2-7: The complete process of conducting simulation in the DDA model

After drawing the analysis geometry, we export the data file and process it in the MatLAB software package. Later, we use the DC software to generate the medium for the simulation, and finally we use DF software to run the simulation. The MATLAB code that reads the Excel file, sorts the file, and writes an input file for program "DC" is provided in Appendix A.

2.3: The RMR rock mass classification and adjustment to DDA

RMR is an observational method used for rock mass rating. It was developed by Bieniawski (1976), based on his personal experience in rock tunneling projects. Over the years, the method underwent several improvements, the most important of which occurred in 1989 (Bieniawski, 1989). The method is characterized by simplicity and applicability to various rock masses, and its ability to assess the expected stand-up time and the required support load. RMR method is based on five parameters:

- Uniaxial compressive strength (UCS)
- Average spacing between joints (RQD)
- Joints condition (length, persistence, roughness, alteration)
- Groundwater condition
- Joint orientation

Each parameter receives a value based on its influence for tunnel stability. The sum of the value ranges between $0 - 100$. Bieniawski defined 5 ranges to determine rock mass condition:

- RMR < 20 very poor
- RMR <20-40 poor rock
- RMR 40-60 fair rock
- RMR 60-80 good rock
- RMR 80-100 very good rock

For each range he also defined a support recommendation and stand-up time for the tunnel top (Figure 2-8). Today, the RMR method is well accepted and is widely implemented by engineering geologists. Thus, it is beneficial to combine RMR with DDA in our recommendation for rock support in rock-burst prone areas.

In this thesis, we use RMR to derive parameters for DDA based on He et al., (2016) work. He et al. (2016) established correlation based on their experience in rock engineering. We use the correlation here by inserting it as DDA parameters based on the rock mass condition we want to analyze. Although He et al. (2016) defined a specific friction angle to each RMR we set the friction angle to the value of 65 degrees. This decision was made in order to set a friction angle higher than the dip inclination angle, which was set to 60 degrees for all the simulations, thus controlling the displacements and avoiding sliding not associated with strain relaxation.

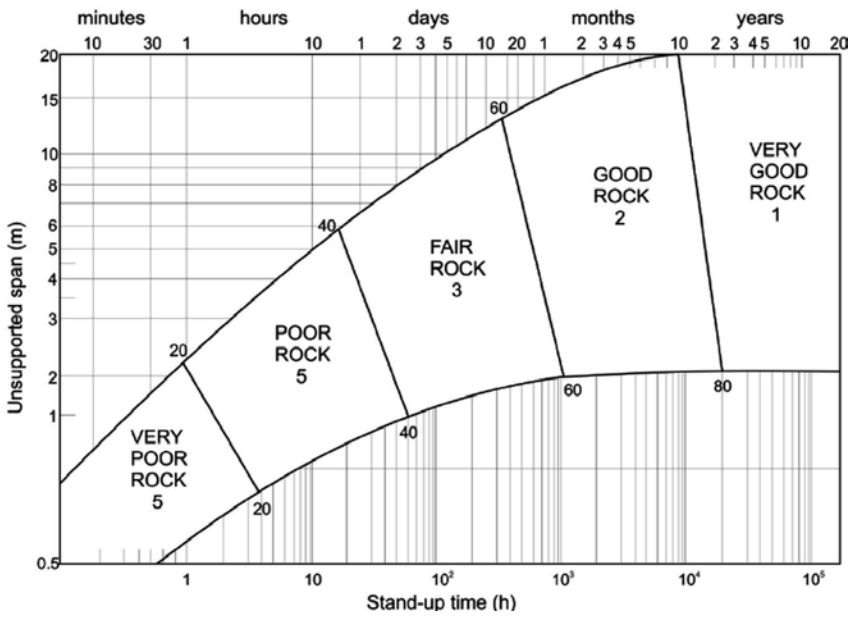

Figure 2-8: The stand-up time of tunnel top as predicted by RMR (Bieniawski, 1989)

Table 2-1: RMR-DDA CORRELATION TABLE

RMR Rating	***Space between discontinuities*** (m)	***Young's modulus*** (GPa)	***Poisson's ratio***	***Friction angle***
65	1	30	0.20	65^o
75	1.5	50	0.21	65^o
85	2.5	70	0.22	65^o
95	5	90	0.23	65^o

Chapter 3 : 'Drop Test' Simulation

Rock-bolts are efficient and economical tool to mitigate rock-burst hazards. They were employed for many years to counter rock-burst risk (Kaiser, 1996). Dynamic tests to examine rock-bolts behavior during such an event are well documented (Hadjigeorgiou and Potvin, 2011; Ortlepp, 1969; Potvin et al., 2010). Hadjigeorgiou and Potvin (2011) mentioned four main types of dynamic rock-bolt tests, including:

1) Simulated large scale experiments by means of blasting.

2) Drop test facilities which apply an impact load on a rock bolt inside a grouted tube.

3) Laboratory tests applying dynamic loads on a core sample.

4) Field monitoring and back analysis of case studies.

In this chapter, we simulated a numerical 'drop test' with DDA. The ‘drop test’ is a laboratory-based test, which delivers kinetic energy to an isolated grouted rock-bolt via sudden loading. This sudden loading is caused by a mass dropped from a fixed height (see Li experiment, Figure 1-4). We use DDA to simulate a ‘drop test’ and study the following issues:

1) The DDA time-step interval parameter.
2) The role of rock-bolt stiffness.
3) Simulation of two bolt system with different time steps to calibrate the preferred stiffness.

3.1: Results of drop test simulation with DDA

This section consists of three simulations with the same geometric configuration. First, we conducted a quasi-static 'drop test' and tested the influence of DDA time step interval g_2 on the simulation results. Next, we checked the performance of the DDA bolt with emphasis on its stiffness. Finally, we studied the behavior of a two rock-bolt system during a 'drop test' and calibrated the correct stiffness value for the next chapters.

Model geometry and mechanical properties

To construct a 'drop test' in the DDA model we used two blocks, one fixed to its position with four fixed points and the other free to move downward due to gravitational / external force. The load of the block due to its self-weight is:

$$W_{block} = m * g * A \tag{28}$$

where m is the block mass per unit area, g is gravity acceleration constant and A is the block area. The blocks are connected using the original bolt connection in DDA. The bolt stiffness for the three simulations are summarized in Table 3-1. In the second simulation we chose very high stiffness values just for saving CPU running time and convenience in showing the results. Because the bolt is one-dimensional, the Young's modulus and the cross section were merged to fixed values. The simulations were conducted with no damping where $k_{01} = 1$. In the dynamic part of the second simulation, gravity is not activated, instead a point load is applied with a vertical force of 250 kN for five seconds from the block center of mass. Figure 3-3 shows the load function input.

The third simulation used the same configuration of the previous simulations with two exceptions: 1) we used two rock-bolts with different stiffness values, the distance between each bolt to the center of the mass is 4 m. 2) we used bigger blocks, which allowed us to visually notice the uneven deformation of the two bolts.

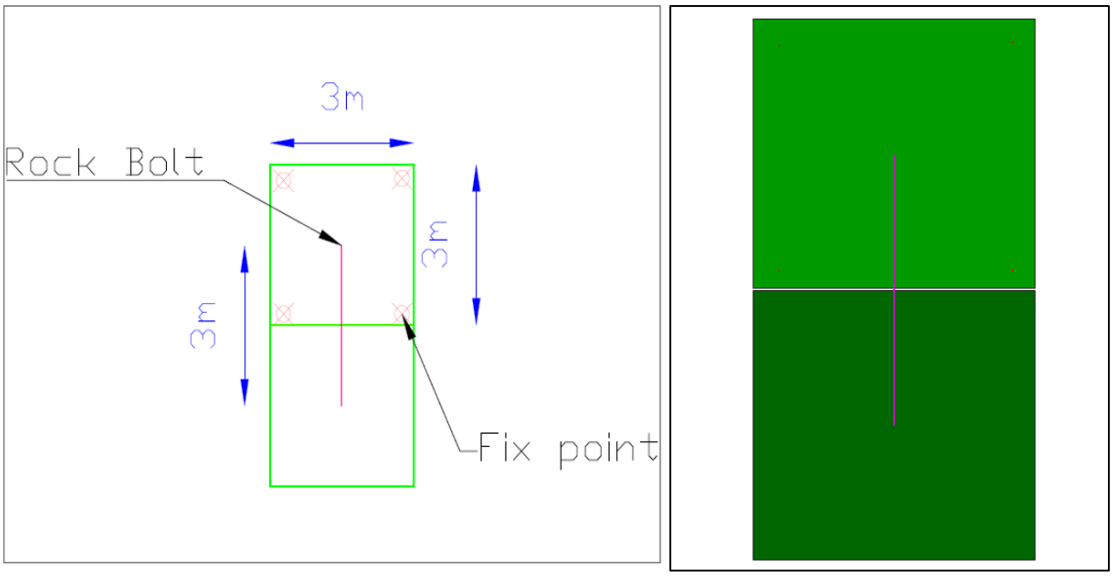

Figure 3-1: The geometric configuration of the static and dynamic 'Drop test' simulations. AutoCAD sketch (left) and the DDA-DC output (right)

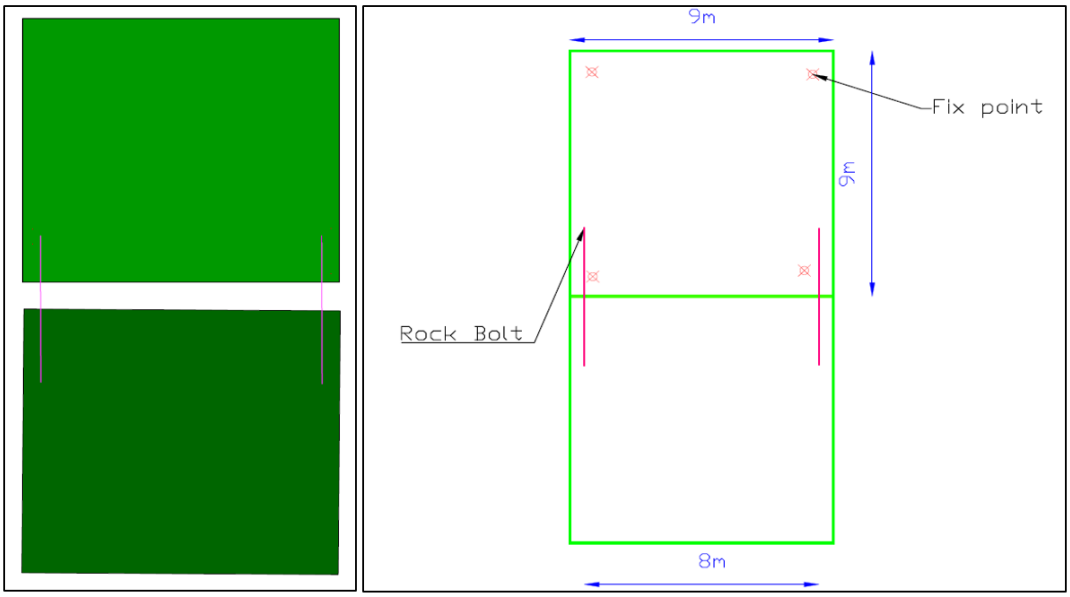

Figure 3-2: The geometric configuration of the System of two bolts 'Drop test'

Table 3-1: THE PARAMETERS FOR THE 'DROP TEST' SIMULATION

	first simulation	*second simulation*	*third simulation*
number of bolts	1	1	2
length (m)	3	3	3
stiffness tested (MN/m)	8	100 500 1500	250 25
block weight (KN)	*225*	225 (static) 0 (dynamic)	1000
Bolt frequency (Hz)	*18.9*	66.7 149.1 258.2	50 15.8

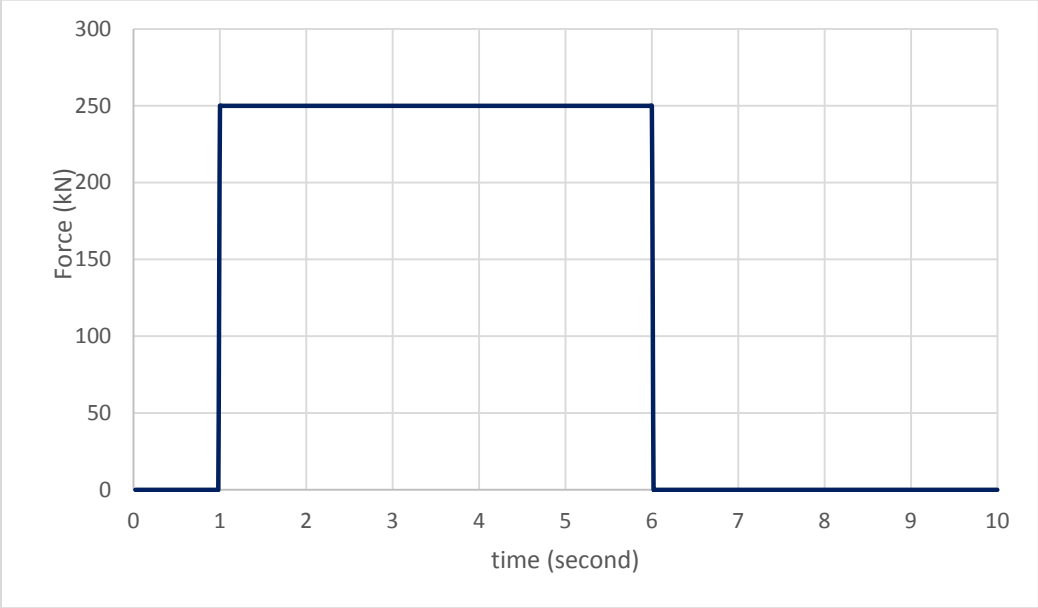

Figure 3-3: The load function of the dynamic simulation, the load is increased abruplly to give the block high initial velocity

Time step interval

In the first simulation we studied the influence of the time step interval on the bolt force as computed with DDA. The results are shown in Figure 3-4. We note high variations between the tested values. Time step interval values shorter than 10^{-3} s did not converge to the expected block weight value, even for an extremely long simulation period of 25 $seconds$. A simple harmonic motion (SHM) of the rock-bolt force continued with minimal damping until the end of the simulation. The only time interval that showed substantial convergence was of 10^{-3} s. The bolt load record displayed more than 93 % convergence to the external force applied after 25 seconds. These results are related to the DDA numerical "algorithmic" damping and will be discussed later in this chapter, but they clearly show the sensitivity of the bolt force calculation to the specified time interval. In dynamic events such as rock bursts, where most of the deformation takes place over a span of several milliseconds, this could pose a great difficulty in capturing the correct force – displacement function of the bolt with DDA.

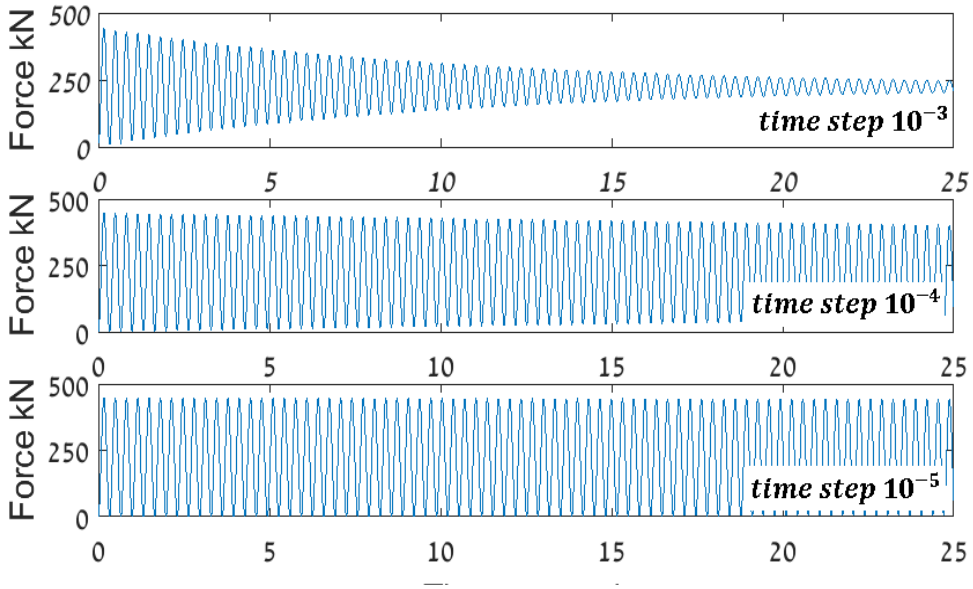

Figure 3-4: Force time history for different time step interval. The allgoritmic damping is dominant only in the high duration time step of 10^{-3} *and negligible in shorter durations*

Bolt stiffness effect – static loading

Under static loading the rock-bolt carries only the block self-weight, in this case $225\ kN$. Figure 3-5 (top) shows the rock-bolt force evolution (colored) compared to the static load (black line); with all bolt stiffness values tested the bolt forces converge to the expected load of the block due to its self-weight. Convergence however, clearly improved with increasing bolt stiffness. It took 2 seconds for convergence with bolt stiffness of $1500\ MN/m$, while stiffness of $100\ MN/m$ and $500\ MN/m$ did not converge even after 2.5 seconds of simulation duration. The energy of the bolts as a function of stiffness is shown in Figure 3-5 (bottom). Since the simulation time is constrained to $2.5\ seconds$, we cannot see the final energy values for softer stiffness which are 50 and $253\ kJ$ for 500 and $100\ MN/m$ respectively. In the end, however, the results of the simulation are equal to the results of the analytical solution.

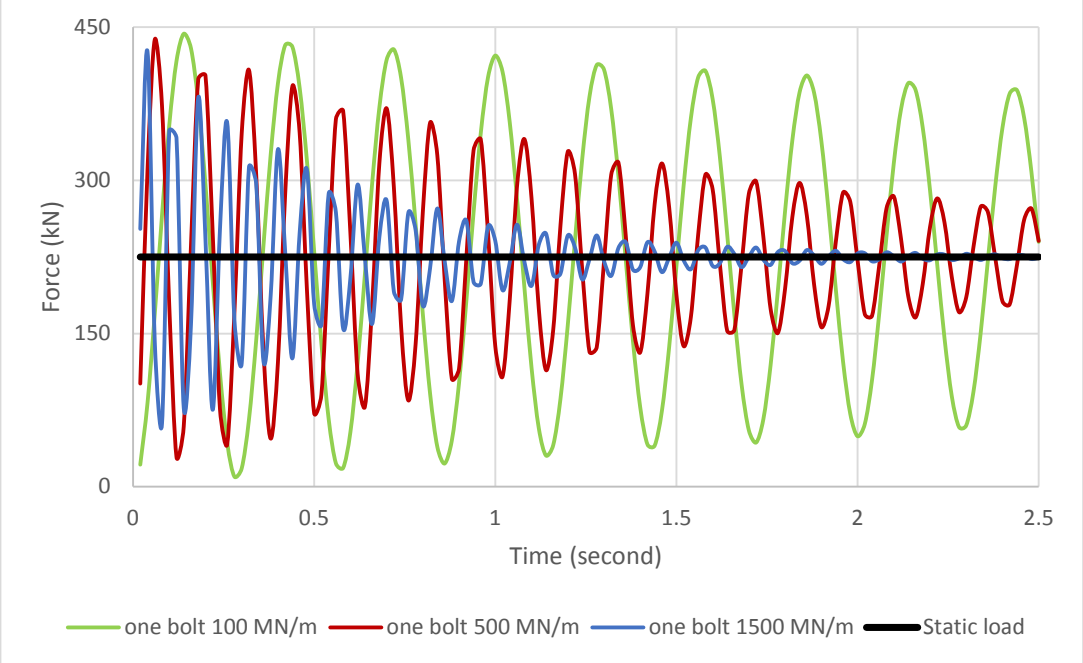

Figure 3.5 (a)

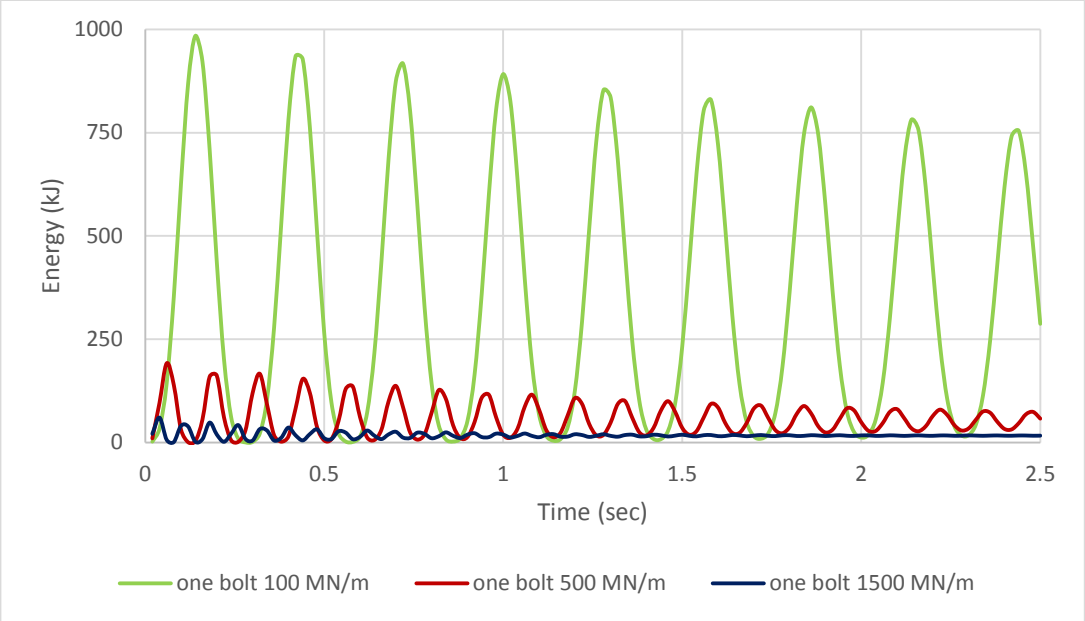

Figure 3.5 (b)

Figure 3-5: Time history of bolt load (a) and energy (b) for static loading condition. The results show the influence of the stiffness in the algoritmic damping process and the influence of energy absorption.

Dynamic load tests

In the second part of the second simulation the bolt was subjected to a dynamic load. A load point rapidly exerts constant load of $250\ kN$ for $5\ second$ as shown in Figure 3-3. From the time history of the bolt load (Figure 3-6) we can detect 3 phases. The first phase $(0-1\ sec)$ shows zero force because the simulation was taken under zero gravity condition. In the second phase $(1-6\ sec)$, during which the load function is applied, the force rapidly increases to **twice** the excreted load, similar to the static simulation. The stiffest bolt exhibits oscillations for two seconds until reaching equilibrium, while the force in the two softer bolts continues to oscillate throughout the duration of loading. Similarly, when the external load was reduced to zero the stiff bolt force converged to zero as well, whereas the forces in the two softer bolts continued to oscillate. The dynamic behavior we received is similar to the static simulations. Namely, the performance of the original bolt connection in DDA is not influenced by the loading velocity but by the magnitude of the applied load.

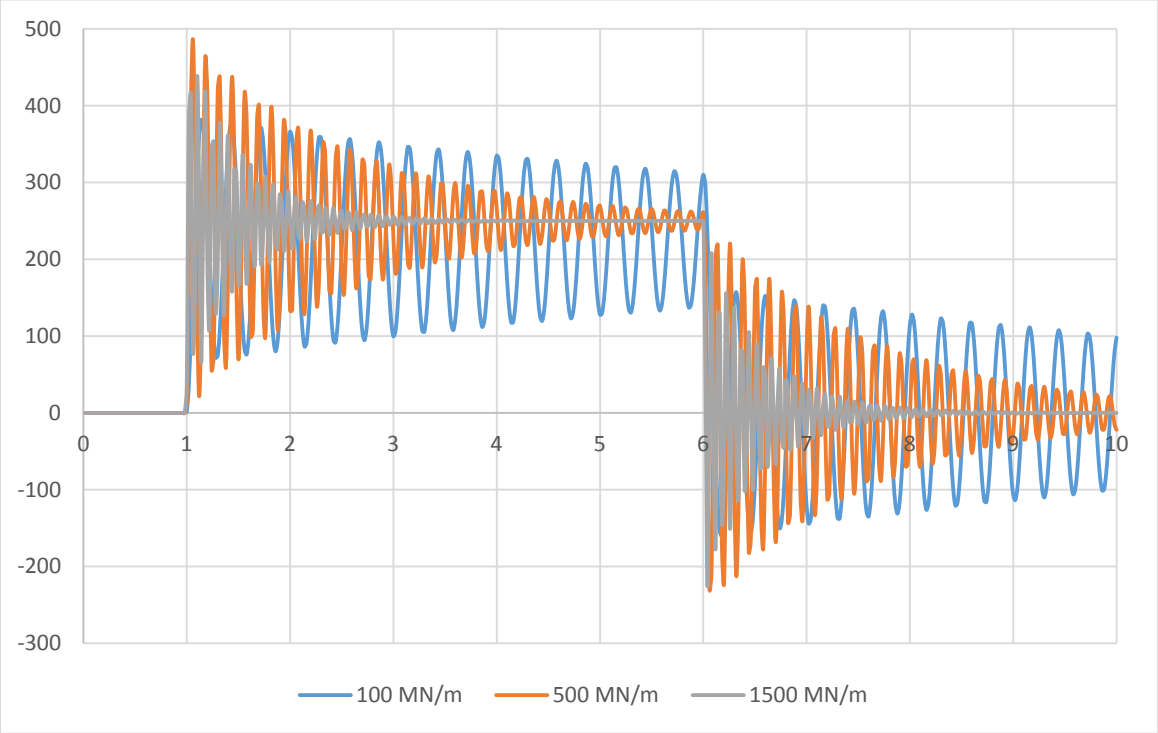

Figure 3-6: Time history of bolt load in dynamically loading condition

Two-bolt system

In this simulation we wish to see what will be the load distribution when two bolts, with different stiffnesses are supporting a single block. The load distribution (Figure 3-7) indicates that after the convergence the load will equally distribute between the two bolts. A rotation angle of 2^o is created between the horizontal line and the hanging block, implying that the displacement does not spread equally between the two bolts. The load in each rock-bolt in the end of the simulation, however, was $1000\ kN$, which is half the total weight of $2000\ kN$. Therefore, the energy of the softer bolt will be higher than the stiff bolts due to the longer extension of the softer bolt. Here we obtained values of $2\ kJ$ versus $20\ kJ$ for the stiff and soft bolt, respectively. The recorded strain of the stiff bolt is 0.4 %, while the recorded strain of the soft bolt is 4 %. The single order of magnitude difference is a direct result of the single of order of magnitude in the specified stiffness of each bolt.

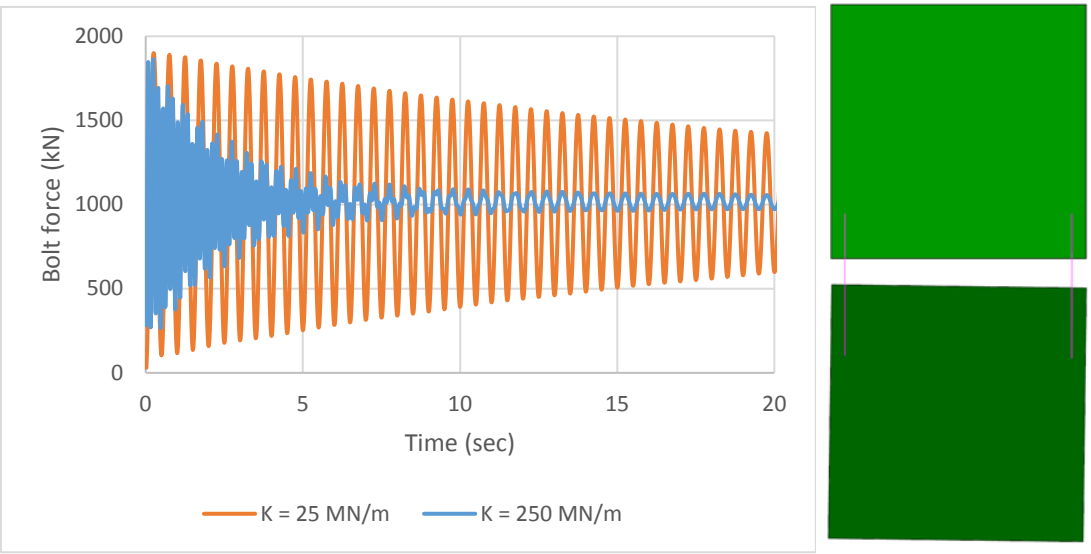

Figure 3-7: Force record of the two different rock bolts and the system after the simulation (left) and the graphic end results (right) note the rotate angle created due to the stiffness variation between the bolts

3.2: Discussion

Bolt stiffness and time step interval

Simulated 'drop tests' are an important means to explore the performance of DDA bolt application. This experimental procedure is both physically and numerically efficient to understanding bolt behavior. The first and second simulations were aimed to clarify the time-step interval and bolt stiffness role on DDA results. Three time-step interval values $[10^{-3}, 10^{-4}, 10^{-5}]$ s were examined. The results suggest that only simulations with relatively large time step of 10^{-3} s converge to the value of the external load within the simulation time duration. The bolt force recorded in the two shorter time step values exhibits a simple harmonic motion, without convergence. These results impose constraints on our study because realistic and practical DDA simulations of rock-burst events require a short time step duration. Regarding bolt stiffness, only the high value of 1,500 MN/m allowed the system to converge in less than two seconds. However, this stiffness is not practical for our research because it does not correspond to realistic rock bolts values which are typically less than 25 MN/m.

Bolt convergence is obtained in DDA through numeric damping (algorithmic damping) that depends on bolt stiffness and time step interval. The numeric damping is implemented in the code to eliminate Simple Harmonic Motions (SHM). Ohnishi et al. (2006) conducted simulations of a mass connected to a fixed body by a linear spring. The analytical solution of such a problem should be in the form of:

$$x = A * \sin \omega t + \phi \tag{29}$$

where x is the spring displacement, A is the amplitude, ϕ is the phase and ω is the angular frequency:

$$\omega = \sqrt{\frac{k}{M}} \tag{30}$$

where k is the spring stiffness and M is the mass.

From equation 27 we can see that the analytical solution does not need to converge and in fact will oscillate endlessly. In the DDA code the SHM is diminished by the algorithmic damping via the 'coefficient of algorithmic damping' λ which is a function of the spring stiffness and time interval (Zhang and Wu, 2003). The spring total energy T_E between two time steps can be shown as follow:

$$T_E = \frac{E_0}{e^{\lambda t}} \tag{31}$$

where E_0 is the initial total energy and t is the simulation running time. From this equation we can see that when the time step interval is high the SHM will exponentially decay faster. The same condition applies for the stiffness as the parameter λ is proportional to it.

Dynamic vs static simulation

We did not find significant difference between the results of static and the dynamic loading. Moreover, the initial velocity does not appear to hold high importance. This could be attributed to the intrinsic behavior of a pure spring. When a spring is subjected to load and has the kinematic freedom to move it will elongate to the maximum length possible, satisfying Hook's law, no matter which loading mechanism is applied, or the mean velocity of the block. The bolt will reach maximum elongation before the resisting force is fully

developed. This has to be taken into consideration when attempting to analyze rock bolt performance with DDA during simulated rock burst deformation.

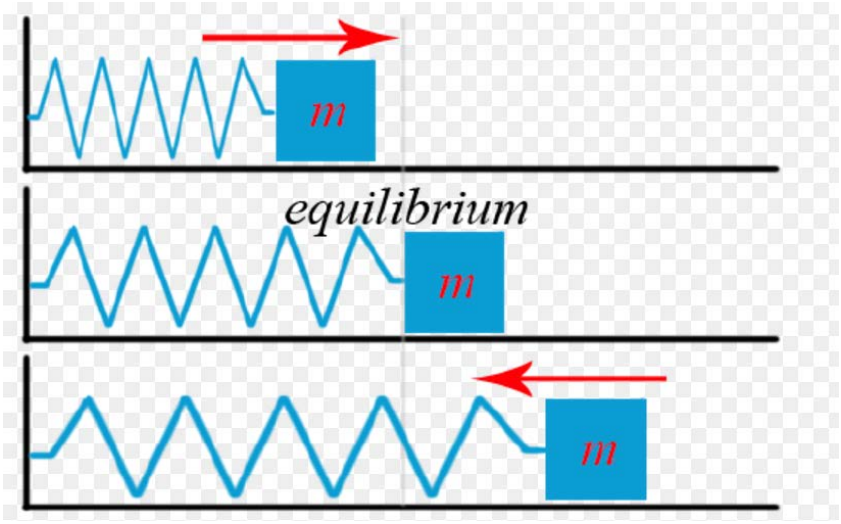

Figure 3-8 illustration of the three phases of harmonic motion

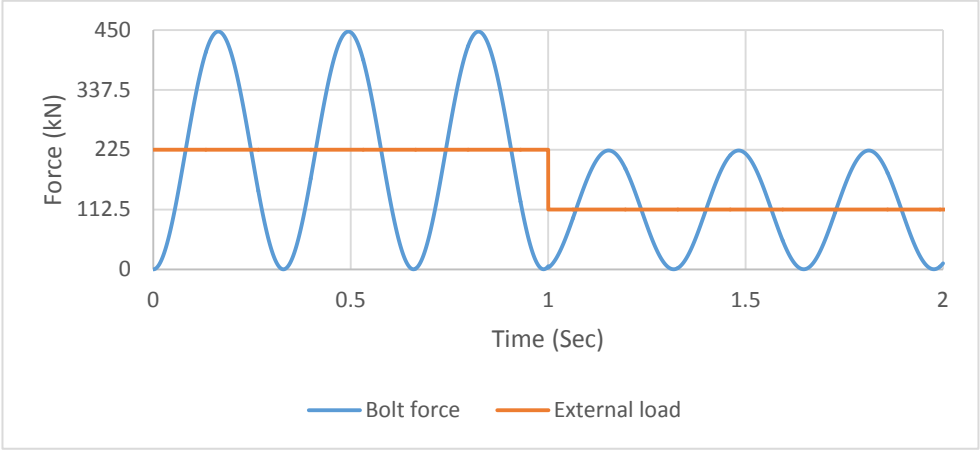

Figure 3-9: Example of the behavior of a spring system, including three phases: negative, equilibrium, and positive (see Figure 3-8). This example was based on the geometry of the second simulation and a stiffness of 100 MN/m. The given external load cycle was 225 kN until 1 second and then reduced to zero. Given a positive external force, the bolt force was twice the amount of the external load in the positive phase and zero in the negative phase. This behavior occurs because of the SHM of a spring in DDA.

Bolt stiffness optimization

The results of the two bolt system showed that stiff rock-bolts absorbed less energy than softer rock-bolts, as is expected from the analytical solution. The softer bolt will elongate

more than the stiffer bolt and a rotation of the block will take place. Because rock-bolts under rock-burst condition endure high deformation and high energy absorption, a stiffness value of 25 MN/m is assumed to be a suitable value for further analysis. This value correlates with a strain value of 4 % for 1000 kN of force, similar to the values reported for energy absorbing rock-bolts (He et al., 2014).

Limitation of the original DDA bolt connection

We found some limitations in using the original DDA bolt model that forced us to make certain assumptions while using the model. The linear one-dimensional behavior $f = kx$ is a simplification of what really occurs in the field. The one-dimensional behavior of the bolt constricts the elongation to only one axis, even though block displacement is two or three dimensional in most cases. The stiffness parameters E, A and l are assumed to be constant with time while the reality in the field is different (Yasar and Celik, 2002).

3.3: Conclusion

Although fast convergence of the SHM was present in the DDA bolt when using a large enough time step interval, realistic simulation of actual rock burst deformation requires a much shorter time step (He et al., 2016; Zelig et al., 2015). It was found that a time step interval of 10^{-5} was the most appropriate to generate rock-burst in DDA. Therefore, we needed to take into consideration the SHM in the results. The DDA bolt connection is load-based rather than velocity-based. It can absorb twice the amount of load in each cycle of oscillation and this constrained the dynamic ejection of blocks in the simulation Figure 3-8 and Figure 3-9. We found that a stiffness value of 25 MN/m produced the best properties in terms of energy, load and strain capacities.

Chapter 4 : Rock-bolt energy study

Developing a good support system based on rock-mass conditions is crucial to project safety and efficiency. Over the years several rock-bolt installation schemes have been suggested by researches around the world. The pioneering engineer, T.A Lang, suggested a set of rock bolt design guidelines concerning tunnel geometry and rock mass conditions. His guidelines, introducing the concept of Reinforce Rock Unit or RRU (Lang and Bischoff, 1982), suggest that every rock-bolt supports a certain rock volume and thus defines a reinforced 'unit' with specified perimeter. It is assumed that a shear radius is created around the rock bolt whereby the rock becomes stronger due to increasing shear resistance along the boundaries of the RRU. However, Lang's concept is not entirely accurate because it does not take into consideration discontinuities in the rock mass or impact dynamic load.

In the 1970's, based on rock mass rating methods, Barton et al., (1978), and later Bieniawski, (1989), separately suggested rock-bolt installation recommendations based on their empirical rock mass rating methods "Q" and "RMR" , respectively. The problem that arises by using those methods is that observational methods are not precise and rock rating can dramatically increase or decrease based on subjective-opinion. These methods also do not take into account dynamic loads.

DDA has also been employed in the study of rock bolt performance. Yeung (1993) was the first to conduct tunnel stability research using the DDA method. He studied the arching effect in underground excavations, which resulted due to the installation of rock bolts. Yeung found that rock bolt significantly affects the arching process because it holds the key blocks of the tunnel roof in place and increases frictional resistance along discontinuities in the rock-block system. Yeung also studied the effect of bolt density, and found that by increasing bolt density, multiple arches can develop in the roof of the tunnel (Figure 4-1), thus stabilizing the structure. Another research study on DDA rock-bolt features, conducted at Ben-Gurion University, by Tsesarsky and Hatzor (2009), examined the role of rock-bolt stiffness in stability of overhanging slopes. The study proposed installation recommendations based on slope parameters. Based on their work on columnar

basalt rock-mass in the Baihetan hydropower plant in China (Hatzor et al., 2015), were able to use DDA bolt feature to demonstrate that Lang's recommendations concerning rock bolt instillation were not valid in an anisotropic rock mass.

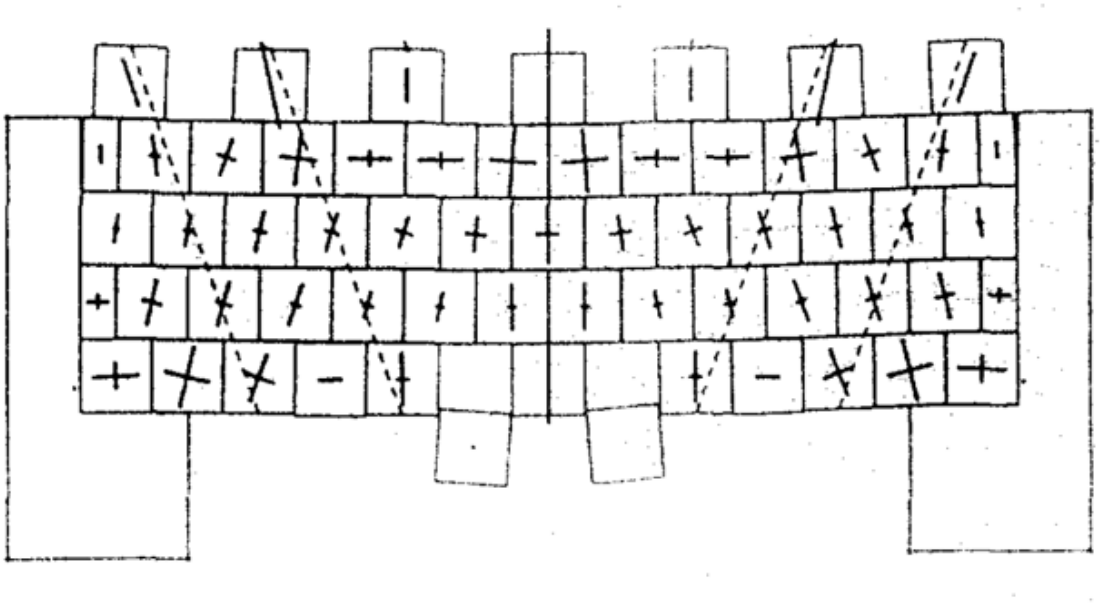

Figure 4-1: The results of Yeung (1993) simulation of rock-bolts functioning in tunneling using the DDA software, Yeung used radial orianted bolt and confirmd their success in stabilazing the structure by creating a stress arch.

It is also important to note that rock-bolts in overstressed environments are different from regular rock-bolts (Cai, 2013). When dealing with rock-burst prone rock-mass we should adopt an energy approach rather than a load approach. The primary objective of static support practice is to mobilize and conserve the inherent strength of the rock-mass in order for it to become self-supporting. However, this approach needs to be modified when considering rock-burst conditions, where absorbing impact load and allowing large deformation becomes the main task of the support system (Hagan et al., 2014).

In deep tunneling projects, a problem frequently arises in determining the exact shock energy that the rock-bolt will need to sustain, during a rock-burst event. Moreover, different rock-masses produce different shock impacts during rock bursting. Ortlepp, (1993) found that the load that developed on the support system depends on rock-mass condition. Damaged rock-masses can produce up to 30 kJ/m^2 with ejection velocities of

$3-8\,m/s$. Kaiser and Cai, (2013) estimated energy absorption value of $80\,kJ/m^2$ and ejection velocities in the order of $1\,m/s$.

In this chapter we study the role of rock-bolt using energy approach. In the first section, a single rock-bolt in high *in-situ* stress condition is tested and the effects of bolt length and stiffness on load, strain, and energy evolution are recorded. The second section extends the analysis to an array of rock-bolts around a circular tunnel and the effect of energy absorption by different array schemes is studied. In the third section, using the best results from the two previous sections, the energy absorption of an array of rock-bolts in varying rock masses is studied by using correlation between RMR and DDA parameters. The excavation sequence is simulated using Tal's sequential excavation enhancement in DDA. The removal of the tunnel occurs at a specific time after the start of the simulation and after the installation of the rock bolts. Figure 4-2 shows the evolution of rock burst occurrence in an unsupported tunnel, which occurs due to tunnel removal, as well as the time history of block velocity and block energy. The analysis domain is 97 meters high and 97 meters wide, with 2 sets of joints inclined 60^o with respect to the horizontal; spacing between the joints is set to 1 meter and a tunnel with a 10 meter diameter is set at the domain center. The discontinuities' friction angle is set to 65 degrees elsewhere in the domain. The hydrostatic *in-situ* stress is set to 55 MPa; this kind of stress field is equivalent to the depth of 2000 meters. The tunnel is removed 0.15 seconds after the start of the simulation and the number of time steps is set to 50,000. Once the material that occupies the tunnel space is removed, the block ejects toward the tunnel space due to rapid strain relaxation. The velocity and energy of the block after tunnel excavation indicates the high energy stored at each block around the tunnel.

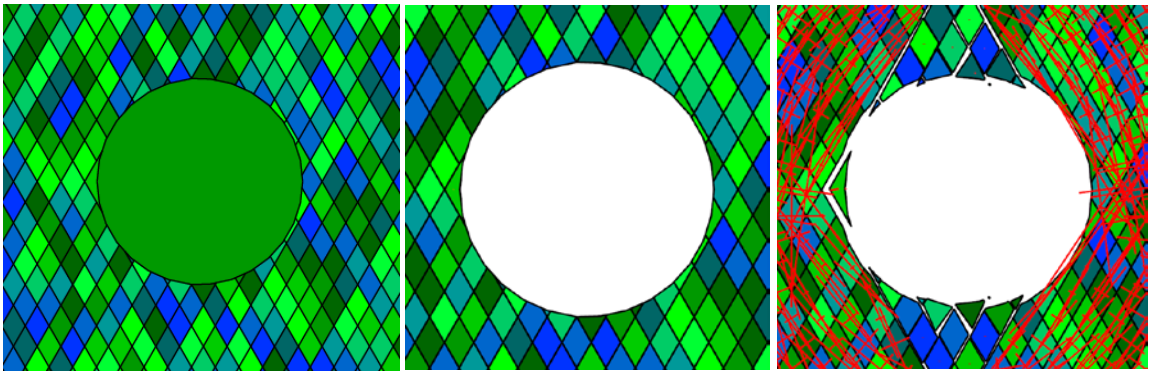

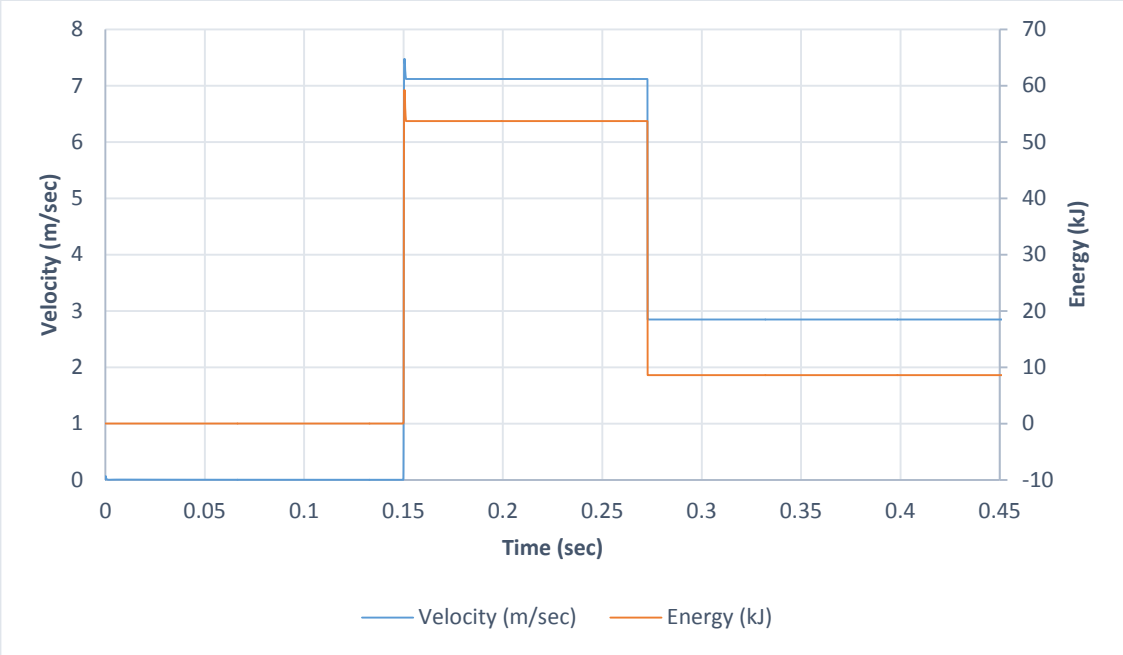

Figure 4-2: The evolution of rock burst event in the DDA simulation. In the upper figure, the sequence of excavation can be seen, first when material fills the space of the future tunnel, followed by the removal of the tunnel, and finally, the outcome of the rock burst event. The lower figure shows the velocity and the energy of the ejected block in the left area of the tunnel.

4.1: Bolt energy

In order to understand how rock-bolts function in overstressed high-deformable environments we test the influence of length and stiffness with a single bolt simulation. We attempt to generate a block system prone to rock bursting with DDA. Bolts are installed, separately, in critical location at the **left area of the tunnel**. Simulations are performed with varying bolt lengths. Since bolt stiffness depends on bolt length the stiffness should change accordingly, therefore we divide the simulation into two paths:

1) Changing the stiffness with length
2) Keeping stiffness fixed with the value of 25 MN/m.

The domain's geometric configuration and the rock's properties are similar to the unsupported simulation mentioned above. The tunnel is removed 1.5 seconds after the start of the simulation. Before tunnel removal, ten rock-bolts, with length ranging between 1 to

10 meters, are installed separately – one in each simulation, in the mesh. We use the stiffness formula:

$$K = \frac{EA}{l}$$

Defining the bolt stiffness in each simulation, where E is a constant value set to 200 GPa.

Table 4-1: ROCK-BOLT PARAMETERS FOR THE SINGLE BOLT SIMULATION. THE BOLT DIAMETER IS IN PARENTHESIS (cm)

length (m)	*Stiffness first simulation (MN/m)*	*Stiffness second simulation (MN/m)*
1	25 (1.3)	25 (1.3)
2	12.5 (1.3)	25 (1.8)
3	8.3 (1.3)	25 (2.2)
4	6.25 (1.3)	25 (2.5)
5	5 (1.3)	25 (2.8)
6	4.16 (1.3)	25 (3.1)
7	3.4 (1.3)	25 (3.3)
8	3.12 (1.3)	25 (3.6)
9	2.77 (1.3)	25 (3.8)
10	2.5 (1.3)	25 (4)

Results

Bolt with varying stiffness: initially we tested ten rock-bolts with varying stiffness as a function of bolt length. Figure 4-4 displays the energy that each bolt sustained during the course of the event. The **left section of the tunnel's key block** displacement shows in Figure 4-5. The results do not exhibit a consistent trend: changing the bolt length led to a large variation in recorded results. The bolt energy record of the different bolts is erratic and range between 10 to 3628 kJ, and is influenced by the geometric trajectory of the rock burst event. This outcome can be attributed to the softer rock-bolt (caused by increasing bolt length), which, in some occasions, fails to hold the key block in place. This then results in continuous failure of additional blocks in the rock mass (Figure 4-5, L=4, L=5) and thus to the total collapse of the left side of the tunnel's structure.

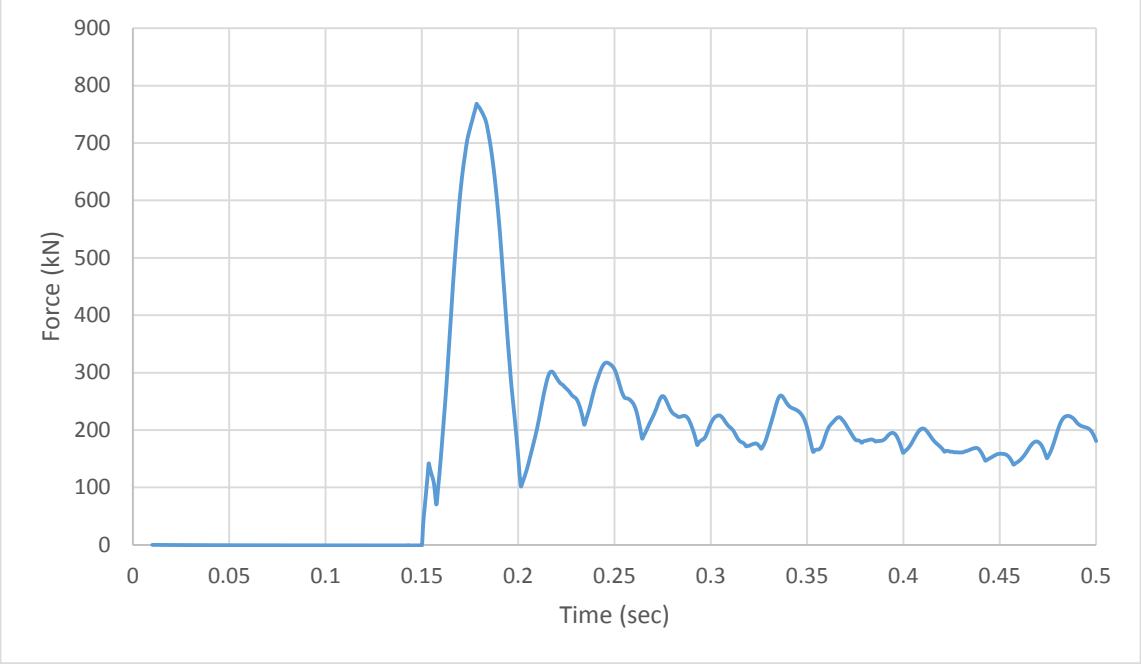

Figure 4-3: The time scheme of the 3 meter length bolt force from the beggining of the simulation. The peak value occurred after the tunnel excavation

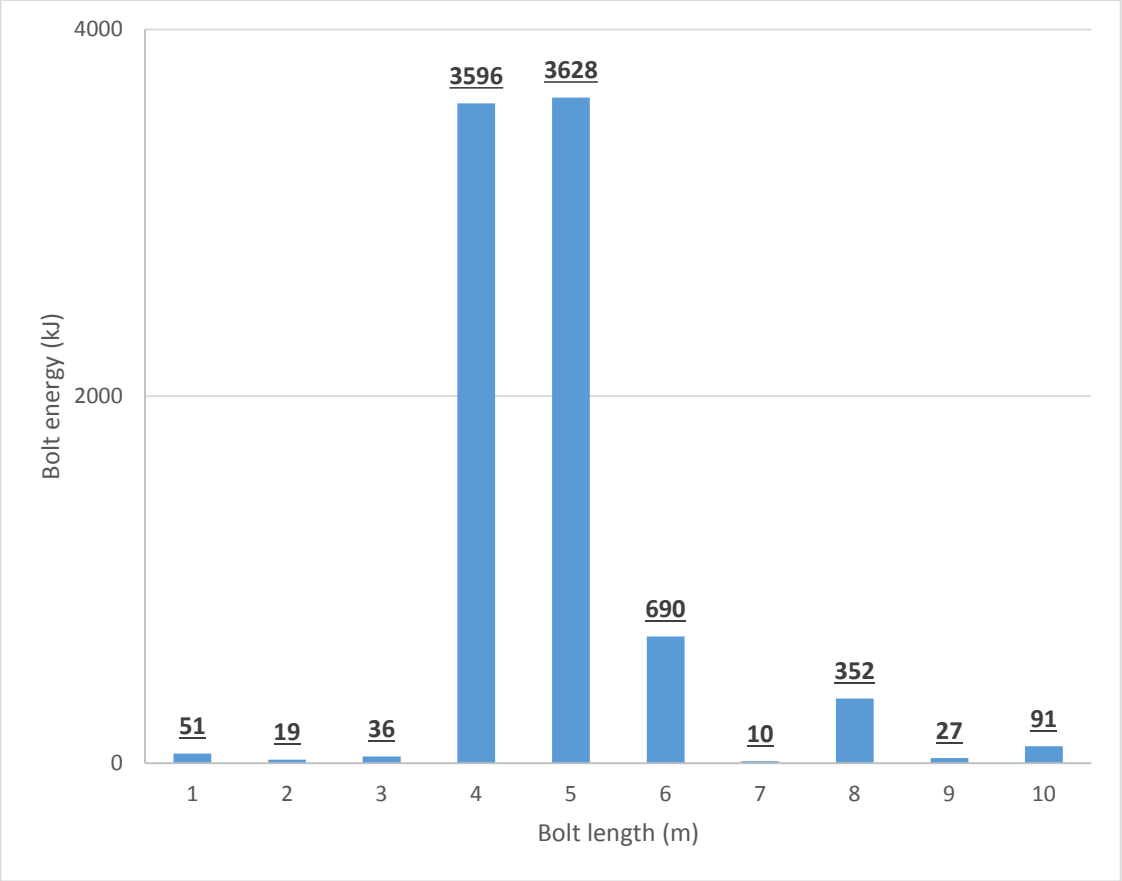

Figure 4-4: The peak energy values for block's kinetic energy. The peak energy values of more than 3500 kJ lead the the failure of the left side of the tunnel.

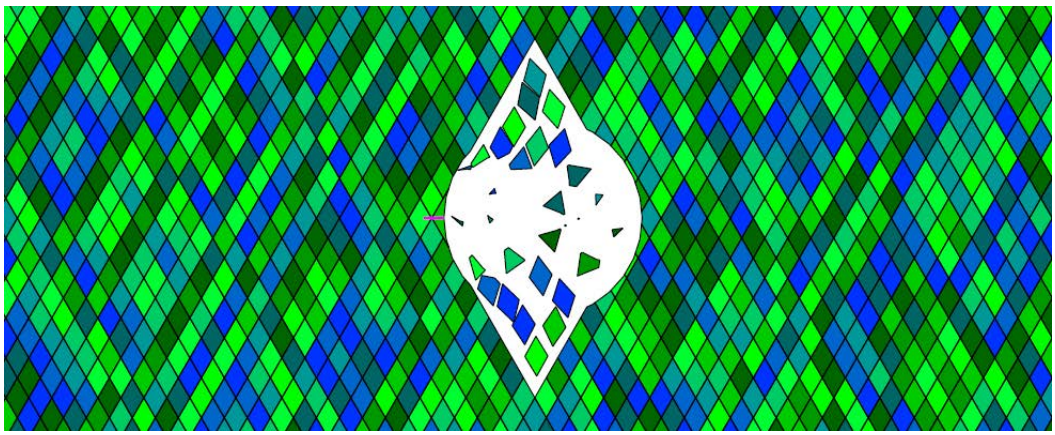

Figure 4.5 (a). L=1

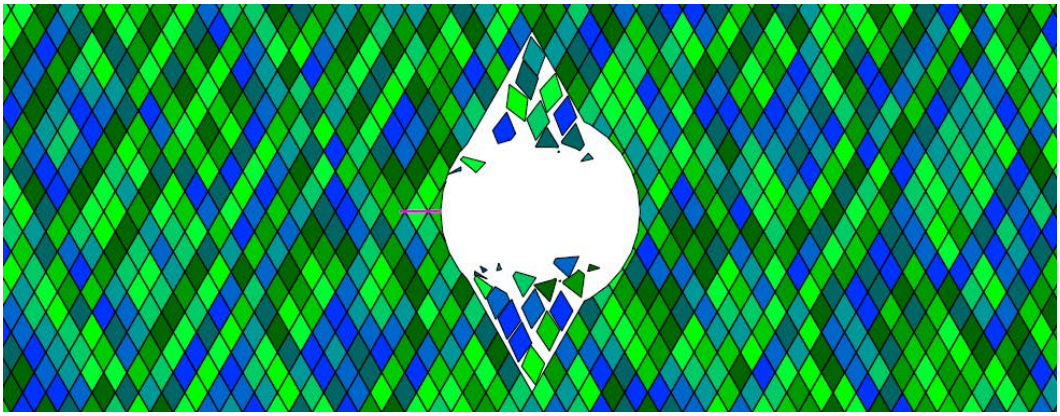

Figure 4.5 (b). L=2

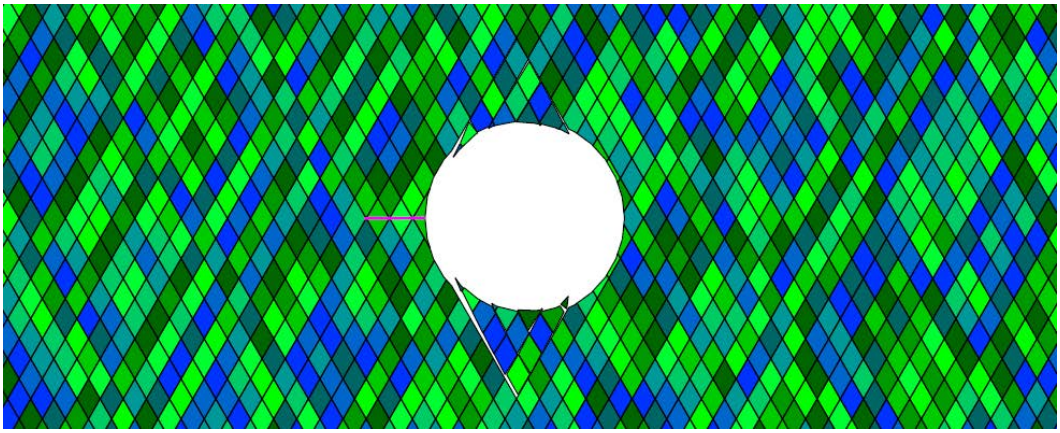

Figure 4.5 (c). L3

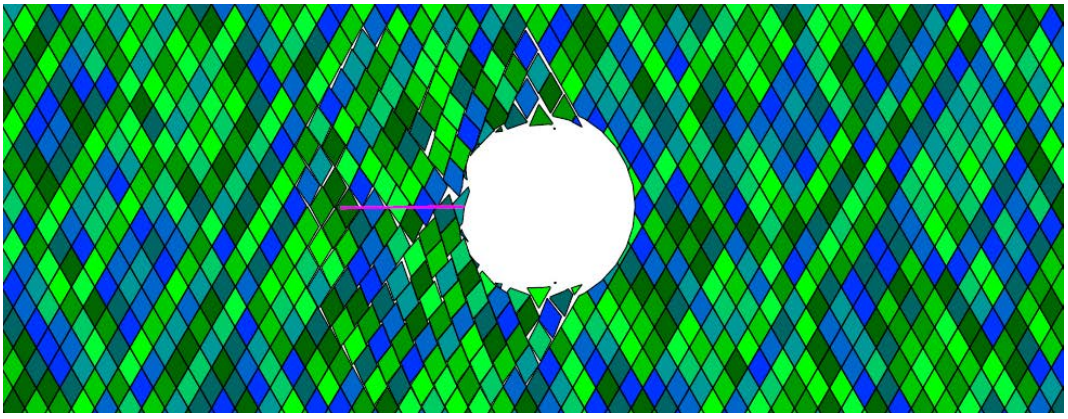

Figure 4.5 (d). L=4

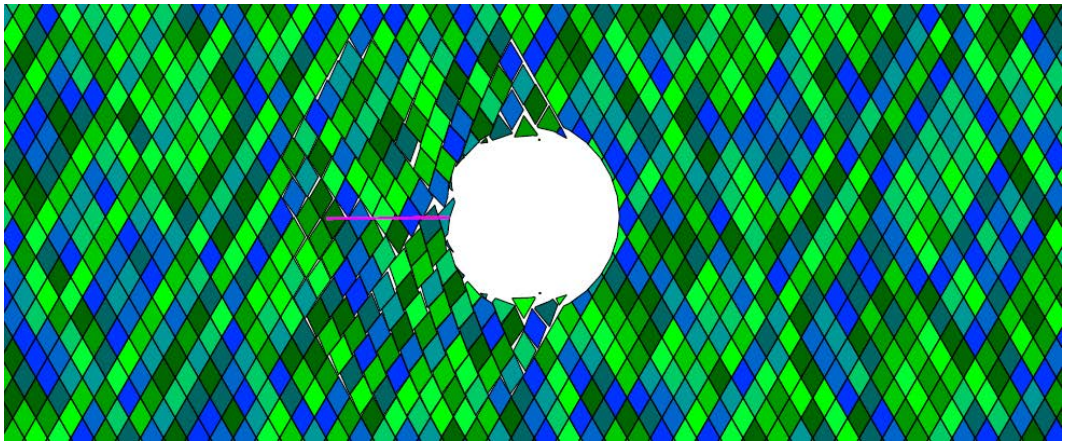

Figure 4.5 (e). L=5

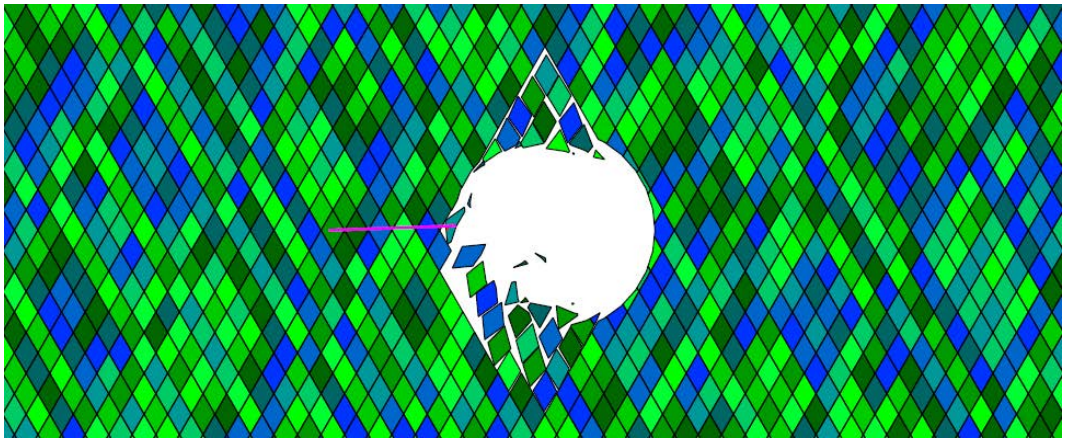

Figure 4.5 (f). L=6

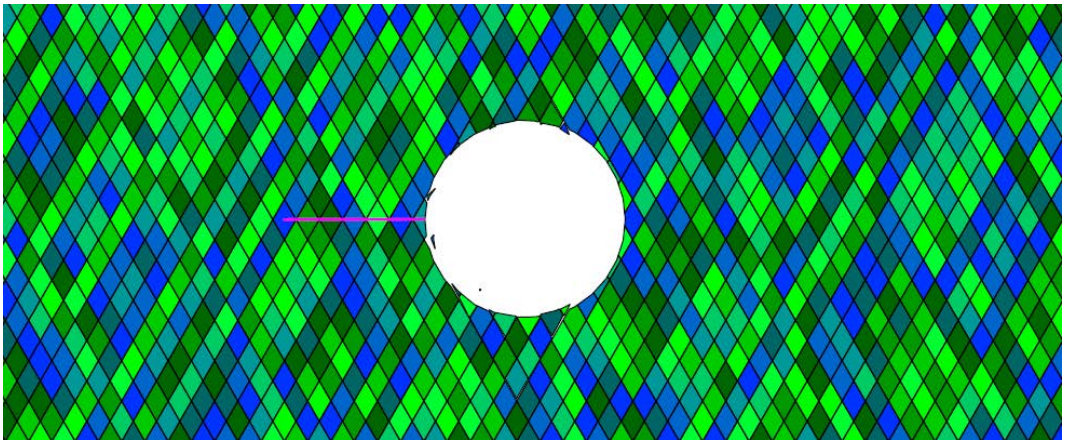

Figure 4.5 (g). L=7

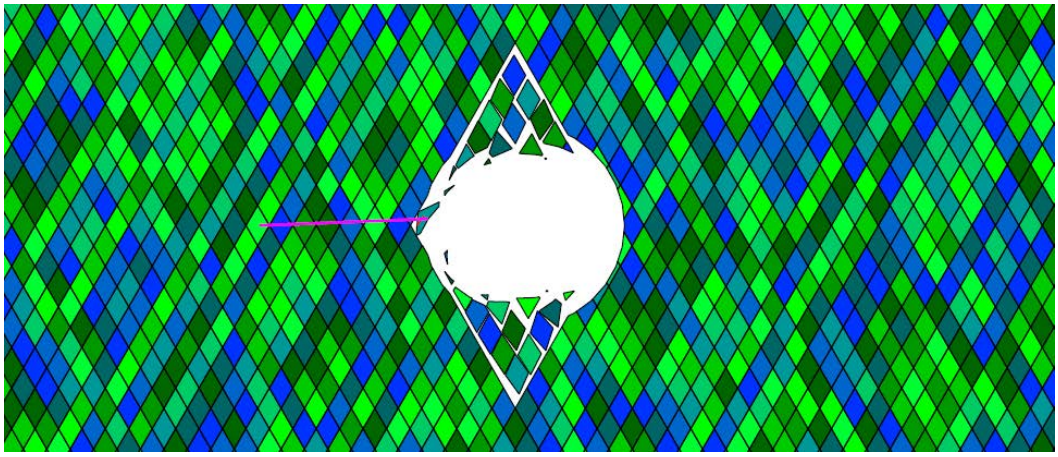

Figure 4.5 (h). L=8

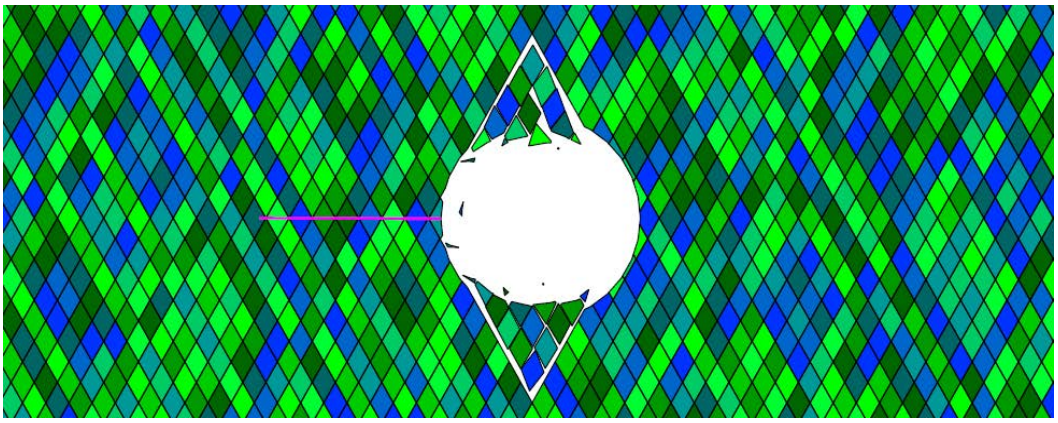

Figure 4.5 (i). L=9

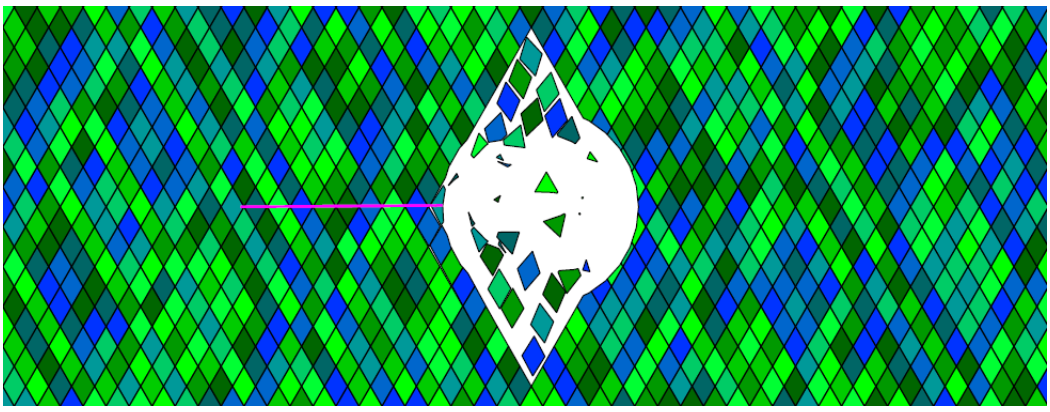

Figure 4.5 (j). L=10

Figure 4-5: The single bolt results at the end of the simulations . It can be seen that the left side of the tunnel collapse due to the failure of the softer bolt to hold the key block in place

***Bolt with constant stiffness**:* after testing the bolts with varying stiffness, we perform the same test using constant stiffness. All ten bolts tested withstood energy in the range of 20 to 100 kJ and the general left section of the structure of the tunnel is preserved.

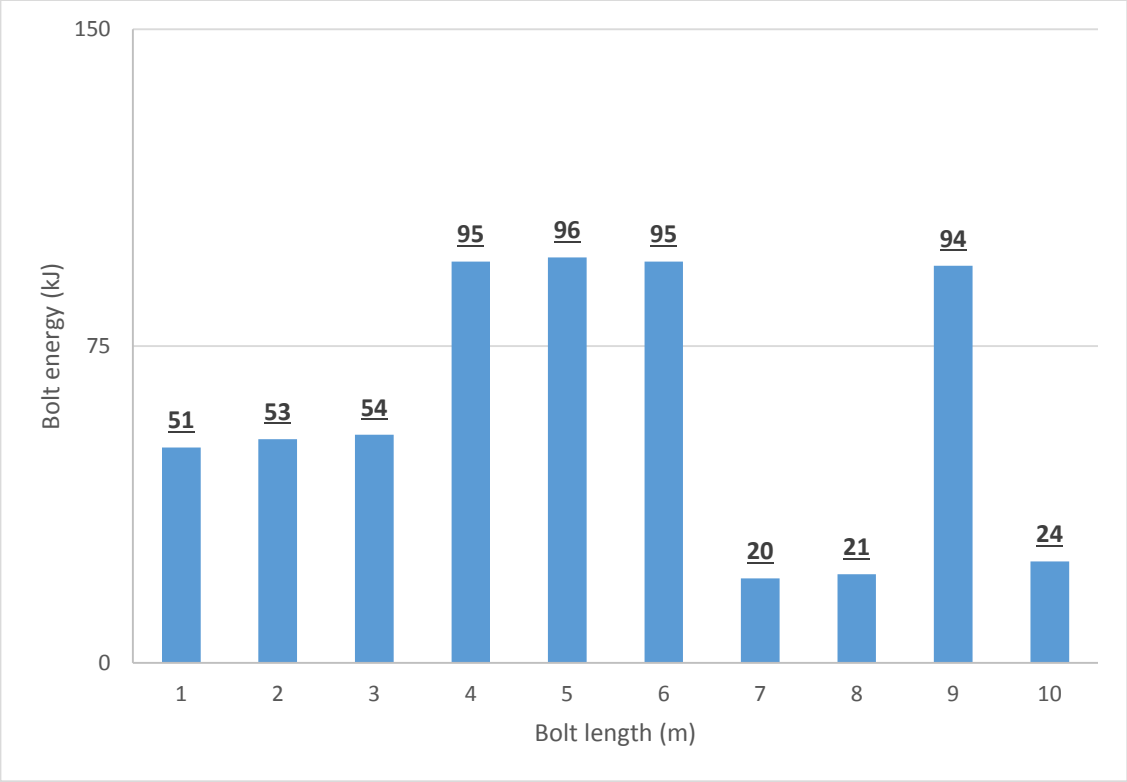

Figure 4-6: Bolt energires for different bolt lengths with fixed stiffness. Bottom - the tunnel at the end of the simulation. Note that the left sidewall remains intact in all simulaitons.

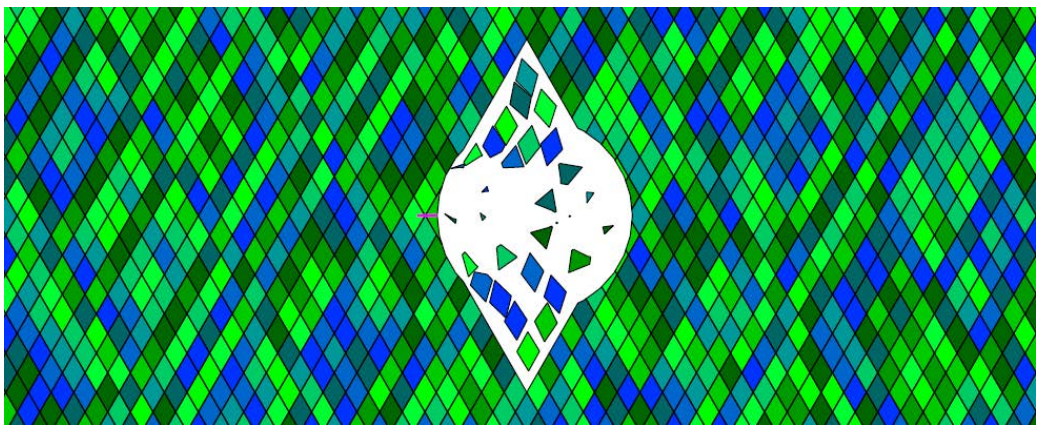

Figure 4.7 (a). L=1

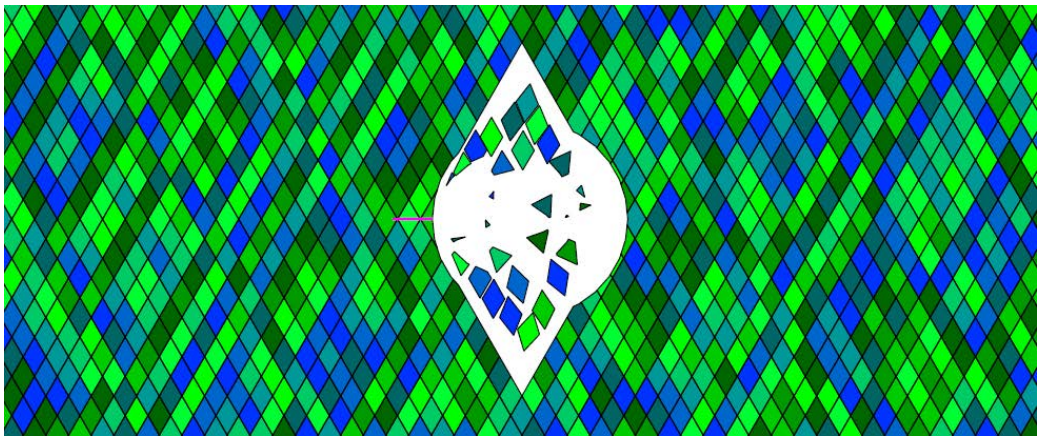

Figure 4.7 (b). L=2

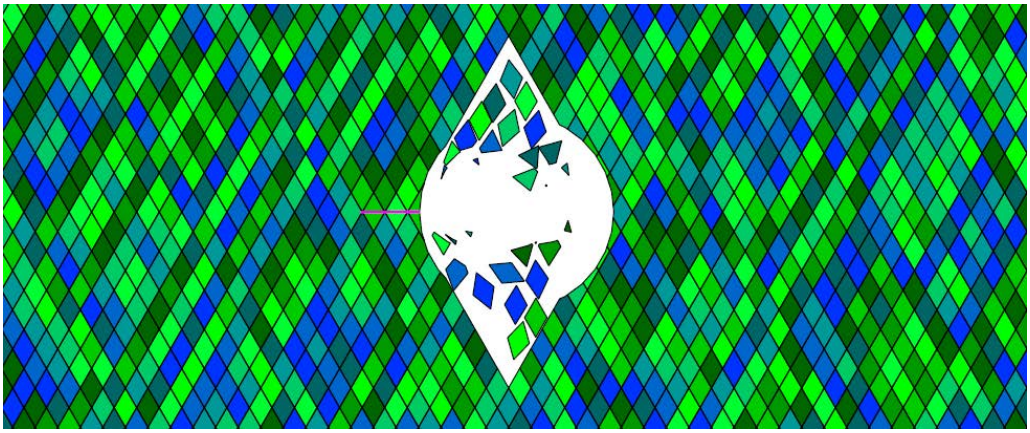

Figure 4.7 (c). L=3

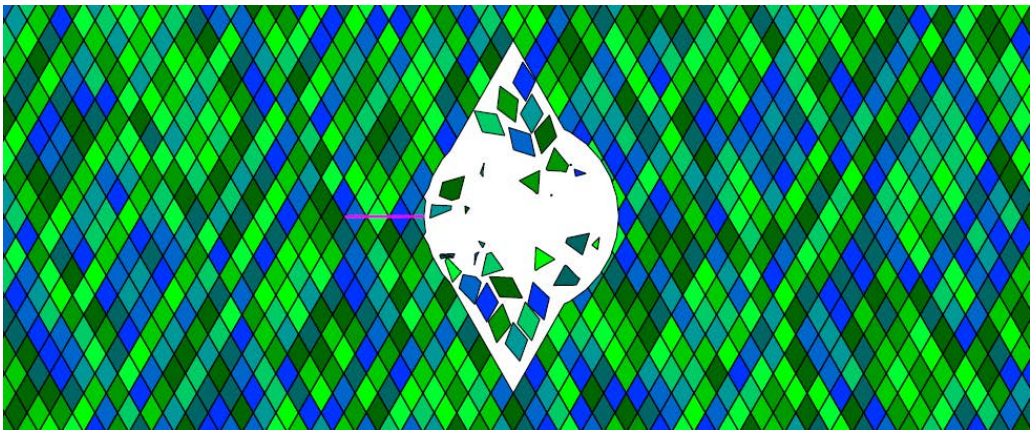

Figure 4.7 (d). L=4

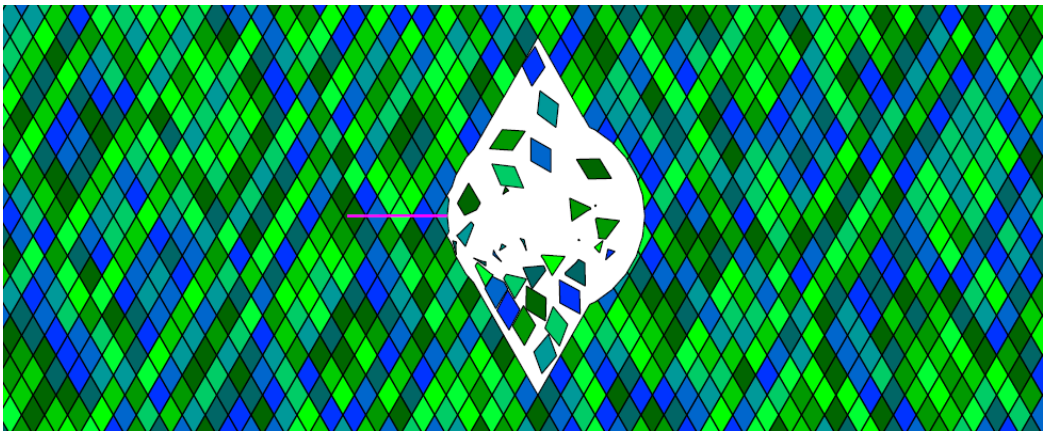

Figure 4.7 (e). L=5

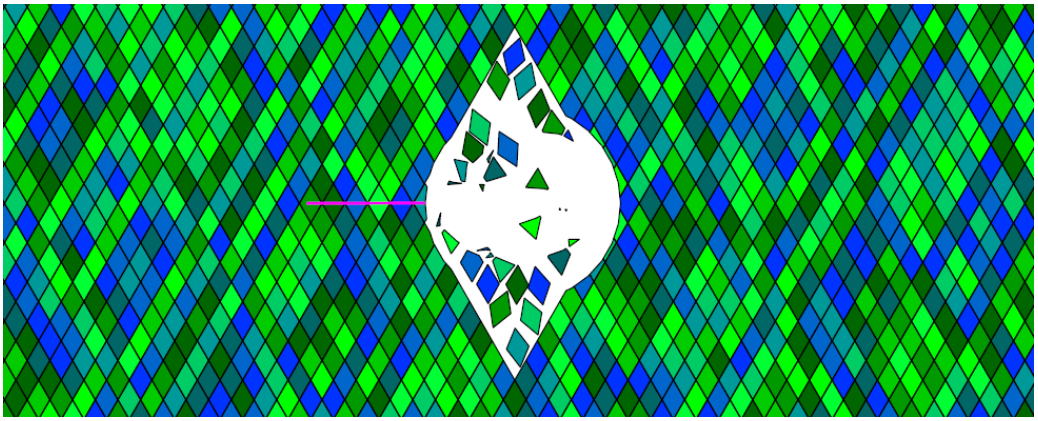

Figure 4.7 (f). L=6

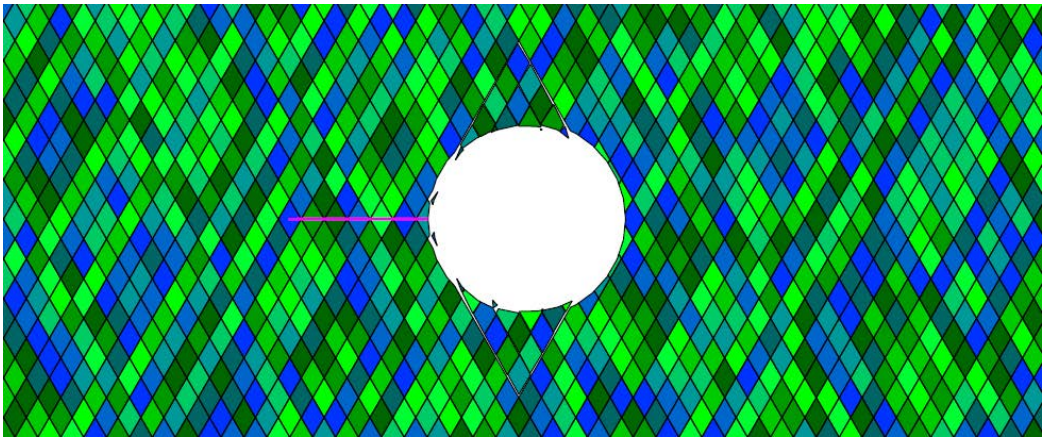

Figure 4.7 (g). L=7

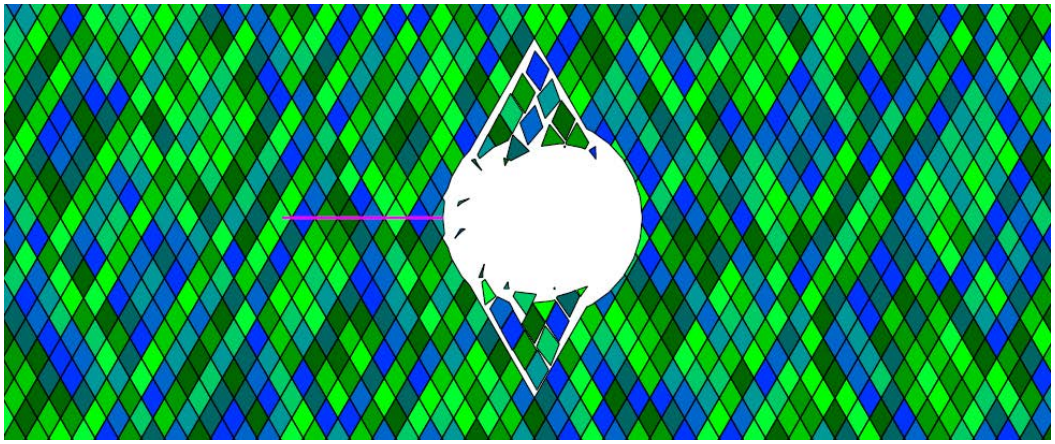

Figure 4.7 (h). L=8

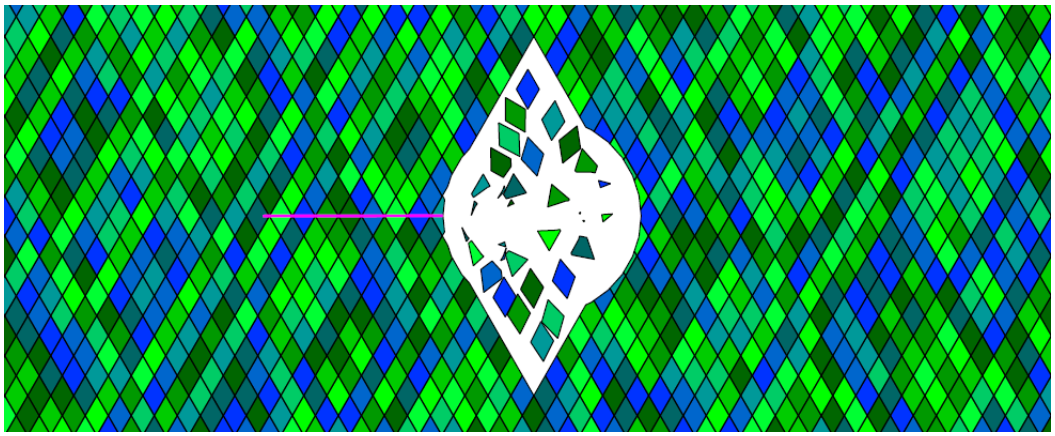

Figure 4.7 (i). L=9

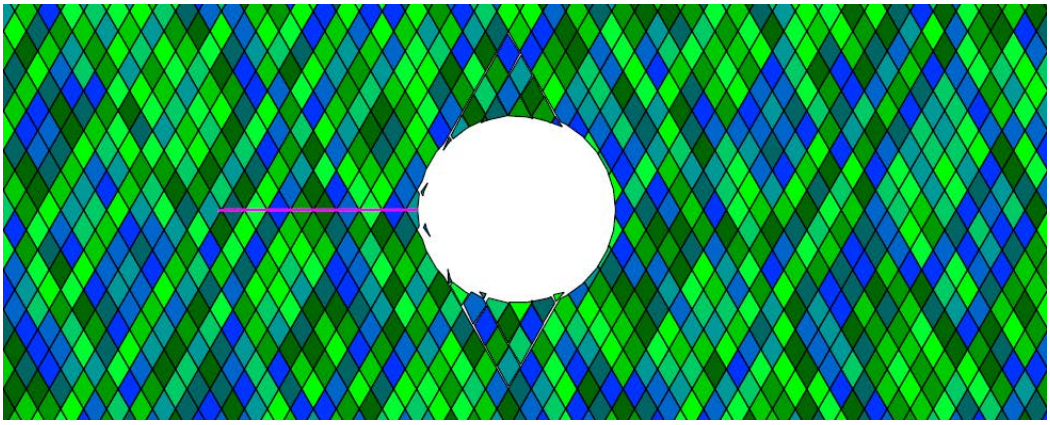

Figure 4.7 (j). L=10

Figure 4-7: The results of the fixed stiffness bolts at the end of the simulations. In contrast to the previous simulations, in this time the bolt retains the key block, keeping the left side of the tunnel intact.

4.2: Bolting Pattern

A parametrical study is carried out in order to understand the role of bolt length and spacing on the performance of the support system. Nine simulations are performed to determine the best energy absorbing support strategy. Based on the previous simulation, the bolt stiffness remains constant, with a stiffness value of 25 MN/m, and therefore not affected by its length. The bolt diameter remains in a range correlated to industry standards, between 180 mm to 330 mm.

The model geometry that is used in this simulation is identical to the geometry used in the previous simulation. The analysis domain is 97 meter high and 97 meter wide, with 2 sets of joints inclined 60^o with respect to the horizontal, spacing between the joints set to 1 meter, and a tunnel with 10 meter diameter that is set at the domain center. The discontinuity friction angle is set to 65 degrees. The hydrostatic *in-situ* stress is 55 MPa, and the tunnel is removed after 0.15 sec from the start of the simulation. Bolts are installed radially around the tunnel automatically using AutoCAD software with bolt parameters as listed in Table 4-2.

Table 4-2: BOLTING PATTERN TESTS.
LEGEND: S = BOLT SPACING, L = BOLT LENGTH, D = EQUIVALENT BOLT DIAMETER

s (m)	L (m) (D, cm)	L (m) (D, cm)	L (m) (D, cm)
1	2 (1.8)	5 (2.8)	7 (3.3)
2	2 (1.8)	5 (2.8)	7 (3.3)
3	2 (1.8)	5 (2.8)	7 (3.3)

Results

The results of the simulations with different bolting patterns suggest that the bolt spacing is the most significant factor. The bolt length also plays an important role in energy absorption of the rock burst event. The peak energy absorbed by the bolts is displays in Figure 4-8. The results may be divided into two groups:

1) *In-effective bolting pattern*: characterized by a **low** energy value, less than $460\ kJ$, with abundant block ejections that can culminate in collapse of the tunnel structure (Figure 4-9). The lower energy value implies that the support system is not functioning properly during the event. These results occurred when we chose a support strategy with **more** than 1 meter spacing between bolts. Because the bolts did not retain the key blocks, a chain reaction ('domino effect') occurred with abundant block ejections.

2*) Effective bolting pattern.* The tunnel structure is preserved with bolt energy in the range of $685 - 1000\ kJ$. These results are obtained only when the spacing between the bolts is 1 meter. The length of the bolts affects the amount of energy absorbed: bolts longer than 5-meters absorb 40 % more than 2 meter bolts. It appears that beyond 5 meter length, the bolts energy remains near $1000\ kJ$. This could indicate that the loosened zone around the tunnel extends to a smaller distance than one tunnel radius.

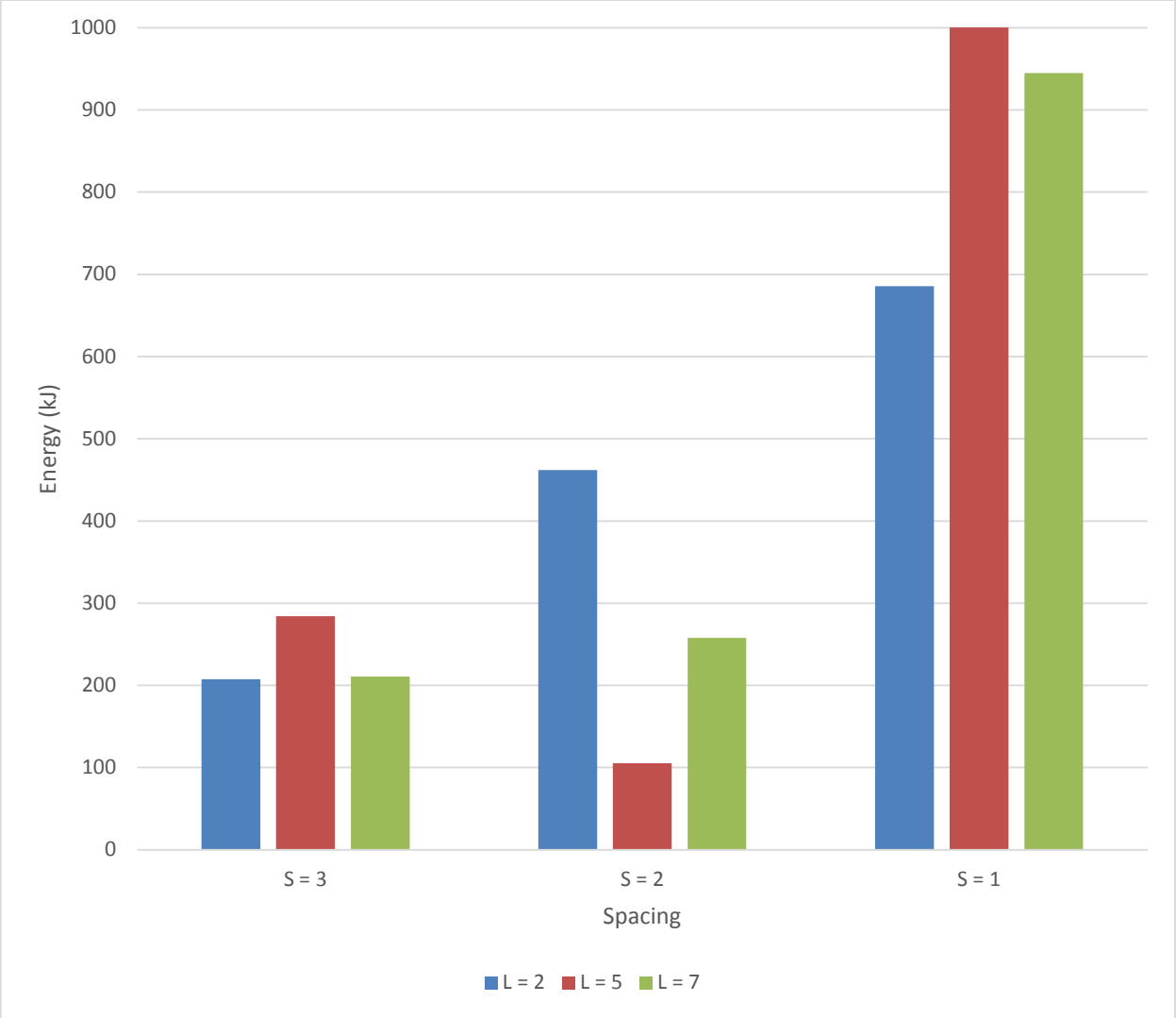

Figure 4-8: Summary of rock-bolt array energy with varying bolt length and spacing. All rock-bolt arrays which have spacing higher then 1 meter suffer energy value indicating failure

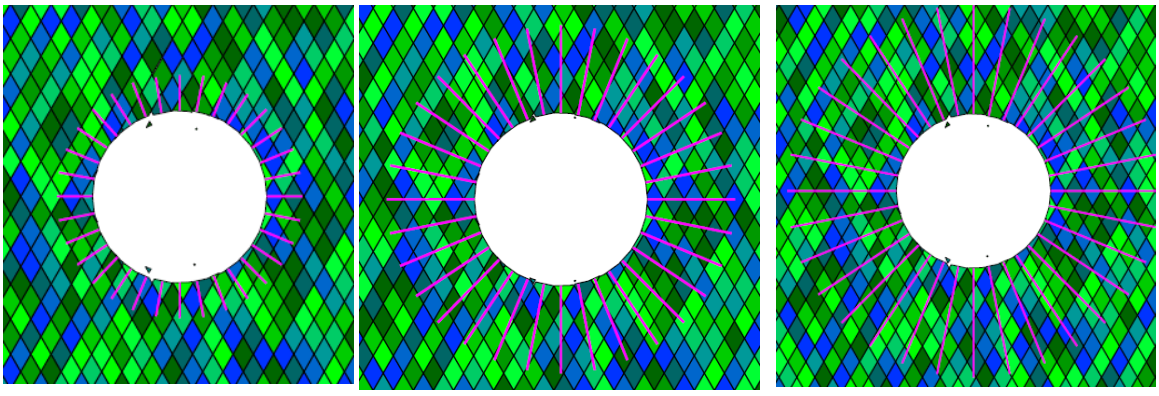

(S=1, L=2) (S=1, L=5) (S=1, L=7)

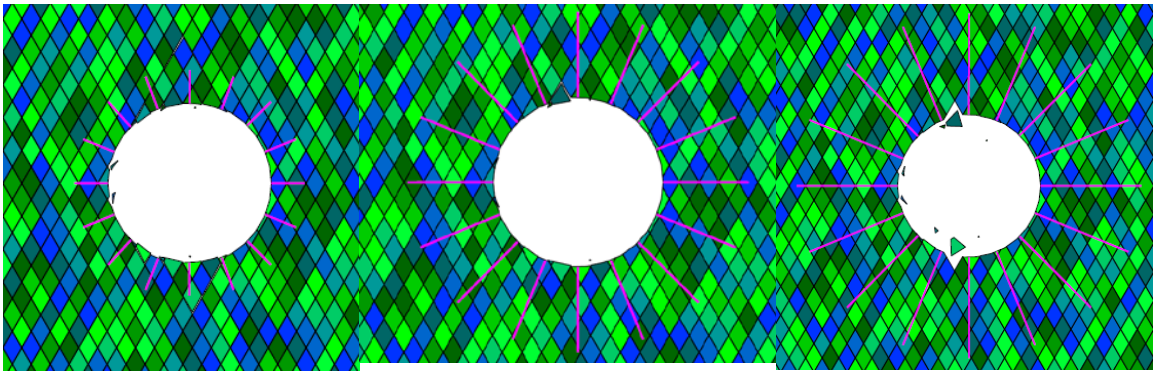

(S=2, L=2) (S=2, L=5) (S=2, L=7)

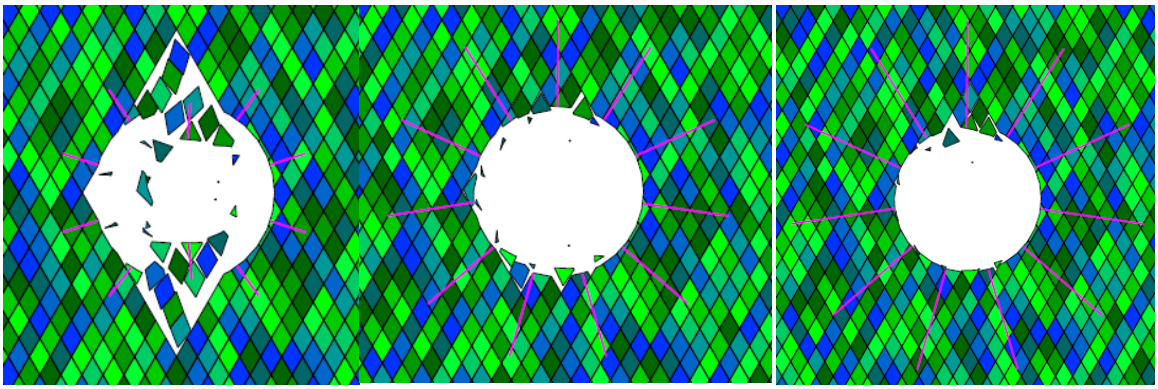

(S=3, L=2) (S=3, L=2) (S=3, L=7)

Figure 4-9: The nine simulations conducted in this section. The results demonstrate the aftermath of the simulation. Even one unsupported key block ejection could lead to the collapse of the entire structure. A medium with 1 meter spacing endures the event with minimal damage.

4.3: The role of rock mass quality

In this section we attempt to establish a relationship between the quality of the rock mass and the energy absorbed by the support system. We use the RMR rock mass rating method with insights reached earlier in this chapter regarding the mechanical and geometrical parameters of the support system.

Different rock masses exhibit different energy release upon excavation, depending on the amount of movement in the rock system and the number of key blocks at the tunnel free surface. Several attempts have been made to find a relationship between the rock mass quality and ejection velocity during rock burst event (He et al., 2016; Ortlepp, 1992b; Reddy and Spottiswoode, 2001). We extend previous work done by He et al., (2016) on the energy balance in the rock mass at the time of the rock burst event by adding another component to the energy balance – the energy absorbed by rock bolts.

The work done by He et al. (2016) uses the theory of elasticity to calculate the energy expected to be released due to the tunnel excavation in a homogenous, continuous, isotropic, linear-elastic, medium. The main assumption in the work is that tunnel excavation is followed by increase in the initial elastic strain energy stored within an annulus that extends to some distance from the tunnel center. This excess energy, combined with the energy which is stored in the annulus before the tunnel is excavated, is the source of the kinetic energy which is released following the excavation in the form of ejected key blocks. He et al., 2016 derived the energy balance associated with tunnel excavation and rock bursting:

$$U_B^0 + \alpha U_A^0 = U_B^* + U_k^* + U_d^* \tag{32}$$

The original stored energy and the energy increase due to excavation are expressed on the left hand side of Equation 25. U_B^0 is the initial elastic energy stored in an annulus around the tunnel to some finite distance, U_A^0 is the energy stored in the tunnel space before excavation, and α is an analytically obtained amplification factor due to formation of the tunnel space, the magnitude of which depends on the radius of the annulus of the affected

zone that is being considered (for more elaborate details and derivation see He et al., 2016). On the right hand side are the energy components that balance this energy increase: U_B^* is the strain energy in the annulus considered after tunnel removal, U_k^* is the kinetic energy released after tunnel removal, and U_d^* is the energy dissipated by frictional sliding along pre-existing discontinuities. The elastic strain energy is calculated using the elastic parameters of the intact rock, E, v and the in-situ stress field:

$$U_0 = \frac{1+v}{2E}\left[(1-v)\left(\sigma_x^0 + \sigma_y^0\right)^2 - 2\sigma_x^0\sigma_y^0\right] \times A_0 \tag{33}$$

where A_0 is the area of the elastic medium and σ_x^0, σ_y^0 are the initial horizontal and vertical stresses, respectively. From this formulation the initial energy U_B^0 and the energy increase in the annulus of consideration, αU_A^0 can be obtained, for derivation see He et al., (2016).

He et al., (2016) investigated the behavior of different rock masses during a rock burst event that occurs spontaneously once the tunnel is removed. Based on their engineering experience, they constructed four DDA block systems to represent graphically four RMR values (95, 85, 75, 65). Here we build on the He et al. (2016) work by adding another component to the energy balance equation, namely, the bolt strain energy accumulated when the bolt is extended. The new equilibrium equation therefore becomes:

$$U_B^0 + \alpha U_A^0 = U_B^* + U_k^* + U_d^* + U_b^* \tag{34}$$

where U_b^* is the bolt energy after tunnel removal.

We use our experience from previous sections to apply different support strategies for each of the rock masses tested. Each RMR rating is accompanied with bolt recommendations, the bolt parameters are shown in table 4-3.

Table 4-3: Bolt RMR PARAMETERS WITH THE TUNNEL INITIAL ENERGY

BOLT GEOMETRIC PARAMETER BY RMR				
RMR	S (m)	L (m)	Number of bolts	Initial energy stored in tunnel space before excavation U_B^0 (kJ)
RMR 65	1	5	32	5257
RMR 75	1	5	32	3245
RMR 85	1	5	32	2381
RMR 95	2	5	16	1900

The geometry of the analysis domain is 97 m high and 97 m wide, with 2 sets of conjugate joints inclined 60^o. A circular tunnel with 10 m diameter is set at the domain center. The initial hydrostatic stress field is 55 MPa, no joint cohesion nor tensile strength are applied during the simulation. The friction angle, Young's modulus, and Poisson's ratio depend on the RMR rating as detailed in Table 2-1. The mass per unit area is 2.65 ton/m^2. The numerical control parameters are time step size : 10^{-5} s, K_{01} set to 1 for non-damping simulation, g_0 = 10 * E, gravity is activated. The bolts are added 0.01 second after the start of the simulation, and the tunnel is removed after 0.15 seconds.

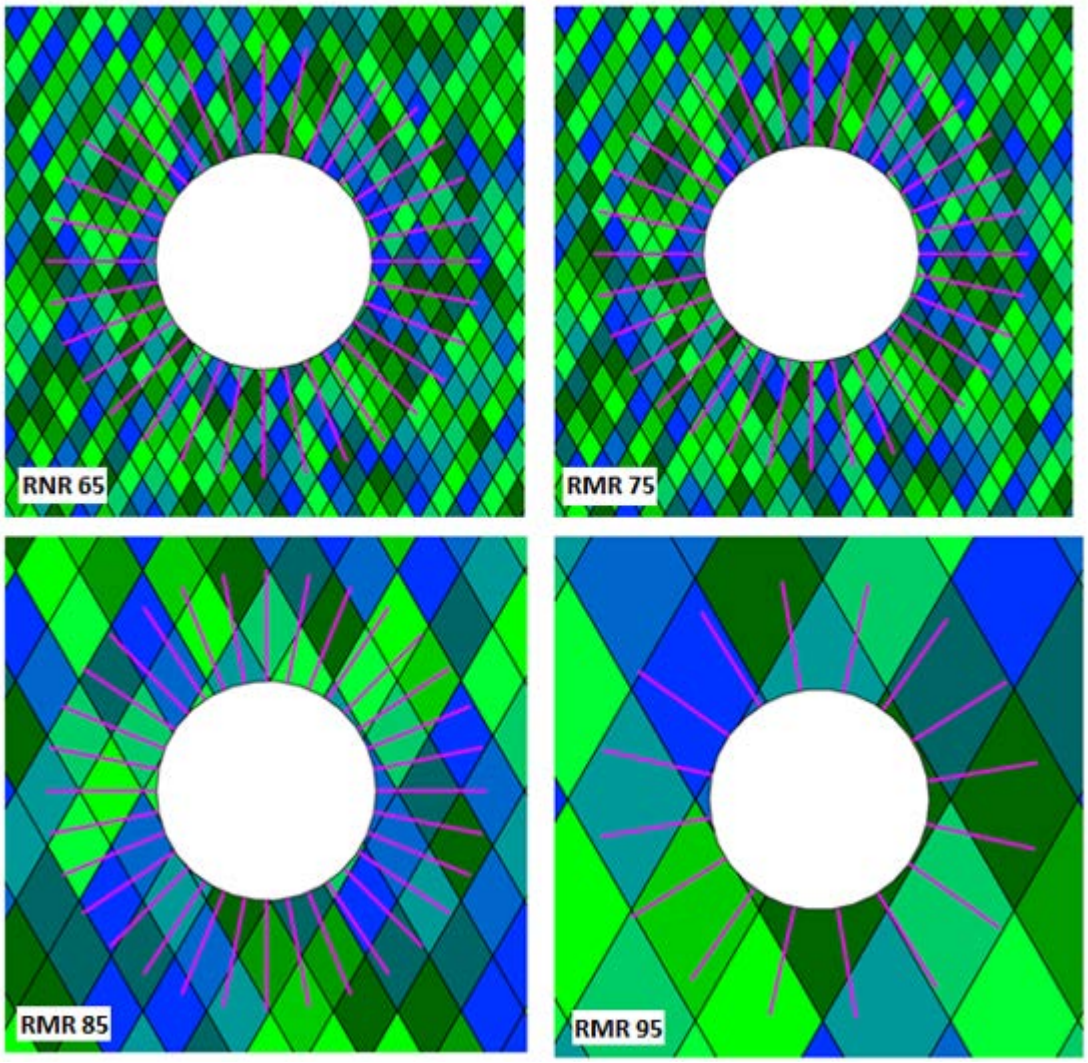

Figure 4-10: RMR rock masses with rock-bolt support

Results

Figure 4-11 tracks the result of the total energy absorbed by the support system in each RMR scenario. It also displays the initial elastic strain energy before excavation. Each rock mass was supported by a conservative support strategy with an identical bolt length of 5 meters and bolt spacing of 1 meter for each rock mass, except the rock mass classified RMR 95, which was supported with a spacing of 2 meters and a length of 5 meters.

The results are displayed with the initial energy in order to understand how much of the initial energy transfers to the support system. He et al., (2016) found that when the initial

energy of the rock mass was high, and the rock mass was heavily jointed the probability of a rock burst event increased significantly.

In all the rock masses that were examined, the tunnel remained intact without any rock burst events. In addition, circular arching stresses developed around the tunnel, which thus preserved the structure of the excavation. The results showed that the energy absorption ranged from $31 - 1002\ kJ$ for the various rock masses. This corresponded to the energy absorption for the unit area of $1 - 32\ kJ/m^2$. These values are within the range of values accepted in the literature. Rock bolts in the poorly rated rock masses of RMR 65 absorbed the highest energy with more than 1000 kJ. Bolts installed in rock masses rated RMR 75 absorbed energy values of 523 kJ. In the beginning, the trend of energy absorption, as a percentage of the initial energy (Figure 4-12), decreased moderately with a simultaneously increasing RMR rating: 19 % (RMR 65) of the initial energy decreased to 15.7 % (RMR 85) of the initial energy. A dramatic decrease was recorded when approaching excellent rock mass rating; only 1.6 % (RMR 95) of the initial energy was absorbed by the support system. This emphasizes the importance of plastic deformation along pre-existing discontinuities in low grade rock mases, in contrast to elastic deformation of intact rock elements in high grade rock masses. Those mechanisms account for the sharp drop in bolt energy for the best rock mass (RMR 95), where the total energy absorbed by the bolting system is only 31 kJ.

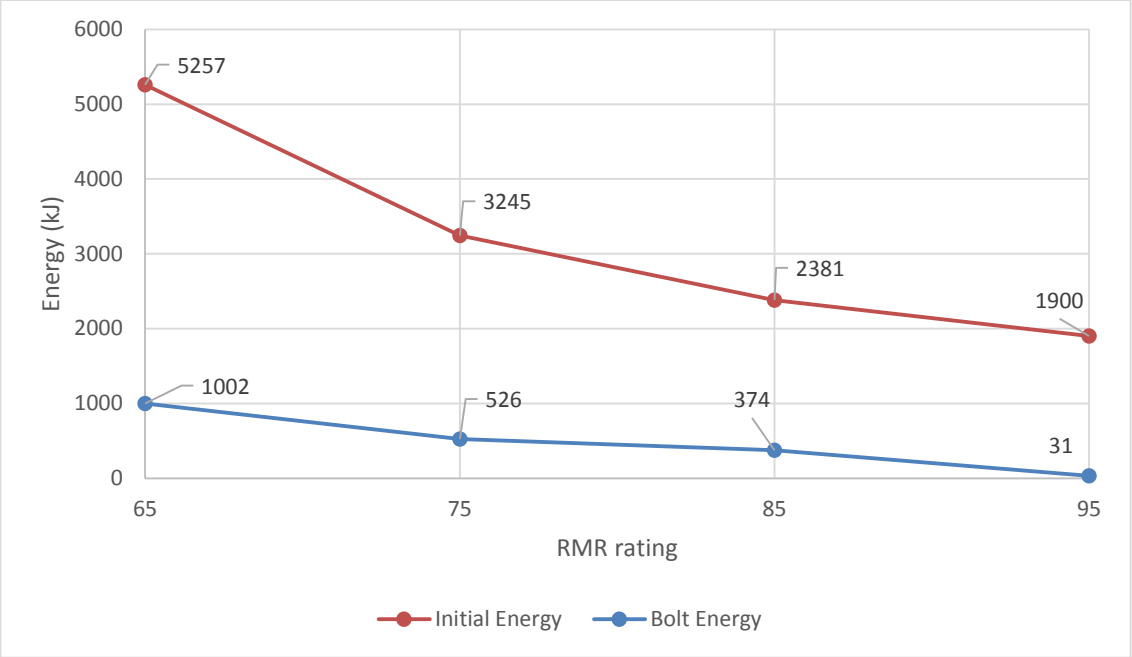

Figure 4-11: Total elastic strain energy in the affected area due to tunneling and the bolts' summation energy absorbed by the support system once the excavation was created.

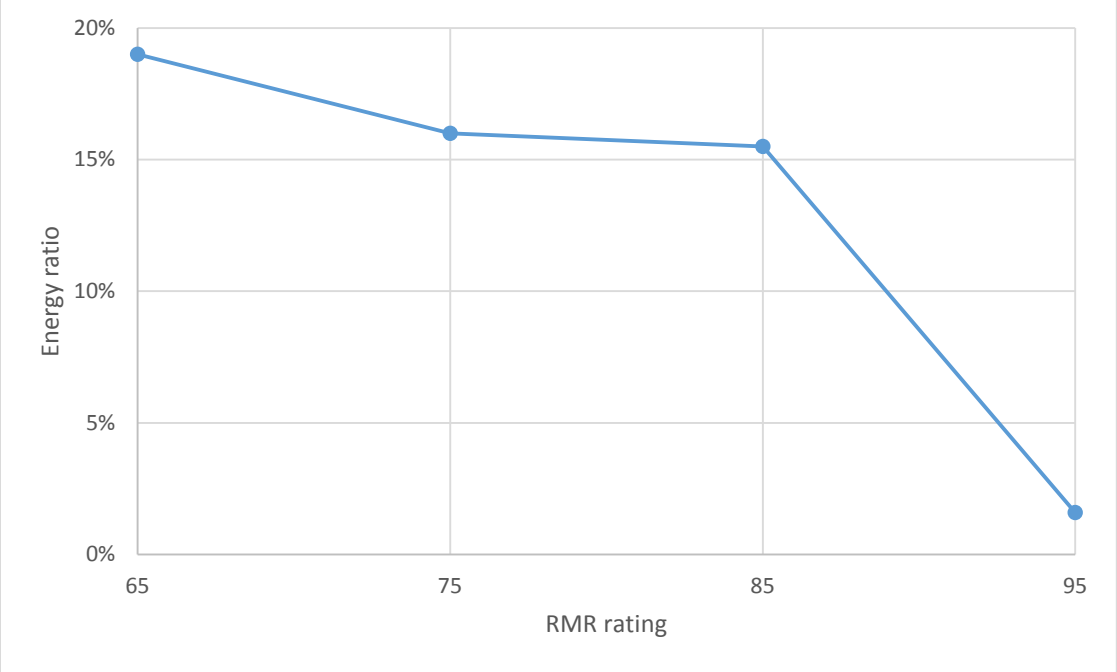

Figure 4-12: Energy amount as a precentage of the initial energy for the four RMR rock masses tested

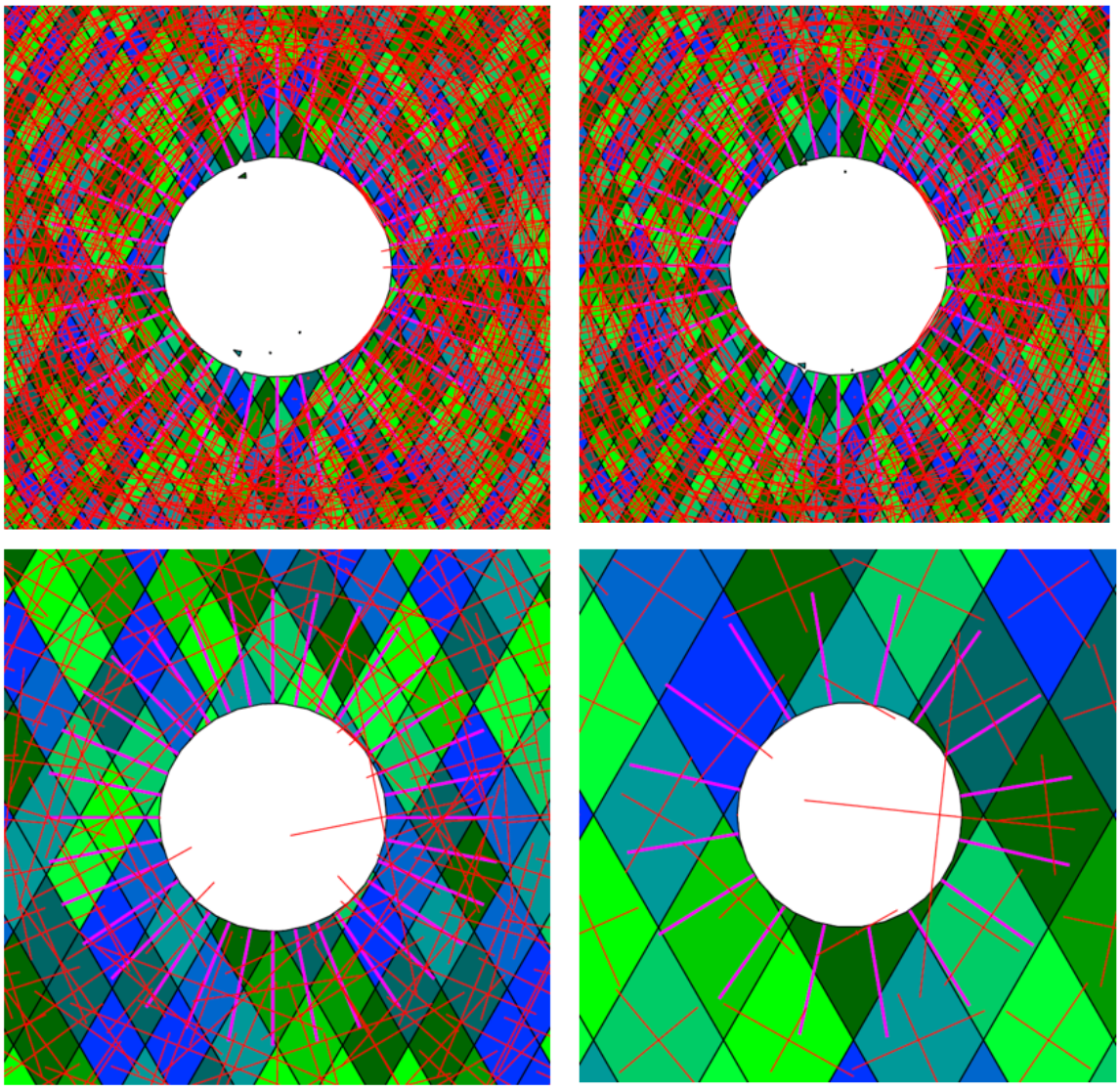

*Figure 13: The end results of the simulation: none of the rock masses experienced a rock burst event. *note the double arch structure created*

4.4: Discussion and Conclusions

In this chapter, the performance of rock-bolts from the perspectives of stiffness, geometry and rock-mass rating was studied.

When studying single bolts, the issue of the modeled bolt stiffness is found to be of paramount importance. Severe events occurred when the stiffness of the bolts was less than $8\,MN/m$ with the left section of the tunnel, which was supported by softer bolts, often completely collapsing. When stiff bolts were installed, regardless of length, the integrity

of the left section of the tunnel structure was generally maintained without rock burst events. We conclude that moderately stiff rock-bolts ($25\ MN/m$) performed better than softer bolts during the rock burst events.

The layout of the rock-bolting pattern, particularly the length and spacing of the rock-bolt pattern, are found to be important in mitigating rock-burst events. We find that the most important parameter is the spacing, which should be as minimal as possible for two reasons: 1) to reinforce as many key blocks for the stabilization of the tunnel free surface 2) to absorb more energy in each individual bolt. Each missed key block had the potential to eject. In addition, because rock-bolts are a type of energy storage device, they had the ability to reduce the potential energy in the system. Supporting strategies, where bolt spacing was greater than 1 meter, experienced rock bursts, whereby the whole structure collapsed. When the bolting pattern was dense enough, a double-arching mechanism was created, which helped the tunnel to be self-supporting. This occurred due to a coupling mechanism between the rock-bolt and the rock blocks; energy transferred via a 'domino effect'. The overall structure was preserved: the bolts provided the force to retain the key blocks and thus the tunnel supported itself.

The bolt length parameter was also found to be an important factor, but secondary to the bolt spacing. Increasing the bolt length provided a stronger rock-bolt anchor to the intact rock mass. Bolts that were anchored in the vicinity of the tunnel surface produced erratic results due to the kinematic processes after excavation. The maximum energy absorbed, without structural failure, was obtained with a bolting pattern consisting of $1\ m$ spacing and $5\ m$ length. We therefore recommend using longer bolts than usual in a rockburst prone environment.

In general, rock-bolt load is a function of two factors, the size of the ejected key block it retains, and the size of the rock volume behind the key block. Figure 4-14 illustrates the situation just described: the purple and the yellow blocks were non-removable until the red block was ejected, once that occurred, the entire area collapsed.

The role of a kinematic block system is also important. The peak rock-bolt force was recorded just after tunnel excavation in the first strain relaxation, in response to kinematical process that resulted from the new excavation. These peak values were not correlated in

time because the bolt forces highly depended on the movements of blocks in the rock mass around the tunnel. The rock mass kinematics acted in the manner of a ‘domino effect' - one block transferred the load to the adjacent block.

Another conclusion that can be drawn from the results in this section is the contribution of the bolting pattern to the apparent formation of a double arching mechanism around the tunnel (Figure 4-15). This phenomenon occurs only when the radial bolting pattern is dense enough to support all of the key blocks around the tunnel free surface.

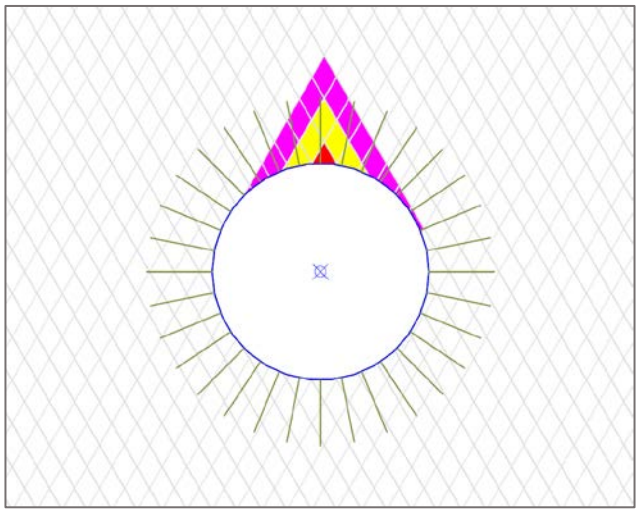

Figure 4-14: illustration of the release zone in the tunnel top

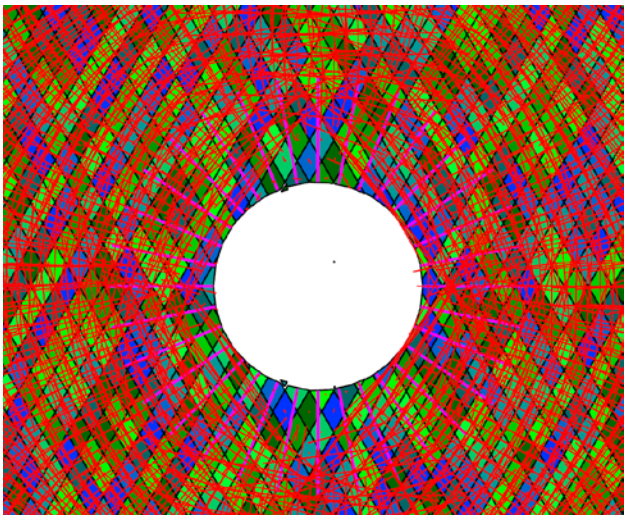

Figure 4-15: Double arch structure that forms around the tunnel

Regarding the role of the quality of the rock mass, the comprehensive studies by He et al. (2016) and Hatzor et al., (2017) both showed that rock-burst hazard, as scaled by the kinetic energy released by block system in the affected zone, increases with deceasing rock mass quality. Our results are in agreement with those conclusions.

Chapter 5 : Rock burst induced by dynamic impact

Dynamic events are common in tunneling excavations. They can occur either due to the effects of far-reaching earthquakes or due to human-induced blasts/vibrations (Cai, 2013; Stacey, 2011). Dynamic events are defined as an energy disruption in the system, which could produce deformation in the rock system. When the rock-mass is a block-like type, the deformation takes place in the form of block sliding, at high velocity.

Up until now, we discussed rock-burst by strain relaxation deformation caused by gravitational driving forces and we studied its influences on different geometric and mechanical properties of the bolts. As opposed to previous chapters in this thesis, where the load was due to stress stored inside the blocks close to the tunnel perimeter, here the rock-burst event origin can be far from the tunnel free surface. The purpose of this section is to explore means to mitigate dynamically induced rockbursts with rock-bolts as support elements.

Rock-burst due to blasting are common. Ortlepp (1994) observed the damage from a real rock-burst that occurred close to a site where mine blasts were conducted. He concluded that the damage produced in the blast was indistinguishable from natural rock-burst damage. Later, Ortlepp and Stacy (1994) noted that there was no simple relationship between the extent and intensity of the rock-burst event and the seismic trigger of the rock-burst.

Reddy and Spottiswoode (2001) studied the influence of local geology and rock mass characteristics on rock-bursts caused by a controlled blasting. They found that the ejected material was bounded mostly by fractures associated with bow-wave fracturing and bedding surfaces, which existed prior to the blast.

Extensive research has been conducted over the years to understand rock-bolt behavior during a dynamic event near the tunnel. The first detailed and thorough testing of a support element, under blast loading, was the underground nuclear explosion testing performed by the U.S. military in the 1950’s (Tannant et al., 1995). In South Africa, Ortlepp was the first to conduct dynamic experiments in deep mines using explosives (Ortlepp, 1969). Later he used both regular rebar rock-bolts and energy absorbing rock-bolts to show that regular

bolts cannot sustain dynamic event energy (Ortlepp, 1976). Based on the work done by Ortlepp, many researches (Hagan et al., 2001; Li, 2010) extended the blast method to test different rock-bolt materials, rock-bolt design, rock-bolt installation geometries, and blast techniques, in the ambition to develop a rock-bolt that could handle high load and high deformation during rock burst event.

Deliberate blast, where explosive charges apply a high pressure P-wave on the surrounding area due to air gas caused by the heat of the explosion, is defined as large scale, rapid and sudden release of energy. The detonation of a condensed high explosive, generates hot gases under a pressure of up to 300 kilo-bar and a temperature of approximately 3000^{o} (Ngo et al., 2007).

Blast tests are useful in understanding rock-bolt performance, even though there are some limitations with this method, as mentioned by Hagan et al. (2014). The challenge in dynamic testing of ground support is to reproduce loading conditions similar to what would be experienced at a supported excavation surface during a rock-burst event. There are certain differences between loading conditions during a rock-burst event and during a simulated rock-burst by means of blasting. A real seismic, shear-type rock burst event first initiates a compressive P-wave followed by a larger amplitude shear S-wave, which carries more energy than the longitudinal wave. Whereas, blast-produced-waves are dominated only by P-waves.

In this chapter, we will study the rock-bolt response to dynamic impact load, based on a blast module suggested for DDA by Zelig et al. (2015). The rock-bolts were tested with varying distances of the blast from the tunnel space, and with different friction angles of the rock-mass. We want to look at the impact of each rock-bolt depending on its position around the tunnel in order to study the effect of the friction angle and the blast distance on the installed rock-bolts.

5.1: Bolt performance under dynamic impact

In this section we will use the non-reflective boundaries (Bao et al., 2012) and sequential excavation (Tal et al., 2014) enhancements proposed earlier for DDA. The method to simulate the blast wave is adopted from Zelig et al. (2015).

It was previously found (Zelig et al. 2015) that the g_2 time step interval should be 10^{-5} s to achieve best accuracy. In addition, the η parameter, which is defining the ratio between the element size and the wave length, needs to be within a certain range:

$$\eta = \frac{\Delta x}{\lambda} \tag{28}$$

where λ is the wave length and Δx is the block length in the propagation direction. Parameter η was originally suggested by Lysmer and Kuhlemeyer, (1969) for dynamic modeling with the Finite Elements method. But it is also useful when studying wave propagation with DDA. Bao et al. (2012) found that a good accuracy with respect to P-wave velocity and stress can be obtained with DDA when the η ratio is between $1/8$ to $1/12$.

The input impact load for DDA includes a characteristic load vs. time function. If the time step interval is smaller than the difference between two successive input time values (t_i, t_{i+1}), a linear interpolation takes place between the two load values, thus:

$$F(t) = intepolation\,[F(t_i), F(t_{i+1})]$$

Because the interpolation depends on the time-step interval, this parameter needs to be calibrated carefully.

The blast load function we adopted is based on research conducted originally by Ma et al. (1998). They tested a 606 kg charge with a loading density of 10 kg/m^3 in the field. The maximum over-pressure of such a charge was 30.23 MPa, the time to peak load was 0.5 $msec$, and the total duration was 2.5 $msec$ (Ma et al., 1998). Usually, the positive impact blast shock could be simplified into two phases: t_1 and t_2 while the negative phase is typically ignored (see Figure 5-1). During the event the hot gas expansion forces out the

volume it occupied, resulting in a blast wave; this is the rise phase, t_1. The second phase, t_2, occurs when the gases expand further and then decay. The negative phase (vacuum) of the blast is ignored here because vacuum is more dominant in fluids and air, but is negligible in a rock-mass. In our simulation, we set the duration of the blast function to 0.8 $msec$ for the rise phase and 2 $msec$ in total to fit the optimal η ratio.

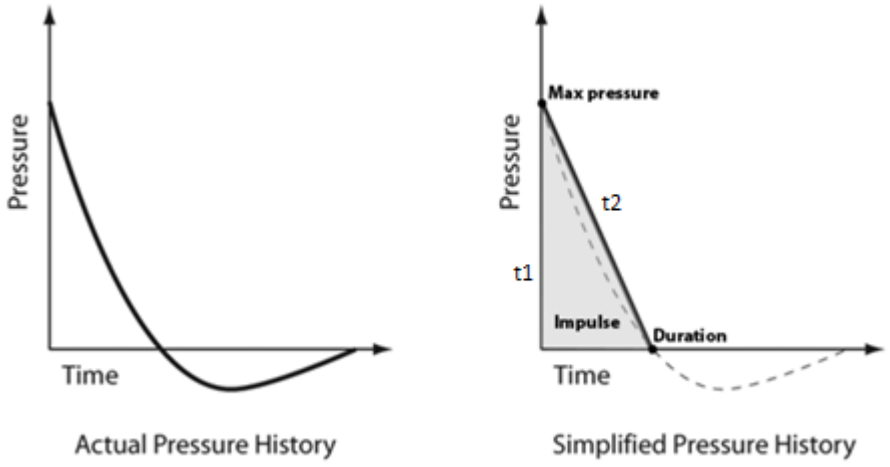

Figure 5-1: Schematic illustration of real blast behavior (left). Simplified linear blast behavior (right) displays a short t1 rise period and a gradual decay t2 phase. The negative vacuum phase is ignored (Martini 2010)

We used the blast element developed by Zelig et al. (2015) for DDA to conduct the blast simulation. We initiated a high impact load of 30 MPa radially, 4.5, 6, and 9 meters from the tunnel free surface. The discontinuity friction angles were changed between $20^o, 40^o, 60^o$ throughout the modeled domain. Unlike in the previous chapter, where we tested rock-burst initiated by strain relaxation, in this simulation we did not use initial stress, in order to render simplicity in the results.

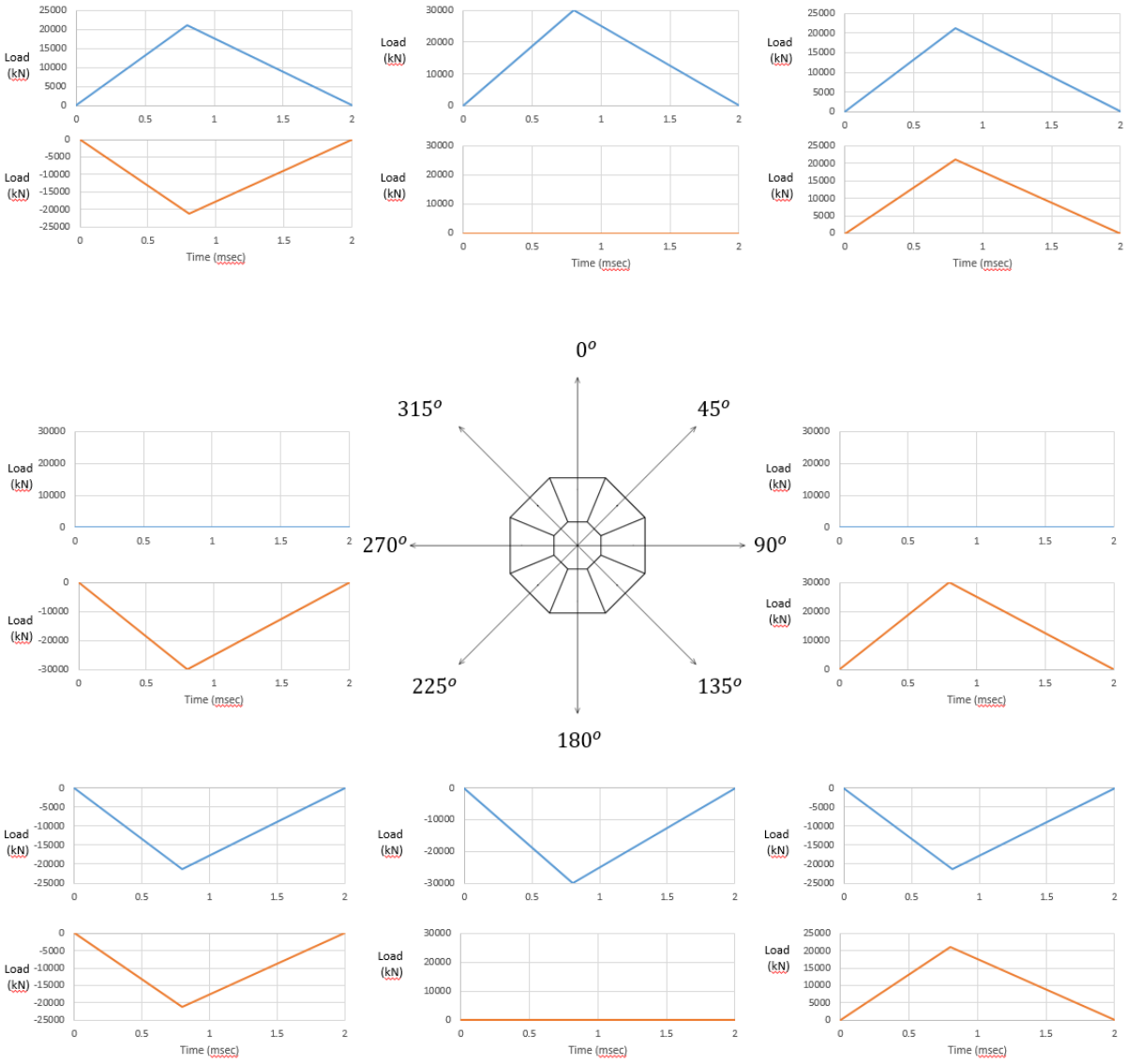

Figure 5-2 The blast function for the radial blast element

We used a block system representing a rock quality of RMR = 65. The analysis domain was 97 m high and 97 m wide and was composed of two sets of 60^o inclined joints with the same spacing of 1 m. A tunnel with 10 m diameter was set at the domain center. Non-reflective boundaries were set at the domain periphery to avoid artificial reflections. Cohesion and tensile strength were not applied at the interfaces. Young's modulus of the intact rock was set to 30 GPa, the Poisson ratio to 0.23, and the mass per unit area was 2.65 ton/m^2. The time step was set to 10^{-5}s, g_0 was set to 10 times E, gravity was not

activated, the tunnel was excavated $0.099\ sec$ after the start of the simulation and the blast was activated at $0.1\ sec$. The bolting pattern parameters were: $S = 1$, $L = 3$. The bolt stiffness (kA/l) was set to $25\ MN/m$. The η parameter was maintained between $1/8$ to $1/12$ in all directions of the rock-mass as the distance between joints depended on the direction of the wave propagation front.

Finally, a simulation with no blast was conducted and the results were subtracted from the tested simulations to filter out the blast load output from the initial load output due to residual strain relaxation.

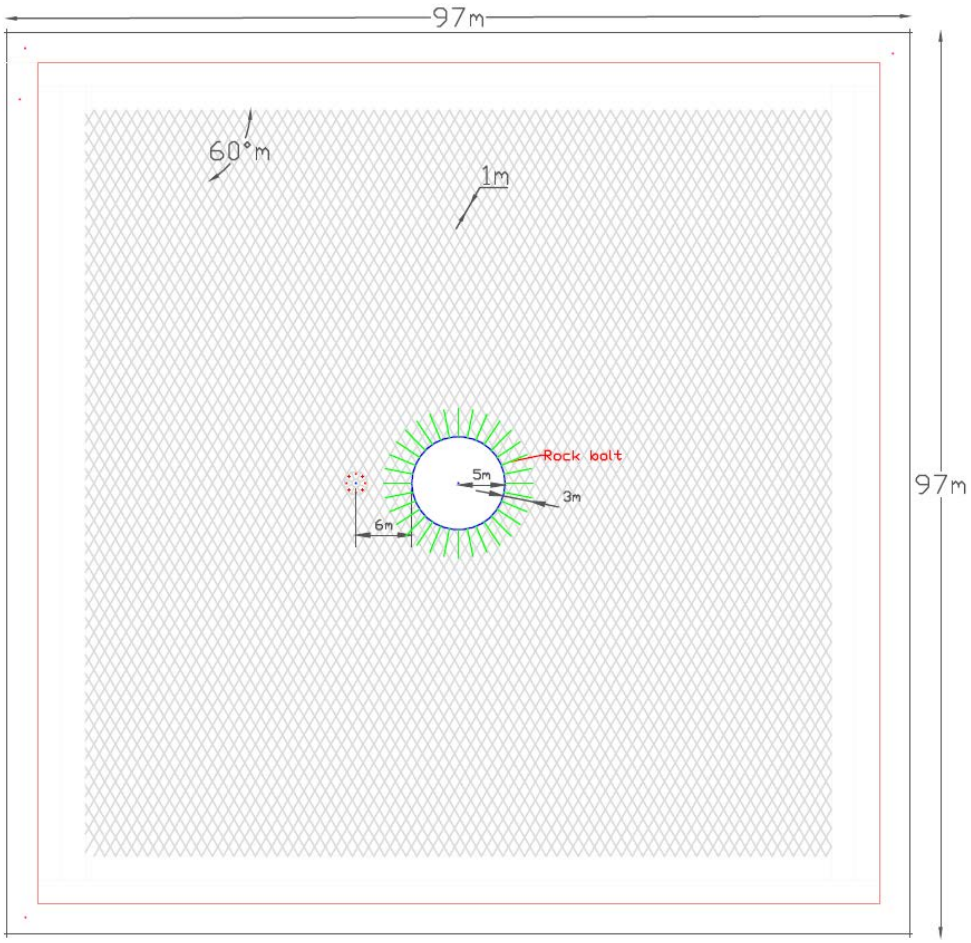

Figure 5-3: Geometry for the blast test is based on RMR 65:, a 10 meter diameter tunnel with blast element in the horizontal axis; in this example the distance between the center of the blast element and the tunnel free surface is 6 meters

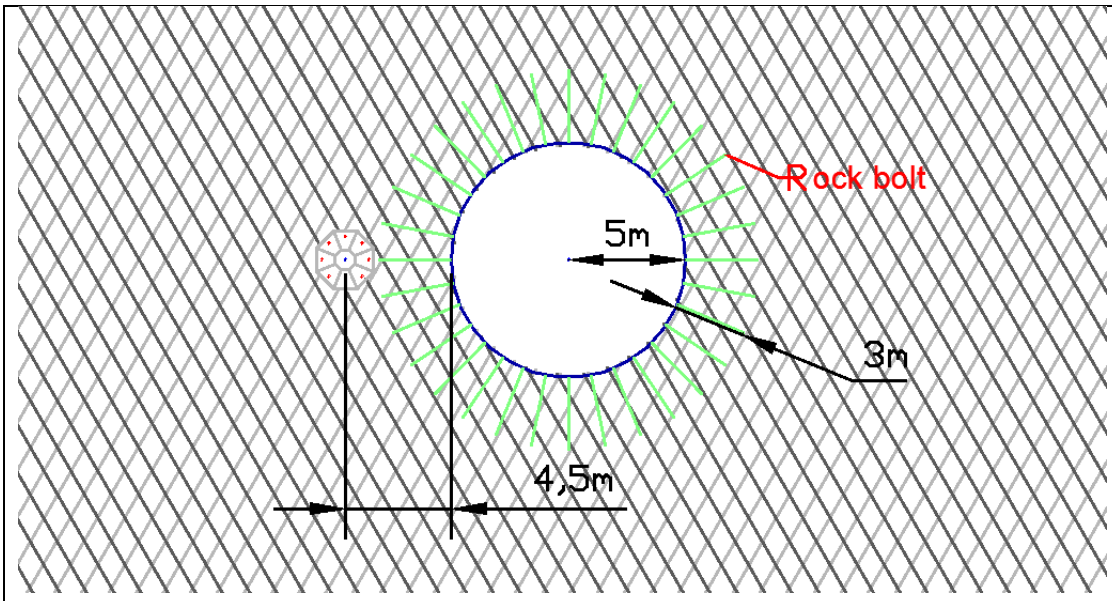

Figure 5-4: Modeled configurations for blast wave propagation

Results

The results of the radial blast simulation are shown in Figure 5-4. The results are presented in three diagrams, each representing a different distance from the blast source. In addition, each diagram includes three curves representing the different friction angles in the rock mass. The diagrams show the energy load (kJ) of the bolts as a radial function of the bolt position relative to the tunnel center. The shape of the radial plot indicates the extent of the bolt load and should be read carefully. From the charts, it can be observed that each distance displays a different load value, however the general shape is almost the same for all simulations conducted. The friction angle plays a major role in influencing the computed load values.

In all of the cases studied, the P-waves generated from the blast elements dispersed in a radial manner and influenced the rock-bolts surrounding the tunnel. It was also apparent that stress enhancements occurred at certain specific bolt angles around the tunnel, mainly on the tunnel roof (349^o) and floor (191^o). The load values decrease when the distance of the blast element from the tunnel free surface increases. The friction angle also plays a

major role in the amount of load absorbed. The highest enhancement is 2.08 kJ in a 4.5 m element 20^o friction angle simulation.

In the simulations where the blast element is positioned at 4.5 meters from the tunnel face, and the friction angle decreases from 40^o to 20^o, the load value increases approximately seven times from 0.3 kJ to 2.08 kJ at the bolt positioned 349^o in the radial pattern. When the friction angle is increased to 60^o, the load values decreases to 0.02 kJ in the same position. In addition only the 20^o friction simulation displays substantial load enhancement, which occur at the left side of the tunnel 281^o, incurring more than 0.6 kJ extra load.

This behavior remains the same when we increase the distance of the blast element to 6 meters; the energy enhancement is three times greater in the 20^o friction simulation than the 40^o friction simulation, for the bolt positioned at 349^o. For the bolt positioned at 191^o, the energy recorded is four times than the 40^o friction angle simulation. In addition, the left wall does not suffer substantial load enhancements in any of the friction angles tested.

When we increase the distance of the blast element to 9 meters, the load value approaches zero at the simulation with 40^o and 60^o friction angles. The simulation with a 20^o friction angle displays bolt energy of 0.3 to 0.6 kJ at the roof, floor, and left wall of the tunnel.

There is a simple explanation for the energy enhancement that results from decreasing the distance of the blast element: the stress wave travels less distance when less energy is lost, due to the friction energy along the discontinuities. The energy differences amongst the friction angles are also most likely due to energy lost by frictional sliding along the discontinuities. The bolt that suffered the highest load among all nine simulations was the bolt with a blast element at a 4.5 meter distance, a 20^o friction angle, and positioned at azimuth 191^o with more than 2.08 kJ of excess load. This is in good agreement with dynamic test values reported in the literature (Li, 2010; Ortlepp, 1992a).

5.2: Discussion and conclusion

In this chapter, we performed a series of simulations to understand the behavior of bolts during a dynamic event resulting from an explosion. We performed a series of nine

simulations to test how the bolts would react when a blast element transmits shock waves in a radial manner next to the tunnel location. Both the distances of the blast element and the rock mass friction angle were varied between simulations. The results determined that both the blast distance and the rock mass friction angle are dominant factors in the amount of load absorbed in the support system. The load was not distributed evenly in the reinforcement scheme; the bolts at the roof, floor, and the wall closest to the blast element, absorbed the majority of the load during the event.

The results demonstrate strong correlation between blast position and rock-bolt energy with a bolt load enhancement of up to 2.08 kJ. Therefore, it is reasonable to recommend that a bolt installed near a potential blast position will have the ability to endure more than an excess $2.08\ kJ$ shock on the already static loaded rock-bolt. The role of the friction angle is more complex than expected because it influences the kinematics of the blocks in the system, and this, in turn, influences the bolt energy. For every distance, we observed that the energy reduction would range between $0.6 - 1.7\ kJ$ when the friction angle increased from 20^o to 40^o . In this case, a numerical model can be a useful tool for predicting and studying dynamic induced rock-burst under varying friction values in the block system. Finally, it important to note that the dynamic simulations were executed without the use of any external stress or gravity, therefore further study should be conducted, which also incorporates initial stresses in the blast study, to determine if this impacts our results.

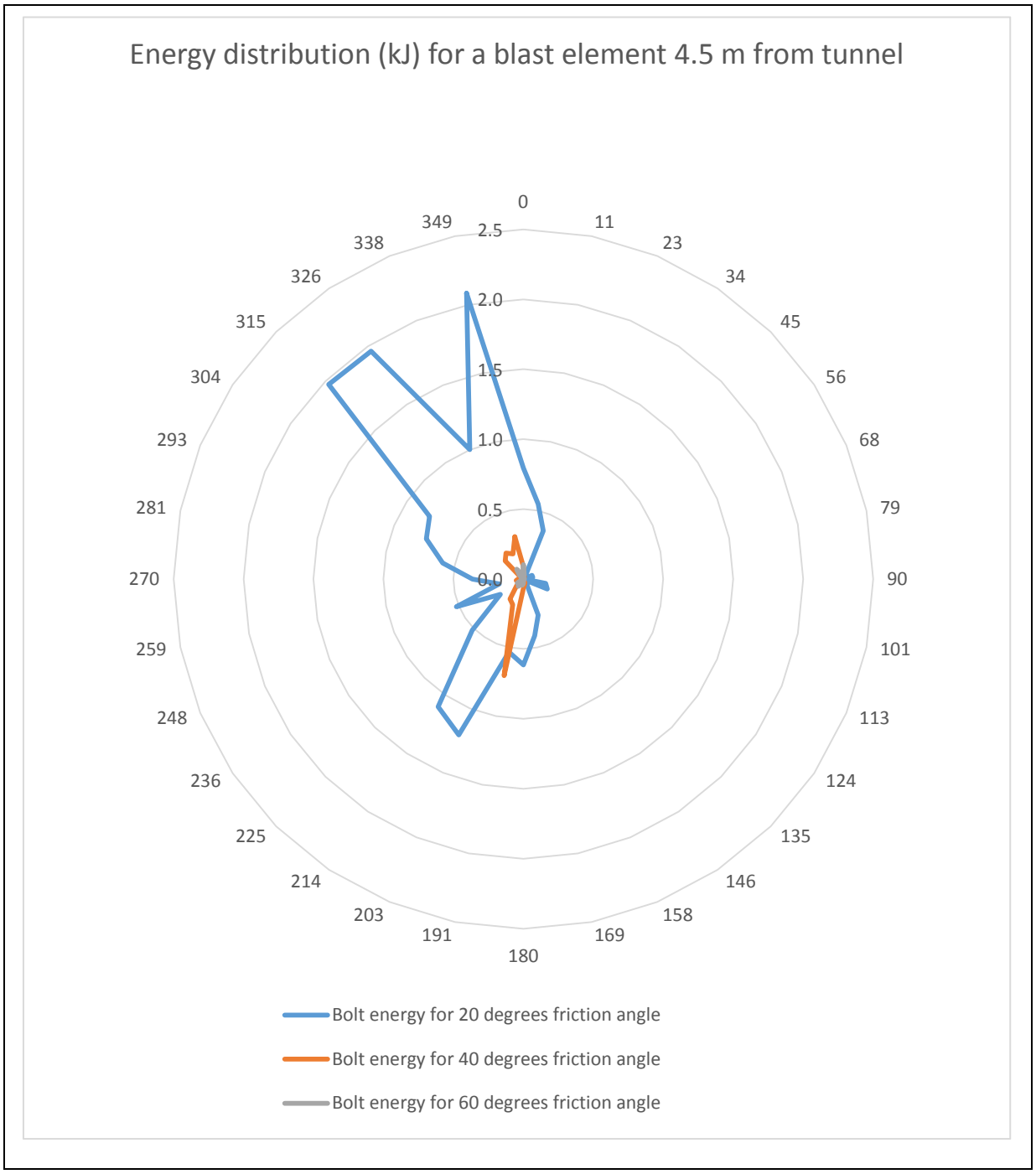
Energy distribution (kJ) for a blast element 4.5 m from tunnel
0
11
23
34
45
56
68
79
90
101
113
124
135
146
158
169
180
191
203
214
225
236
248
259
270
281
293
304
315
326
338
349
2.5
2.0
1.5
1.0
0.5
0.0
Bolt energy for 20 degrees friction angle
Bolt energy for 40 degrees friction angle
Bolt energy for 60 degrees friction angle


Energy distribution (kJ) for a blast element 6 m from tunnel
0
11
23
34
45
56
68
79
90
101
113
124
135
146
158
169
180
191
203
214
225
236
248
259
270
281
293
304
315
326
338
349
1.2
1.0
0.8
0.6
0.4
0.2
0.0
Bolt energy for 20 degrees friction angle
Bolt energy for 40 degrees friction angle
Bolt energy for 60 degrees friction angle

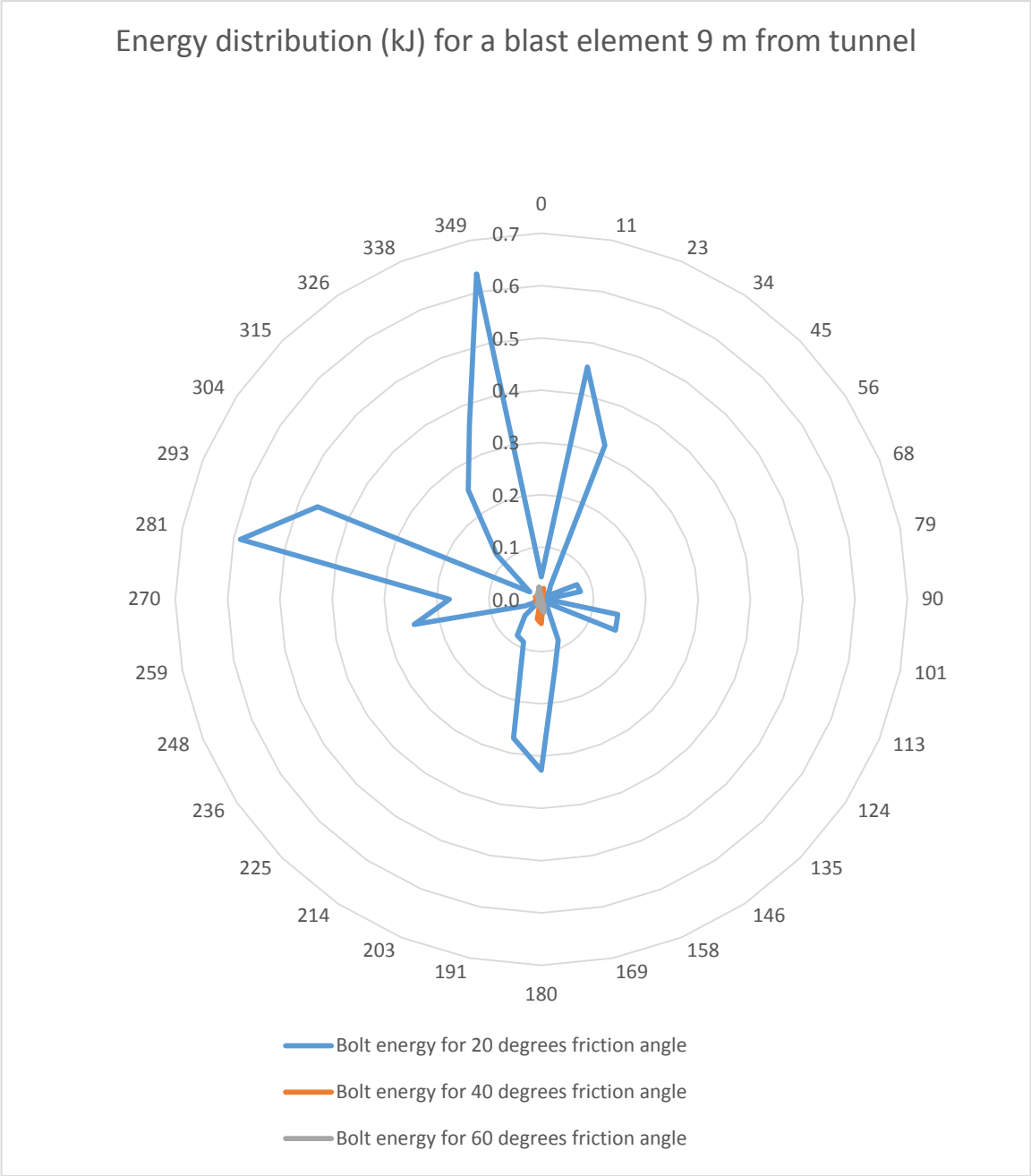

Figure 5-5: The radial bolt energy map showed the energy (kJ) enhancement in all directions, the bolt excess load increasde when the blast element distance and friction angle decreased. The shape of the excess load changed according to the distance

Chapter 6 : Thesis summary

Rock-burst is a very complex phenomenon. Even in our simplified DDA model – with a hydrostatic stress field, dry conditions, perfect geometric shapes, 2-D DDA with full face excavation sequence and without material degradation – it is still difficult to predict which removable key block will experiences rock-burst ejection and what will be the extent of it. The 'domino effect' of block-block and block-bolt kinematics also plays a significant role in the event, and it is hard to isolate a single block as the source of rock-burst event. This study conducted research about rock-bolt behavior in DDA under dynamic condition and dynamic load sources. Little work was done in the past to address DDA rock-bolt behavior in dynamic conditions (see work on columnar basalt rock-mass in the Baihetan hydropower plant in China (Hatzor et al., 2015)), and to compare static and quasi-static conditions (Tsesarsky and Hatzor, 2009). The use of DDA rock-bolt proves to be accurate under specific assumptions (see chapter 3).

In this thesis, we wanted to answer two key questions:

1. Can rock bolts mitigate the rock burst phenomenon, and if so, how can they accomplish this, in terms of bolt parameters?
2. And, what will be the energy load, on the bolt system, during the time of the event?

We discovered that rock bolts can reduce, or prevent, a rock burst event by absorbing the majority of the event energy. The energy absorption heavily depends on the rock mass condition, bolt stiffness, bolt length, and bolt spacing. The bolt stiffness should be at least 25 MN/m. The recommended bolt spacing in rock burst prone areas should be as minimal as possible, while the length should be more than one tunnel radius.

We found that in such an event the energy absorption ranged between 1 to 32 kJ/m^2.

The conclusions of this thesis consist of three parts:

1) The role of rock-bolts in the DDA model: we conducted three simulations to check the influence of time step interval, bolt stiffness and bolt reaction on varying load conditions. Both static and dynamic loading conditions displayed the same behavior, implying that the

bolt model is force-based, whereas rock-burst is an energy-based phenomenon. Other problems include the spring-like behavior of the bolt, which produces a multitude of errors including SHM, non-plastic deformation, stiff and fixed connection between bolt edges, and finally not considering bolt cross section, length and elastic modulus **separately**. Never the less, realistic values for the support elements could still be obtained from the model.

2) The performance of rock-bolts in strain relaxation induced rock bursts: we tested a single bolt, a bolting pattern, and rock mass quality as scaled by RMR. We showed that DDA could be a useful tool to conduct a pre-investigation of future tunnel sites, and produce close to reality results of the performance of system of rock-bolt pattern during event. Moderately stiff, long, and dense pattern of bolts can absorb the event energy, thus keeping the tunnel safe. These results prove to be valid throughout varying rock-mass conditions.

3) The effect of dynamic blast load on rock-bolts: we demonstrated the dominant influence of blast distance and rock mass friction angle on the support system. As the blast element position traveled away from the tunnel free surface, the amount of load decreased substantially. The role of the increasing friction angle was also important in terms of energy reduction, therefore, numeric modeling should be carried out to understand the influence on future tunnel sites.

Chapter 7 : Bibliography

Bao, H., Hatzor, Y. H., & Huang, X. (2012). A new viscous boundary condition in the two-dimensional discontinuous deformation analysis method for wave propagation problems. *Rock Mechanics and Rock Engineering*, *45*(5), 919–928.

Barton, N., & others. (1978). Suggested methods for the quantitative description of discontinuities in rock masses. *ISRM, International Journal of Rock Mechanics and Mining Sciences & Geomechanics Abstracts*, *15*(6).

Bieniawski, Z. T. (1976). Rock mass classification of jointed rock masses. *Exploration for Rock Engineering. Johannesburg: Balkema*, *97*, 106.

Bieniawski, Z. T. (1989). *Engineering rock mass classifications: a complete manual for engineers and geologists in mining, civil, and petroleum engineering*. John Wiley & Sons.

Cai, M. (2013). Principles of rock support in burst-prone ground. *Tunnelling and Underground Space Technology*, *36*, 46–56.

Clark, J., & Chorley, S. (2014). The greatest challenges in TBM tunneling: experiences from the field. *North American Tunneling: 2014 Proceedings, Los Angeles, USA*.

Doolin, D. M., & Sitar, N. (2004). Time integration in discontinuous deformation analysis. *Journal of Engineering Mechanics*, *130*(3), 249–258.

Durrheim, R. J., Roberts, M. K. C., Haile, A. T., Hagan, T. O., Jager, A. J., Handley, M. F., … Ortlepp, W. D. (1998). Factors influencing the severity of rockburst damage in South African gold mines. *JOURNAL-SOUTH AFRICAN INSTITUTE OF MINING AND METALLURGY*, *98*, 53–58.

Fu, G. Y., & Ma, G. W. (2014). Extended key block analysis for support design of blocky rock mass. *Tunnelling and Underground Space Technology*, *41*, 1–13.

Goodman, R. E., & Shi, G. (1985). *Block theory and its application to rock engineering*. Prentice-Hall Englewood Cliffs, NJ.

Hadjigeorgiou, J., & Potvin, Y. (2011). A critical assessment of dynamic rock reinforcement and support testing facilities. *Rock Mechanics and Rock Engineering*, *44*(5), 565–578.

Hagan, P., Chen, J., & Saydam, S. (2014). The load transfer mechanism of fully grouted cable bolts under laboratory tests.

Hagan, T. O., Miley, A. M., Spottiswoode, S. M., Hildyard, M. W., Grodner, M., Rorke, A. J., … Le Bron, K. B. (2001). Simulated rockburst experiment-an overview. *JOURNAL-SOUTH AFRICAN INSTITUTE OF MINING AND METALLURGY*, *101*(5), 217–222.

Handbook, I. B. (2011). International Society of Explosives Engineers, 18 th.

Hatzor, Y. H., Feng, X.-T., Li, S., Yagoda-Biran, G., Jiang, Q., & Hu, L. (2015). Tunnel reinforcement in columnar jointed basalts: the role of rock mass anisotropy. *Tunnelling and Underground Space Technology*, *46*, 1–11.

Hatzor, Y. H., He, B.-G., & Feng, X.-T. (2017). Scaling rockburst hazard using the DDA and GSI methods. *Tunnelling and Underground Space Technology*, *70*, 343–362.

He, B.-G., Zelig, R., Hatzor, Y. H., & Feng, X.-T. (2016). Rockburst generation in discontinuous rock masses. *Rock Mechanics and Rock Engineering*, *49*(10), 4103–4124.

He, M., Gong, W., Wang, J., Qi, P., Tao, Z., Du, S., & Peng, Y. (2014). Development of a novel energy-absorbing bolt with extraordinarily large elongation and constant resistance. *International Journal of Rock Mechanics and Mining Sciences*, *67*, 29–42.

K\il\ic, A., Yasar, E., & Celik, A. G. (2002). Effect of grout properties on the pull-out load capacity of fully grouted rock bolt. *Tunnelling and Underground Space Technology*, *17*(4), 355–362.

Kaiser, P. K. (1996). *Canadian Rockburst Support Handbook: 1996*. Geomechanics Research Centre.

Kaiser, P. K., & Cai, M. (2013). Critical review of design principles for rock support in

burst-prone ground--time to rethink! In *Proceedings of the Seventh International Symposium on Ground Support in Mining and Underground Construction* (pp. 3–37).

Kamai, R., & Hatzor, Y. H. (2008). Numerical analysis of block stone displacements in ancient masonry structures: A new method to estimate historic ground motions. *International Journal for Numerical and Analytical Methods in Geomechanics*, *32*(11), 1321–1340.

Kim, Y.-I., Amadei, B., & Pan, E. (1999). Modeling the effect of water, excavation sequence and rock reinforcement with discontinuous deformation analysis. *International Journal of Rock Mechanics and Mining Sciences*, *36*(7), 949–970.

Kutter, H. K., & Fairhurst, C. (1971). On the fracture process in blasting. In *International Journal of Rock Mechanics and Mining Sciences & Geomechanics Abstracts* (Vol. 8, pp. 181–202).

Lang, T. A., Bischoff, J. A., & others. (1982). Stabilization of rock excavations using rock reinforcement. In *The 23rd US symposium on rock mechanics (USRMS)*.

Li, C. C. (2010). A new energy-absorbing bolt for rock support in high stress rock masses. *International Journal of Rock Mechanics and Mining Sciences*, *47*(3), 396–404.

Lysmer, J., & Kuhlemeyer, R. L. (1969). Finite dynamic model for infinite media. *Journal of the Engineering Mechanics Division*, *95*(4), 859–878.

Ma, G. W., Hao, H., & Zhou, Y. X. (1998). Modeling of wave propagation induced by underground explosion. *Computers and Geotechnics*, *22*(3), 283–303.

Moosavi, M., & Grayeli, R. (2006). A model for cable bolt-rock mass interaction: Integration with discontinuous deformation analysis (DDA) algorithm. *International Journal of Rock Mechanics and Mining Sciences*, *43*(4), 661–670.

Ngo, T., Mendis, P., Gupta, A., & Ramsay, J. (2007). Blast loading and blast effects on structures--an overview. *Electronic Journal of Structural Engineering*, *7*(S1), 76–91.

Nie, W., Zhao, Z. Y., Ning, Y. J., & Guo, W. (2014). Numerical studies on rockbolts mechanism using 2D discontinuous deformation analysis. *Tunnelling and*

Underground Space Technology, *41*, 223–233.

Ohnishi, Y., Nishiyama, S., & Sasaki, T. (2006). Development and application of discontinuous deformation analysis. In *The 4th Asian rock mechanics symposium, Singapore* (pp. 59–70).

Ortlepp, D. W. (1976). Selection of Design of Tunnel Support. *Rock Mechanics Principles in Practical Underground Mine Design, South African Institute of Mining and Metallurgy, University of the Witwatersrand, Johannesburg, South Africa, August*, 2–6.

Ortlepp, W. D. (1969). An empirical determination of the effectiveness of rockbolt support under impulse loading. In *Proc. Int. Symp. on Large Permanent Underground Openings, Oslo* (pp. 197–205).

Ortlepp, W. D. (1992a). Implosive-load testing of tunnel support. *Rock Support in Mining and Underground Construction*, 675–682.

Ortlepp, W. D. (1992b). The design of support for the containment of rockburst damage in tunnels-an engineering approach. *Rock Support in Mining and Underground Construction*, 593–609.

Ortlepp, W. D. (1993). High ground displacement velocities associated with rockburst damage. *Rockbursts and Seismicity in Mines*, *93*, 101–106.

Ortlepp, W. D. (1994). Grouted rock-studs as rockburst support: a simple design approach and an effective test procedure. *Journal of the Southern African Institute of Mining and Metallurgy*, *94*(2), 47–63.

Potvin, Y., Wesseloo, J., & Heal, D. (2010). An interpretation of ground support capacity submitted to dynamic loading. *Mining Technology*, *119*(4), 233–245.

Reddy, N., & Spottiswoode, S. M. (2001). The influence of geology on a simulated rockburst. *JOURNAL-SOUTH AFRICAN INSTITUTE OF MINING AND METALLURGY*, *101*(5), 267–274.

Shi, G. (1993). *Block system modeling by discontinuous deformation analysis* (Vol. 11).

Computational mechanics.

Stacey, T. R. (2011). Support of excavations subjected to dynamic (rockburst) loading. In *Proceedings of the 12th international congress of the international society of rock mechanics* (pp. 137–145).

Tal, Y., Hatzor, Y. H., & Feng, X.-T. (2014). An improved numerical manifold method for simulation of sequential excavation in fractured rocks. *International Journal of Rock Mechanics and Mining Sciences*, *65*, 116–128.

Tannant, D. D., Brummer, R. K., & Yi, X. (1995). Rockbolt behaviour under dynamic loading: field tests and modelling. In *International journal of rock mechanics and mining sciences & geomechanics abstracts* (Vol. 32, pp. 537–550).

Tsesarsky, M., & Hatzor, Y. H. (2009). Kinematics of overhanging slopes in discontinuous rock. *Journal of Geotechnical and Geoenvironmental Engineering*, *135*(8), 1122–1129.

Tsesarsky, M., Hatzor, Y. H., & Sitar, N. (2002). Dynamic block displacement prediction--validation of DDA using analytical solutions and shaking table experiments. In *Stability of rock structures: Proceedings of the Fifth International Conference of Analysis of Discontinuous Deformation. Lisse: Balkema Publishers* (pp. 195–203).

Wang, C. Y., Chuang, C.-C., & Sheng, J. (1996). Time integration theories for the DDA method with finite element meshes. In *Proceedings of 1st Int. Forum on Discontinuous Deformation Analysis (DDA) and Simulations of Discontinuous Media* (pp. 263–287).

Yagoda-Biran, G. (2008). *Seismic hazard estimation along eastern margins of Sea of Galilee by back analysis of seismically induced natural and structural failures*. BGU Ben-Gurion U.

Yagoda-Biran, G., & Hatzor, Y. H. (2010). Constraining paleo PGA values by numerical analysis of overturned columns. *Earthquake Engineering & Structural Dynamics*, *39*(4), 463–472.

Yeung, M. R. (1993). Analysis of a mine roof using the DDA method. In *International*

journal of rock mechanics and mining sciences & geomechanics abstracts (Vol. 30, pp. 1411–1417).

Zelig, R., Hatzor, Y. H., Feng, X.-T., & others. (2015). Rock-Burst Simulations with 2D-DDA: Preliminary Results. In *49th US Rock Mechanics/Geomechanics Symposium*.

ZHANG, G., & Wu, X. F. (2003). Influence of seepage on the stability of rock slope-coupling of seepage and deformation by DDA method. *Chinese Journal of Rock Mechanics and Engineering*, *22*(8), 1269–1275.

Chapter 8 : Appendix

Converting AutoCAD configuration to a DDA file

The scripts listed below convert the AutoCAD geometric data to DDA operation file, dc and df. An excel file is loaded into the MatLAB software, processed and then a new files are created for numerical simulation execution.

```
% This code produce a DC and a DF files' based on AutoCAD drawing. One
should use a special
% template excel file to use this code
% Note - the fixed lines, inserted in AutoCAD as point
clear;
clc;
bolt_stifness_matrix = [0]; % The bolts stiffness use in the DC file
addpath(genpath('')) % Add the data file folder into MatLAB folder
base_number= ; % Name of loaded file
[line_cord,   layer]=xlsread(strcat(int2str(base_number),'','.xls'));   %
read the Excel file coordinates

% DC file
[row,column]=size(layer);
line_cord = cellfun(@str2double, layer);
frame=[]; % the frame of the domain: (1x4)*n
Joint_1=[]; % first joint set identifier number
Joint_2=[]; % second joint set identifier number
tunnel=[]; % tunnel boundary set identifier number
fixed_lines=[]; % the fix point of the domain: (1x4)*n
measurement_points=[]; % point of measure: (1x2)*n
new_bolts=[]; % botls (1x4)*n
removed_blocks=[]; % processing hole point
non_reflective_boundery=[]; % the reflective boundary of domain: (1x4)*n
% the next loops will sort the file 'coordinates' in to the different
% matrix

for i=2:row
   switch layer{i}
       case {'frame'}
          frame=[frame; line_cord(i, 2:5),1];
       case {'Joint_1'}
          Joint_1=[Joint_1; line_cord(i, 2:5),2];
       case {'Joint_2'}
          Joint_2=[Joint_2; line_cord(i, 2:5),3];
       case {'tunnel'}
          tunnel=[tunnel; line_cord(i, 2:5),4];
       case {'fixed_lines'}
          fixed_lines=[fixed_lines;    line_cord(i,    6:7),line_cord(i,
6:7)];
       case {'measurement_points'}
          measurement_points=[measurement_points; line_cord(i, 6:7)];
       case {'new_bolts'}
```

```
          new_bolts=[new_bolts;            line_cord(i,            2:5),
bolt_stifness_matrix(1),0 ,0];
       case {'removed_blocks'}
          removed_blocks=[removed_blocks; line_cord(i, 6:7)];
       case {'non_reflective_boundery'}
          non_reflective_boundery=[non_reflective_boundery; line_cord(i,
2:5)];
       otherwise
          disp(layer(i));
   end
end

% this section count the number of each element that after that will
insert
% to the list of the DC file
minimum_edge_node_distance=0.001 ;
number_of_joints=size(frame,1)+size(Joint_1,1)+size(Joint_2,1)+size(tun
nel,1) ;
number_of_fixed_lines=size(fixed_lines,1);
number_of_measurement_points=size(measurement_points,1);
number_of_new_bolts=size(new_bolts,1);
number_of_removed_blocks=size(removed_blocks,1);
new_bolts=sortrows(new_bolts);
number_of_matirial_line = 0 ;
number_of_bolt_elements = 0 ;
number_of_loadind_point = 0 ;
number_of_hole_points = 0 ;
% %% writing the dc file
% open file for writing
fid_1=fopen(strcat('dc','.txt'), 'wt');
% write to file minimum edge length parameter
fprintf(fid_1, '%d \n', minimum_edge_node_distance);
% write to file total number of lines and boundry lines
fprintf(fid_1, '%d  %d \n', number_of_joints , 0);
% write to file number of the list of point
fprintf(fid_1,   '%d   \n%d   \n%d   \n%d   \n%d   \n%d   \n%d   \n%d   \n',
number_of_matirial_line, number_of_bolt_elements, number_of_fixed_lines,
number_of_loadind_point,                    number_of_measurement_points,
number_of_hole_points, number_of_new_bolts, number_of_removed_blocks);
% write to file the frame
fprintf(fid_1, '%d  %d  %d %d %d \n', frame');
% write to file the J_1
fprintf(fid_1, '%d  %d  %d %d %d \n', Joint_1');
% write to file the J_1
fprintf(fid_1, '%d  %d  %d %d %d \n', Joint_2');
% write to file the tunnel
fprintf(fid_1, '%d  %d  %d %d %d \n', tunnel');
% write to file the  fixed line matrix
fprintf(fid_1, '%d %d \n', fixed_lines');
% write to file the measured point matrix
fprintf(fid_1, '%d  %d \n', measurement_points');
% write to file the bolts
fprintf(fid_1, '%d  %d  %d %d %d %d %d\n', new_bolts');
% write to file the removed blocks matrix
fprintf(fid_1, '%d  %d\n', removed_blocks');
% write to file the wave velocity reduction ratio and number of absorbing
boundary lines
```

```
fprintf(fid_1, '%d  %d \n%d \n',1 , 1,4);
% write to file the absorbing boundry matrix
fprintf(fid_1, '%d  %d %d %d \n', non_reflective_boundery');
% write to file the number of traction lines
fprintf(fid_1, '%d \n', 0.0);
% close the file
fclose(fid_1);


% Df file

bolt_file=1; % parameter of the type of simulation, if there are bolt in
the mesh
young=30E+06; % elastic deformation modulus (KPa)
poisson=0.20; % Poisson's ratio (~)
f_angle=35; % friction angle

% define elastic parameters:
remove=[];
density=2.653;  % density ton/m^3
G=0; % gravity (m/s^2)
wight=density*G; % kPa/m
initalstress=[-55000 -55000 0]; % stress [Sx Sy Txy]kPa
cohesion=0; % rock mass cohesion KPa
t_strength=0; % rock mass tensile strength KPa

%  define numerical parameters:
Ko=1; %damping factor, should be zero before tunnel formed
time_step=0.00001; % DDA time step interval
nt_steps=32000; % calculate the number of the time step needed for the
real time
g0=young*10; % contact spring g2 stiffness
fix_node=zeros(1,number_of_fixed_lines);

% the next if is in a case of late excavation
for m=1:size(removed_blocks) ;
   remove=[remove,1,30000];
end

%bolt matrix
bolt_time_step_array=29000:1:29000+size(new_bolts)-1 ;

%how many time steps to print the results to “output”
print_time=10;

% write the df file
fid_2=fopen(strcat('df','.txt'), 'wt'); % open file for writing
fprintf(fid_2, '%f \n', Ko); % write to file Dynamic/Static
fprintf(fid_2, '%i \n',round(nt_steps)); % write to file number of time
steps
fprintf(fid_2, '%d \n%d \n%d \n%d \n%d \n', 1, 1,0.0001, time_step,g0  );
% write to file number of the different numeric parameters
fprintf(fid_2, '%d  %d  %d  %d\n',fix_node'); % write to file the fix_node
matrix
fprintf(fid_2, '%d %d \n',remove'); % write to file removed block matrix
```

```
    if bolt_file
        fprintf(fid_2, '%d \n', bolt_time_step_array');% write to file
the time step bolt install
    end
fprintf(fid_2, '%d \n', print_time'); % write to file when to print the
results to "output" file (in how many time steps?)
fprintf(fid_2, '%d  %d  %d  %d  %d\n', density, 0,wight,young, poisson );
% write to file elastic parameters
fprintf(fid_2, '%d  %d  %d \n', initalstress'); % write to file the inital
stresses matrix
fprintf(fid_2, '%d  %d  %d \n%d  %d  %d\n', 0, 0 ,0,0,0,0); % write to
file the incremental initial normal stresses and initial velocity
fprintf(fid_2, '%d  %d  %d \n',f_angle,cohesion,t_strength); % write to
file the friction angle, cohesion,  tensil strength [F/L]
fprintf(fid_2, '%d \n%d %d %d \n%d \n', 1.4,0,0,0,0); % write to file
thefactor of over-relaxation used by SOR iteration method
fclose(fid_2);

fclose('all'); % close the file
```